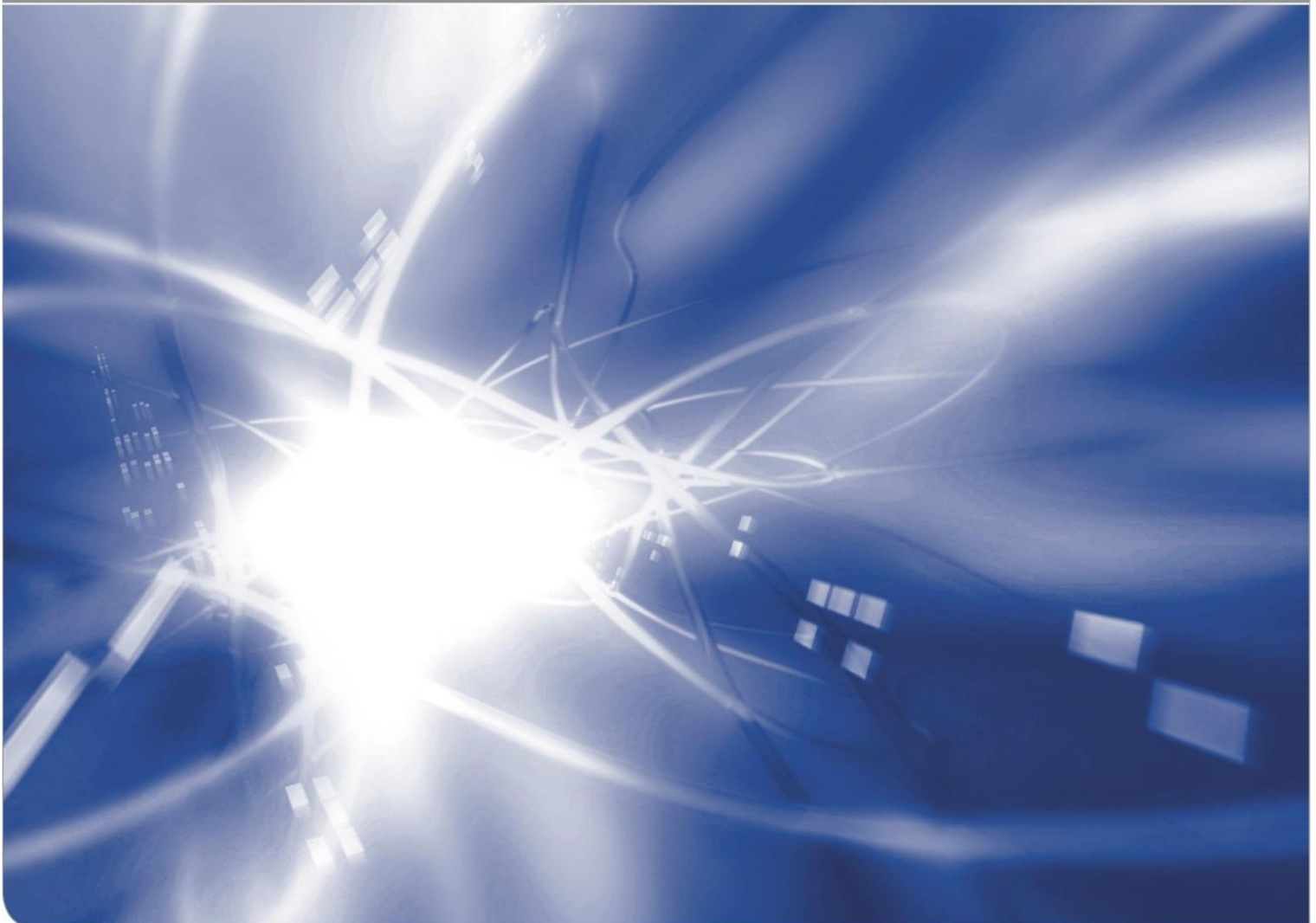


# Annual Report 2021 of the Institute for Thermal Energy Technology and Safety

Walter Tromm (Ed.)

KIT SCIENTIFIC WORKING PAPERS 207



Institute for Thermal Energy Technology and Safety  
Hermann-von-Helmholtz Platz 1  
76344 Eggenstein-Leopoldshafen  
<https://www.ites.kit.edu>

### **Impressum**

Karlsruher Institut für Technologie (KIT)  
[www.kit.edu](http://www.kit.edu)



This document is licensed under the Creative Commons Attribution – Share Alike 4.0 International License (CC BY-SA 4.0): <https://creativecommons.org/licenses/by-sa/4.0/deed.en>

2022

ISSN: 2194-1629

## Content

<b>Institute for Thermal Energy Technology and Safety</b> .....	<b>1</b>
Structure and Activities of the Institute for Thermal Energy Technology and Safety (ITES).....	1
Resources.....	1
<b>Group: Magnetohydrodynamic</b> .....	<b>3</b>
Magnetohydrodynamics for liquid-metal blankets.....	3
Magneto-convective flows around two differentially heated cylinders .....	3
Magnetohydrodynamic flow in stepwise bent circular pipes .....	8
MaPLE facility .....	10
Further work.....	12
References.....	12
<b>Group: Severe Accident Research</b> .....	<b>15</b>
SAR/ITES research activities in 2021 .....	15
Some Publications .....	17
<b>Group: Multiphase Flow</b> .....	<b>19</b>
Multiphase flows with heat transfer- subcooled boiling water flows up to boiling crisis.....	19
Introduction .....	19
COSMOS-L.....	19
COSMOS-H .....	21
Outlook.....	23
Acknowledgements.....	23
References.....	23
<b>Group: Karlsruhe Liquid metal Laboratory (KALLA)</b> .....	<b>25</b>
Liquid Metal Technology for Energy Conversion, Storage and Process Technology .....	25
Introduction KALLA .....	25
Thermal fluid dynamics of liquid metals.....	25
Liquid metal based thermal energy storage.....	28
LIMELISA - Development of a High Temperature Liquid Metal Loop for Testing Future Process Engineering Key Components.....	28
Liquid metal based process technology.....	29
References.....	32
<b>Group: Accident Management Systems</b> .....	<b>35</b>
Key Advancements in the Research Area of Energy System Resilience and Crisis Management in 2021 .....	35
Introduction .....	35
Resilient and Sustainable Energy Systems .....	35
Artificial Intelligence for predicting Critical Supply States.....	36
Integration of FLEXPART into JRODOS .....	37
Assessment of uncertainties affecting dosimetric calculations for Intake of Radon and NORM .....	39
Modelling the biokinetic behaviour of Americium in the human body with and without the presence of decorporating agents.....	40
References.....	41

<b>Group: Hydrogen</b> .....	<b>43</b>
Fundamental Behaviour of Hydrogen to Applied Accident Consequence	
Analysis for Hydrogen as a Safe Energy Carrier .....	43
Introduction.....	43
Quantitative Corona Infection Risk Assessment.....	43
Contributions to the Innopool Project “Solar Hydrogen” .....	46
Simulation of High Pressure Hydrogen Injection .....	48
References .....	50
<b>Group: Energy and Process Engineering</b> .....	<b>51</b>
First experimental results of a supercritical Organic Rankine cycle turbine	
using propane as working fluid.....	51
The MoNiKa power plant.....	51
Components description .....	52
Instrumentation.....	53
Simulation Software GESI.....	54
Stodola’s law.....	56
Summary .....	58
References .....	59
<b>Group: Framatome Professional School</b> .....	<b>61</b>
Introduction Framatome Professional School (FPS).....	61
CFD Validation .....	61
References .....	62
Reduced Order Model (ROM) of Standard K- $\epsilon$ Turbulence Model.....	62
References .....	63
Weak curvature asymptotics for Debye layers as electrohydrodynamic	
discontinuities.....	63
References .....	65
Analysis of Flow Blockages in a Typical Fuel Assembly of a Liquid Metal	
Cooled Reactor employing CFD, Coarse Grid-CFD and POD-ROM	
methodologies .....	65
References .....	66
PDF Methods for Two-Phase flows .....	66
References .....	67
Measurement and modeling of the boiling crisis in a rod bundle on	
Accident Tolerant Fuel (ATF) cladding materials.....	67
References .....	68
<b>List of Publications</b> .....	<b>69</b>

## Institute for Thermal Energy Technology and Safety

### Structure and Activities of the Institute for Thermal Energy Technology and Safety (ITES)

Walter Tromm

The Institute for Thermal Energy and Safety (ITES) is situated with its offices and research laboratories in Campus North of Karlsruhe Institute of Technology (KIT).

The research of ITES focuses on conversion from thermal power to electric power for future power systems without CO<sub>2</sub> emission including hydrogen technologies and on safety. In the past ITES concentrated on safety features and on methods to mitigate severe accidents for nuclear power plants. Nowadays, ITES uses these competences, gained from a profound experience in numerical simulation and in design and operation of large-scale experimental facilities to apply this knowledge mainly in the area of renewable energies.

The combination of science and technology with education and training is a systematic approach at KIT, and ITES is contributing accordingly to courses in mechanical engineering, supervises several bachelor and master theses each year and coordinates master programs in energy technologies. Compact courses on energy technologies are given also in executive master programs and in the Framatome Professional School, which is funded by industry and managed by ITES.

#### Resources

The employees of ITES contribute to the research-programs Materials and Technologies for the Energy Transition (MTET), Energy System Design (ESD), Fusion (FUSION), and Nuclear Waste Management, Safety and Radiation Research (NUSAFE) in the research field energy of the Helmholtz Association (HGF).

By the end of 2021, around 80 scientists, engineers and technicians have been working at ITES on this wide range of CO<sub>2</sub>-free technologies for energy conversion. Fig. 1 illustrates that still more than 50 % of the ITES employees were working for the NUSAFE program, but steadily reduced in recent years. Around two third of the employees were funded in 2021 by the Helmholtz Association (HGF), the others by third party funds of the European Commission, by industry, by German ministries or by other research funds. Doctoral students as well as students of the Baden-Wuerttemberg Cooperative State University (DHBW) were filling around 20% of these positions at ITES. In addition, students perform their bachelor or master theses or spend an internship in the research laboratories of ITES.

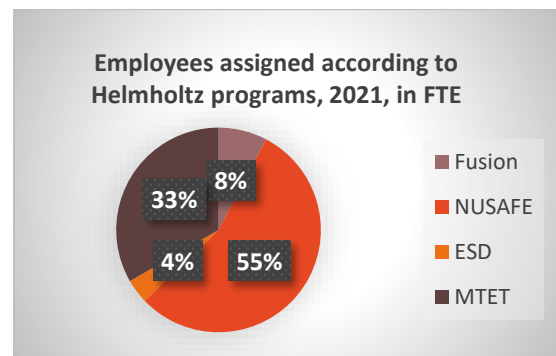


Fig. 1 Assignment of ITES personnel to Helmholtz programs.

An overview of the structure of ITES is given by the organization chart, Fig. 2. Because all working groups are embedded in the research field energy of the Helmholtz association (HGF) a close collaboration within the groups is guaranteed.

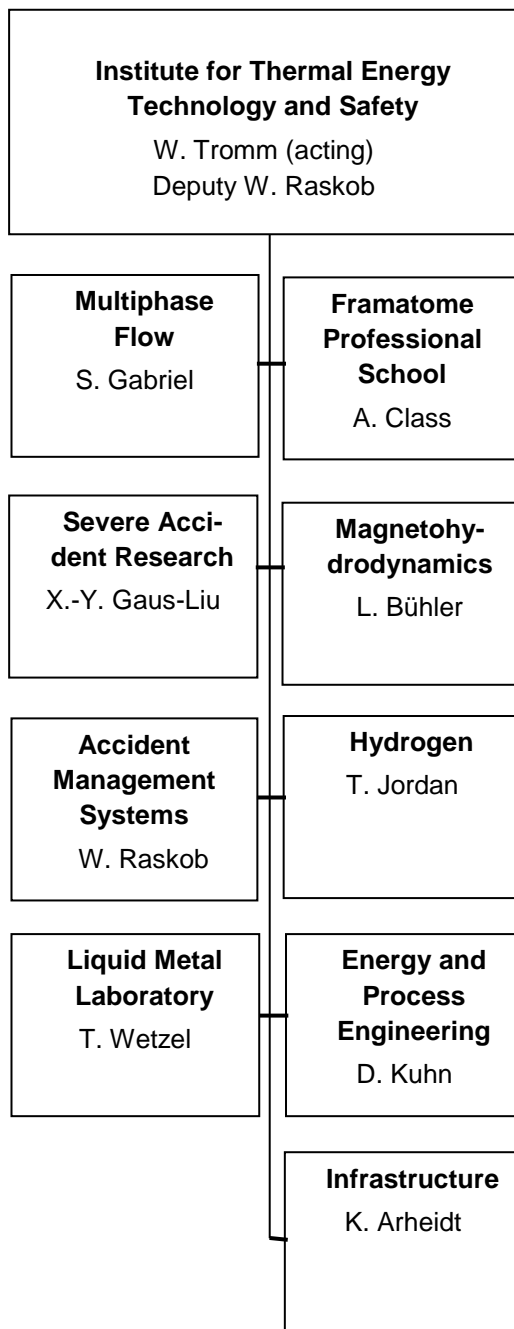


Fig. 2 : Organization chart of the Institute for Thermal Energy Technology and Safety

Working groups on Severe Accident Research, on Multi-Phase Flow as well as the Framatome Professional School still concentrated in 2021

primarily on nuclear applications, whereas the Karlsruhe Liquid Metal Laboratory (KALLA) and the Hydrogen group were addressing nuclear as well as renewable energy technologies. The working group on Magneto-Hydrodynamics is primarily working on nuclear fusion applications, whereas the working group on Energy and Process Engineering is concentrating on geothermal energies. The working group Multiphase Flows is mainly experimentally investigating technically relevant, complex flow phenomena. The field of activity currently focuses on the build-up of the complex structure of the COSMOS-H high-pressure loop. The working group on Accident Management Systems continued to extend the application of its simulation models not only to nuclear emergency cases but to several critical infrastructures within the program ESD. Thus, the institute covers a wide field of different energy technologies and related safety investigations. The share of personnel resources on the different research topics reflects the requirements of the Helmholtz Association's energy research field.

They are all supported by a joint infrastructure, comprising a metal workshop, manufacturing urgent test components, a welding shop, and an electromechanical workshop. Other tasks of the infrastructure include the IT-administration, business administration and public website of the ITES. The Infrastructure team is active as well in education and training activities.

Every year, several students of the Baden-Württemberg Cooperative State University are employed by ITES, managed by the Infrastructure group, to work with the research teams as part of their educational program.

Working in a research area with industrial application ITES practices a Quality Management System appropriate to EN ISO 9001.

Group: Magnetohydrodynamic

## Magnetohydrodynamics for liquid-metal blankets

*L. Bühler, B. Lyu, H.-J. Brinkmann, C. Courtessole, V. Klüber, C. Köhly, C. Mistrangelo, J. Roth*

### Magneto-convective flows around two differentially heated cylinders

In the frame of the European fusion research program coordinated by EUROfusion, liquid metal blanket concepts are developed, which will be experimentally tested in the International Thermonuclear Experimental Reactor (ITER). In the water-cooled lead lithium (WCLL) blanket concept, currently under investigation in the EUROfusion research activities, the heat is removed by a large number of cooling tubes immersed in the liquid metal that flows in the breeding units. The design of the WCLL test blanket module for ITER consists of modules stacked along the poloidal direction. Liquid lead lithium serves as tritium breeder, neutron multiplier and heat carrier. Since in the WCLL blanket the forced flow is relatively slow and temperature gradients are large, it is expected that buoyancy dominates and determines the flow pattern as a result of a balance with electromagnetic Lorentz forces. The arrangement of cooling tubes in the breeding zones plays a critical role to assess the blanket feasibility. The present study sheds some light on magneto-convective heat transfer around obstacles, such as the cooling pipes, and provides insight in major flow phenomena, by predicting 3D circuits of electric currents and flow patterns [1].

For systematic investigation of liquid metal heat transfer in strong magnetic fields, a generic model problem has been defined as shown in Figure 1. A magnetic field  $\mathbf{B}$  is imposed in  $y$  - direction parallel to gravity. Walls perpendicular to the applied magnetic field are called Hartmann walls, while those parallel to  $\mathbf{B}$  are named side walls. Two differentially heated isothermal pipes aligned

with the  $x$  direction penetrate the end-walls at  $x=\pm 100\text{mm}$ . The selected geometrical configuration corresponds to the one used in an experimental campaign carried out in the liquid metal laboratory MEKKA at KIT in which the eutectic liquid metal alloy GalSn is used as model fluid [2]. A temperature gradient that drives the buoyant flow is realized in the experiments by setting a temperature difference between the two copper pipes immersed in the liquid metal. One tube is heated, while the other pipe is cooled to serve as heat sink. The pipes are maintained at constant temperatures  $T_1 < T_2$  during the experiments.

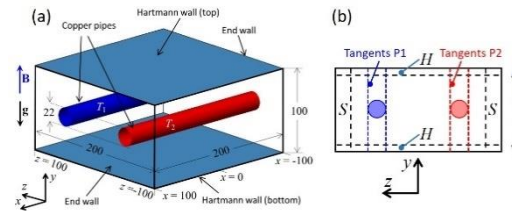


Figure 1 (a) Geometry used for simulations. Dimensions are given in mm. (b) Side ( $S$ ) and Hartmann layers ( $H$ ) are schematically indicated together with internal layers tangent to pipe walls.

The physical parameters characterizing the MHD-convective flow are the Hartmann number and the Grashof number,

$$Ha = BL\sqrt{\frac{\sigma}{\rho_0\nu}}, \quad Gr = \frac{g\beta\Delta TL^3}{\nu^2},$$

where  $L$  denotes a typical length scale of the problem. The former one gives a non-dimensional measure for the strength  $\mathbf{B}$  of the imposed magnetic field and  $Ha^2$  quantifies the

relative importance of electromagnetic and viscous forces. The second one represents the ratio of buoyancy to viscous forces and is proportional to  $\Delta T=(T_2-T_1)/2$ .

The physical properties of the fluid, such as the reference density  $\rho_0$ , the kinematic viscosity  $\nu$ , the volumetric thermal expansion coefficient  $\beta$ , and the electric conductivity  $\sigma$  are considered constant.

The numerical code used for simulations consists of an extension of the hydrodynamic open source code OpenFOAM for MHD applications [3].

### **Fully developed flow**

In this section, we analyze fully developed MHD buoyant flows, like the one expected, in a certain range of parameters, at some distance from the end-walls and in particular on the symmetry plane  $x=0$ . A parametric study has been carried out to investigate the influence of the magnetic field strength and the applied temperature difference  $\Delta T$  on flow distribution and heat transfer. Let us first consider the flow at  $Gr=2.5 \cdot 10^7$  and different Hartmann numbers. For  $Ha < 40$  time-dependent flow patterns appear triggered by the increased buoyancy effects as shown in Figure 2. The unstable flow is characterized by a large-scale recirculation formed by the fluid that moves upwards in the boundary layers around the warm pipe. The layers detach from the tube and merge again at some distance behind the cylinder while flowing towards the upper wall of the box. The ascending thermal plume impinges against the cavity top wall and turns downwards, flowing towards the low-temperature pipe. The cold boundary layer flow detaches from the cylinder and recombines to feed the region near the bottom of the container.

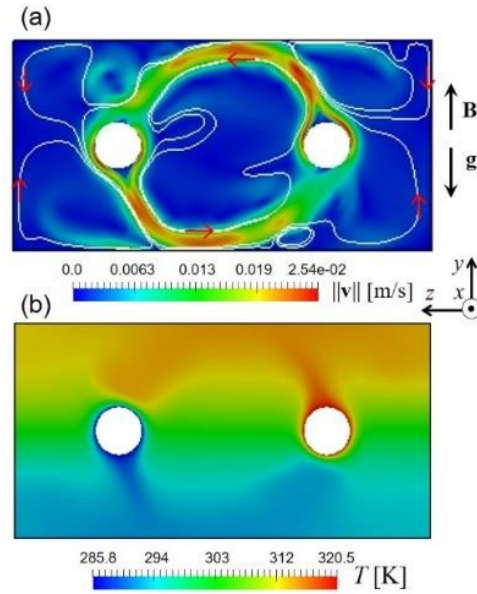


Figure 2 Instantaneous contours of velocity magnitude (a) and temperature (b) displayed for the axially fully developed magneto-convective flow at  $Gr=2.5 \cdot 10^7$  and  $Ha=25$ . White paths in (a) are velocity streamlines.

By further increasing the Hartmann number, the flow becomes stationary and temperature contours tilt progressively such that isotherms tend to become vertical, as in a pure conduction case, since convection is damped by more intense Lorentz forces. This can be observed in Figure 3, where contours of temperature (top), velocity magnitude (middle) and axial current density (bottom) are plotted for axially fully developed magneto-convective flows at  $Gr=2.5 \cdot 10^7$  and two Hartmann numbers. For larger  $Ha$ , the velocity distribution becomes regular and well organized. The flow is characterized by two convective cells located between side walls and pipes and a central, almost square, convective cell between the tubes. This is due to the fact that the intensity of braking electromagnetic forces becomes much larger than the buoyant forces. The highest velocities are found in internal layers tangent to the pipe walls and aligned with the magnetic field direction.

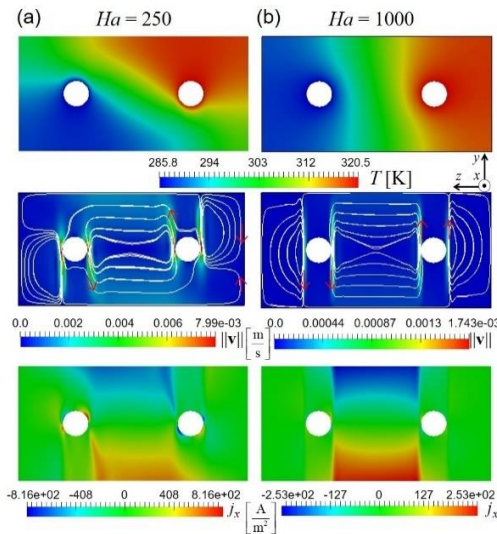


Figure 3 Fully developed flow at  $Gr=2.5 \cdot 10^7$  and two Hartmann numbers,  $Ha=250$  (a), 1000 (b). Contours of temperature (top), velocity magnitude and streamlines (middle) and axial current density (bottom).

### Three-dimensional flow

Three-dimensional numerical simulations have been performed considering the real geometry of the test-section with finite axial length as used for experiments. The aim is on one hand, to verify possible limitations of the assumption of fully developed flow in 2D simulations, and on the other hand, to provide a complete description of the phenomena involved by allowing current closure in parallel layers along end-walls. Moreover, numerical results complement experimental data and facilitate their interpretation.

In Figure 4a, the temperature distribution is plotted on the upper Hartmann wall and on the horizontal symmetry plane  $y=0$ , for the flow at  $Ha=500$ ,  $Gr=2.5 \cdot 10^7$ . In regions close to the end-walls, the temperature varies along the axial direction, while temperature contours on the middle plane of the test-section resemble the ones obtained by 2D simulations. On the two end-walls, a different temperature distribution is present as a result of an increased convective heat transfer near these vertical planes. This is caused by higher velocities in the boundary layers that

develop at walls parallel to the magnetic field, as displayed in Figure 4b, where 3D contours of the velocity distribution in the box are plotted on different planes.

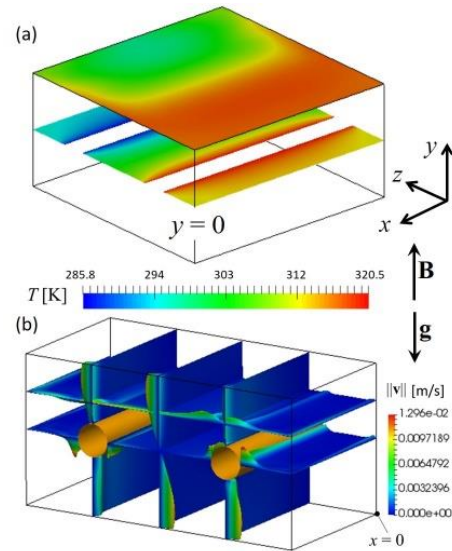


Figure 4 Flow at  $Ha=500$ ,  $Gr=2.5 \cdot 10^7$ . (a) Temperature distribution on planes perpendicular to the magnetic field, at  $y=0$  (middle plane) and on the top Hartmann wall. (b) Velocity distribution in the test-section. Here only half geometry is shown.

### Heat transfer

The rate of heat transfer between pipes and liquid metal is expressed in nondimensional form by the Nusselt number  $Nu=hL/k$  evaluated at the cylinder walls. Here  $h$  is the heat transfer coefficient and  $k$  the thermal conductivity. In Figure 5  $Nu$  is plotted as a function of the combined parameter  $Gr/Ha^2$ , which quantifies the relative importance of buoyancy to electromagnetic forces.

Results for the Nusselt number obtained by assuming fully developed thermal and hydraulic conditions along  $x$  (2D simulations), and from 3D calculations for the real geometry of the test-section, are compared with the ones measured in the experimental campaign. Simulations have been performed for  $4 \cdot 10^6 < Gr < 5 \cdot 10^7$  and  $25 < Ha < 2000$ .

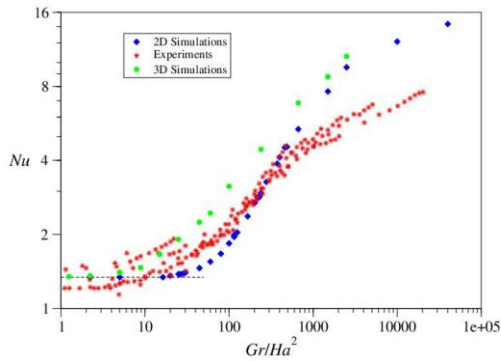


Figure 5 Comparison of Nusselt number measured in the experiments (stars) and values calculated by 3D (circles) and 2D (rhombus) simulations. The black dashed line indicates the Nusselt number for  $Gr=0$ , i.e. in case of pure conduction,  $Nu_0=1.339$ .

When the Nusselt number increases, it indicates that the convective heat transfer becomes more preponderant over the purely conductive one. The conduction-dominated regime with  $Nu_0=1.339$  is found to occur for  $Gr/Ha^2 \leq 15$  in 2D simulations, while in 3D calculations for  $Gr/Ha^2 \leq 2.5$ . This lower threshold value observed when considering the full geometry is explained by the fact that, when assuming fully developed flow conditions in 2D simulations, a significant fraction of the total heat exchanged by the convective motion near the end-walls is not taken into account. This is also the reason why 3D simulations predict higher Nusselt numbers than the 2D calculations.

### Experimental study

As already mentioned above, the theoretical work was motivated by experiments performed in the MEKKA. Eutectic GalSn was used as a model fluid such that experiments could be performed at room temperature. Electric potential and temperature were measured at selected wall locations as well as in the center of the cavity. Experiments were performed over a broad range of parameters  $0 < Ha < 3000$  and

$1.0 \times 10^6 < Gr < 5.0 \times 10^7$  for which heat transfer has also been characterized (see Figure 5).

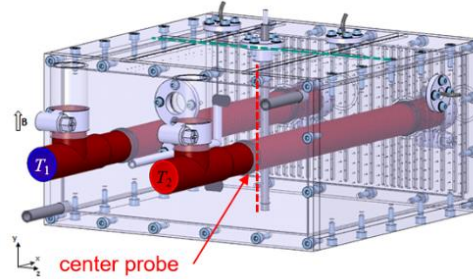


Figure 6 Sketch of the test section.

The results obtained from the time-average temperature distributions recorded in the center of the cavity and shown in Figure 7 hint at a possible relaminarization of the core flow due to turbulence suppression by the magnetic field. For instance, data collected for  $Gr = 2.5 \cdot 10^7$  show that the temperature amplitude in the center of the test section first increases with  $Ha$  in favor of the reduction of turbulence mixing. It reaches a maximum value for  $Ha \approx 200$  before collapsing to almost zero at the strongest magnetic field applied as the convective motion gets eventually almost completely damped by the Lorentz force.

This interpretation is supported by the statistical analysis of the data recorded at the center probe. Profiles of standard deviation of nondimensional temperature derived from a sample of 1090 data points collected at different times are shown in Figure 8. When no external magnetic field is imposed, temperature fluctuations of up to 1.5% reveal the occurrence of an unstable or turbulent convective cell located between the pipes. Recordings obtained in the presence of an external magnetic field show a strong suppression of temperature oscillations in the core flow even at the lowest magnetic fields investigated here. For instance for  $Ha \approx 50$ , the statistical deviations of the signals are of

the same order or smaller than the resolution of the measurements, i.e. 0.025 °C.

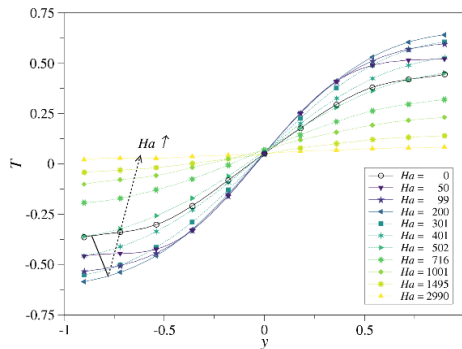


Figure 7 Nondimensional temperature distribution measured along the magnetic field direction in the center of the cavity for  $Gr=2.5 \cdot 10^7$  and various  $Ha$  numbers.

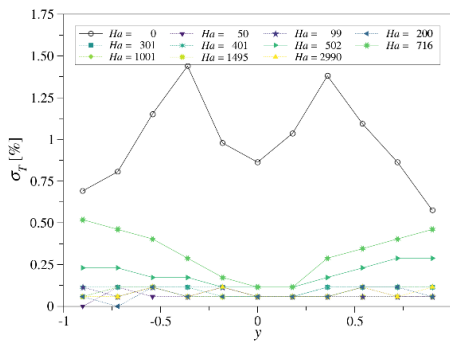


Figure 8 Profiles of standard deviation of temperature along the vertical direction  $y$  in the center of cavity for  $Gr=2.5 \cdot 10^7$

The critical parameters at which this transition occurs were further investigated for various Grashof numbers. The onset of the re-laminarization of the core flow was identified from transient temperature signals recorded by the center probe. The core flow was considered laminar when temperature fluctuations measured by all 11 thermocouples of the center probe dropped below the uncertainty of the measurement, i.e. 0.025 °C. Since the transition was expected to occur at low  $Ha$  in the range of  $Gr$  investigated, the power supply of the electromagnet was replaced with one that allows finer control of

the magnetic field with 1 mT increments. A map of flow regimes obtained by these measurements is shown in Figure 9

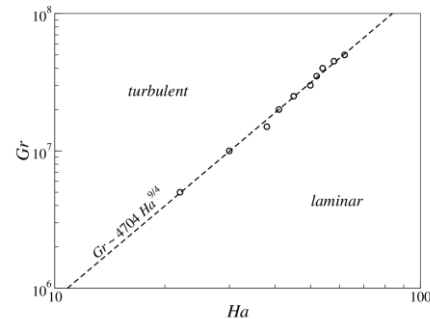


Figure 9 Map of flow regimes showing transition from turbulent to laminar magneto-convective flow upon increasing  $Ha$ .

### Conclusions

In order to investigate fundamental aspects of magneto-convective flows relevant for WCLL blankets, numerical simulations and experiments have been performed for a model problem, where two isothermal parallel cylinders immersed in a box filled with liquid metal are kept at differential temperatures. Numerical results show that electromagnetic forces significantly slow down the convective motion that results from the non-uniform thermal conditions caused by the imposed temperature difference between the cylinders. With increasing magnetic field, residual turbulent fluctuations are suppressed. Under intense magnetic fields, the flow features a central, almost square convective cell bounded by the fluid layers, which develop parallel to the magnetic field and tangent to the pipes. In the rest of the container, the fluid velocity is very small. Eventually, when  $Ha$  becomes large enough, the problem tends to an asymptotic behavior where the heat transfer is completely dominated by conduction and the temperature field is characterized by vertical isotherms. The intensity of convective heat transfer has been quantified by the Nusselt number calculated by performing both 2D and 3D numerical simulations. The outcome

clearly shows that the increased convective heat transfer near the end-walls of the box contributes significantly to the total transferred heat. Therefore, a pure 2D analysis cannot be used to accurately quantify the heat exchanged between pipes and fluid in a geometry of finite axial extension.

### Magnetohydrodynamic flow in stepwise bent circular pipes

Asymptotic analyses and numerical simulations have been performed to predict liquid metal flow in an electrically conducting circular pipe that exhibits stepwise bends in a strong uniform magnetic field. The present work is motivated by applications in nuclear fusion engineering, where such step-shaped double bends are foreseen in the shield behind the liquid metal test blanket module to be tested in ITER. Although the geometry is relatively simple, quite complex and unexpected flow patterns are observed, depending on the orientation of the magnetic field. For that reason, the present type of flow constitutes an interesting fundamental problem in magneto-hydrodynamics.

The flow is governed by two non-dimensional parameters, the Hartmann number  $Ha$  and the interaction parameter  $N$ , and the conductivity of the wall is characterized by the wall conductance parameter  $c$ ,

$$Ha = B_0 L \sqrt{\frac{\sigma}{\rho \nu}}, \quad N = \frac{\sigma L B_0^2}{\rho \nu_0}, \quad c = \frac{\sigma_w t_w}{\sigma L},$$

where  $Ha^2$  and  $N$  denote the ratios of electromagnetic to viscous and inertia forces, respectively, and  $c$  defines the relative conductance of the wall with thickness  $t_w$  and electric conductivity  $\sigma_w$  compared to the conductivity of the fluid region.

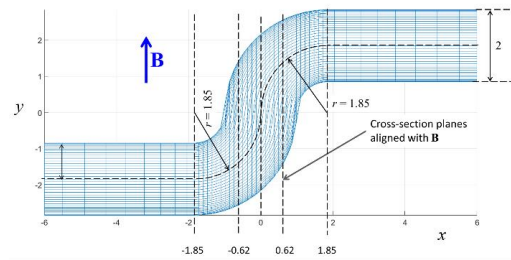


Figure 10 Coarse grid on the model geometry and indication of cross sections on which results are presented later. Calculations have been performed with higher resolution. Dimensions and coordinates are scaled with the pipe radius  $L=3.25\text{cm}$ .

The performed 3D analysis is based on an asymptotic theory valid for strong magnetic fields, i.e. assuming  $N \rightarrow \infty$  and  $Ha \gg 1$ . Under these conditions, electromagnetic forces dominate over inertia forces and viscous boundary layers along walls are very thin. It is known that strong 3D MHD effects occur in bends that turn the flow in a plane aligned with magnetic field lines [4] and the investigated geometry contains two of these bends in series, as shown in Figure 10.

### Results from asymptotic theory

Simulations discussed in this section are performed for the ITER-relevant Hartmann number  $Ha=3495$ , results are universal and apply for other  $Ha$  as well, as long as the boundary layers are thin and the wall is better conducting than the Hartmann layers.

Figure 11 shows colored contours of electric potential plotted on the surface of the geometry. In the fully developed region, at the entrance, the potential is constant along magnetic field lines with variations along the transverse direction  $z$ , as expected for fully developed flows.

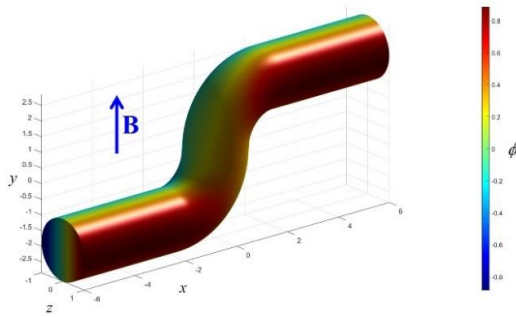


Figure 11 3D view on contours of non-dimensional potential at the fluid-wall interface for radial-toroidal-radial flow.

Highest values of potential magnitude are found near the sides,  $\phi(x \rightarrow \pm\infty, z = \pm 1) = \pm 0.889$ , in agreement with predictions for fully developed pipe flow in electrically conducting pipes [5], where  $\phi_{fd}(z = \pm 1) = (1+c)^{-1} = 0.890$ . When approaching the bends, a reduction of the magnitude of wall potential can be observed near the sides. One could argue that some fluid now flows parallel to  $\mathbf{B}$  which reduces the strength of the induced electric field  $\mathbf{v} \times \mathbf{B}$ , and therefore the potential at the sides is smaller as well. Another explanation is found when discussing the flow in terms of cross-sections aligned with  $\mathbf{B}$ . If we imagine that the geometry is sliced by vertical  $yz$  planes, it is clear that cross-sections defined in this way vary with  $x$  as depicted in Figure 10. Since the flow rate is constant, and the cross-sectional areas increase in the bend, the average velocity along  $x$  reduces, and so does the induced electric field. Consequently, the magnitude of potentials at the sides are smaller near  $x=0$ .

In Figure 12, the potential is plotted along center and sides of the pipes. For  $-2 < x < 2$ , we observe axial variations of electric potential, which give rise to 3D electric currents  $\mathbf{j}_{3D}$  and additional Lorentz forces that affect the flow.

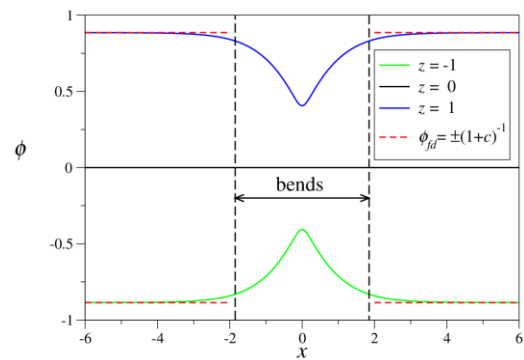


Figure 12 Variation of potential along center and sides of the pipes.

The situation is sketched schematically in Figure 13 and, for simplicity, it is projected onto a horizontal  $xz$  plane.

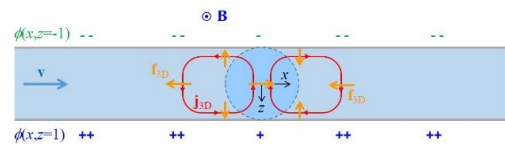


Figure 13 Sketch of distribution of side potential, 3D current loops  $\mathbf{j}_{3D}$ , and Lorentz forces  $\mathbf{f}_{3D}$ .

When the fluid moves in a magnetic field, the flow-induced electric field  $\mathbf{v} \times \mathbf{B}$  produces a difference in potential between the sides of the pipes. The higher values of potential magnitude are indicated by double-symbols ++ and --, whereas the reduced values near  $x=0$  by single + and - signs, respectively. The axial variation of potential near the sides leads to local axial gradients in the fluid, which drive additional 3D currents. The latter converge towards  $x=0$  for  $z > 0$  and they diverge from  $x=0$  for  $z < 0$ . Current circuits close via the core of the bends (in the virtual cylinder introduced below) near  $x=0$ . Here currents interact with the magnetic field and create streamwise extra Lorentz forces which reduce, or even reverse, the pressure gradient necessary to drive the flow. These phenomena occur preferentially inside a virtual cylinder of unit radius that forms around the  $y$ -axis (dashed circle in the sketch shown

in Figure 13). Its circumference is formed by magnetic field lines that are tangent to the wall in the symmetry plane  $y=0$ , where both bends join together. Outside of the tangent cylinder, i.e. for  $x^2+z^2>1$ , 3D currents have different orientation and create either transverse or upstream oriented Lorentz forces, which increase the pressure gradient in the close external neighbourhood of the virtual cylinder.

### **Conclusions**

Numerical simulations show that MHD flows in stepwise double bends in a plane parallel to the magnetic field experience strong 3D effects caused by extra Lorentz forces due to additional 3D current loops. The flow region splits into three cores. We find an upstream core, where velocity and pressure vary strongly when approaching the central “tangent” virtual cylinder with radius one that forms around the  $y$ -axis. The volume inside this virtual cylinder represents the central core in which the pressure is almost constant. Downstream of the virtual cylinder, in the third core, the flow exhibits again very strong 3D distortions with increased pressure drop in the center of the pipe. The most surprising result, however, is that despite very strong 3D effects on velocity and pressure distribution, the overall pressure drop is not increased compared to the one in a straight pipe flow of same axial length.

### **MaPLE facility**

MaPLE (Magnetohydrodynamic PbLi Experiment) is a facility to investigate, understand and predict multiple MHD effects and interactions of eutectic lead-lithium (PbLi) flow with strong magnetic fields for fusion applications. The focus of future experiments is on free, forced and mixed convection flows with heat transfer. In particular, tests are foreseen for measuring techniques (pres-

sure, flow rate, electric potential) and investigations of heat transfer, with the aim of gaining in addition experience in long-term operation of a PbLi MHD facility. With MaPLE, MHD flows in heated test sections can be investigated for different orientations with respect to gravity and flexible orientations of the magnetic gap (horizontal, inclined, vertical) for various strengths of the magnetic field, different PbLi velocity and arbitrary heat flux.

MaPLE, has been built in the US at UCLA [6] and it was substantially upgraded with contributions from EUROfusion before it was decided to relocate the facility to the MEKKA laboratory of KIT. First parts arrived beginning 2021. The reconstruction of the facility is in progress and shall be finished in October 2022. After commissioning, MaPLE will extend significantly the experimental capabilities in the MEKKA laboratory.

The MaPLE facility consists of two major components, a large magnet and a PbLi loop, which can be seen in Figure 14.

*Magnet:* A 20-ton electromagnet capable to produce a uniform magnetic field of up to 1.8 T in a  $80 \times 15 \times 15 \text{ cm}^3$  volume. The magnet is mounted on a hydraulic positioning frame and can be lifted up to 2 m in vertical direction. For magneto-convection experiments, the magnet can be rotated by  $\pm 90^\circ$  around its horizontal axis.

*PbLi loop:* It can operate at up to  $500^\circ\text{C}$ . It is equipped with a 70 kW heat rejection system (air-cooler), a high efficiency EM pump with a maximum pressure head of 6 bars, flow meter, expansion vessel, storage tank, and a vacuum box, which contains the test section. The entire loop sits on a translation cart on rails so the loop can be moved in and out of the magnet gap. The liquid metal loop has been designed to be easily reconfigured and to allow tilting a test article to any angle between 0 and 90 degrees.

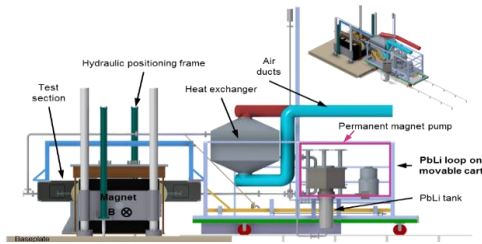


Figure 14 MaPLE facility with liquid metal PbLi loop and magnet.

Prior to relocating the MaPLE facility to KIT the MEKKA laboratory had been reorganized and prepared to accommodate the new facility. One action was the dismantling and removal of the superconducting solenoid magnet CELLO that is no longer needed.



Figure 15 The CELLO magnet still visible in the red frame has been removed.

In order to provide electricity to the MaPLE magnet, the existing power supply had been extended by new power switches, and a new transformer, transductor and rectifier for the MaPLE magnet were installed. A view into the new electrical building is shown in Figure 16.



Figure 16 Upgraded power supply (transformers, rectifiers, power switches) for MEKKA and MaPLE in new building.

The magnets for MEKKA and MaPLE are resistive magnets that need to be water-cooled during operation to remove up to 500 kW of power dissipated in their copper coils. The available chilled-water circuit was upgraded. The pumps and the heat exchanger were moved into a more suitable room and a tap-water separator and 2 booster pumps were added on the primary side of the heat exchanger (see Figure 17). The control system for the cooling circuit and magnet control was completely updated and it allows now control of both magnets for MEKKA and MaPLE.



Figure 17 Pumps for water cooling circuits for MEKKA and MaPLE magnets at new location.

The stream of fresh air for MaPLE heat-rejection system is provided by an air-blower. Penetrations through the building walls for

intake and exhaust, and noise silencers have been installed to meet regulations.



Figure 18 Air-blower fitted with new noise silencer and building lead-trough.

*Status of MaPLE reconstruction:* The MaPLE magnet has been installed and mechanically and hydraulically connected with the lifting/ tilting system. The water circuit is connected with the main water supply and the electric wiring finalized. The MaPLE magnet has been successfully commissioned and is ready for operation.



Figure 19 MaPLE magnet installed in the MEKKA building.

Further steps in commissioning MaPLE at KIT are modifications to meet EU standards in particular for all electrical systems. For future operation of the MaPLE loop with larger scaled mockups of blanket modules, it is required to extend the PbLi inventory. For this purpose, a large storage tank will be installed and the connection with the liquid metal loop will be achieved via a SPS-controlled safety valve.

First experiments for heat transfer in vertical and horizontal ducts are foreseen by the end of 2022 and WCLL related studies for MHD heat transfer at internal obstacles will start in 2023.

### Further work

In addition to the topics described above, the MHD group at ITES KIT contributed with scientific papers to blanket-relevant MHD topics [7, 8, 9, 10, 11].

### References

- [1] Mistrangelo, C., Bühler, L., Brinkmann, H.-J., Courtessole, C., Klüber, V. and Koehly, C.; "Magneto-convective flows around two differentially heated cylinders. Part I. Numerical simulations," *International Journal of Heat and Mass Transfer*, p. submitted, 2022.
- [2] Courtessole, C., Brinkmann, H.-J. and Bühler, L.; "Magneto-convective flows around two differentially heated cylinders. Part II Experiments," *International Journal of Heat and Mass Transfer*, p. Submitted, 2022.
- [3] Mistrangelo, C. and Bühler, L.; "Development of a numerical tool to simulate magnetohydrodynamic interactions of liquid metals with strong applied magnetic fields," *Fusion Science and Technology*, vol. 60, no. 2, pp. 798-803, 2011.

- [4] Molokov, S.; "Liquid metal flows in manifolds and expansions of insulating rectangular ducts in the plane perpendicular to a strong magnetic field," Tech. Report Kernforschungszentrum Karlsruhe, KfK 5272, 1994.
- [5] Miyazaki, K., Konishi, K. and Inoue, S.; "MHD pressure prop of liquid metal flow in circular duct under variable transverse magnetic field," *Journal of Nuclear Science and Technology*, vol. 28, no. 2, pp. 159-161, 1991.
- [6] Smolentsev, S., Li, F.-C., Morley, N., Ueki, Y., Abdou, M. and Sketchley, T.; "Construction and initial operation of MHD PbLi facility at UCLA," *Fusion Engineering and Design*, vol. 88, pp. 317-326, 2013.
- [7] Bühler, L., Lyu, B., Brinkmann, H.-J. and Mistrangelo, C.; "Reconstruction of 3D MHD liquid metal velocity from measurements of electric potential on the external surface of a thick-walled pipe," *Fusion Engineering and Design*, vol. 168, p. 112590, 2021.
- [8] Mistrangelo, C., Bühler, L., Koehly, C. and Rikapito, I.; "Magnetohydrodynamic velocity and pressure drop in WCLL TBM," in *Proceedings of the 28th IAEA Fusion Energy Conference*, May 10-15, Virtual, 2021.
- [9] Mistrangelo, C., Bühler, L., Koehly, C. and Rikapito, I.; "Magnetohydrodynamic velocity and pressure drop in manifolds of a WCLL TBM," *Nuclear Fusion*, vol. 61, p. 096037, 2021.
- [10] Mistrangelo, C., Bühler, L., Smolentsev, S., Klüber, V., Maione, I. and Aubert, J.; "MHD flow in liquid metal blankets: major design issues, MHD guidelines and numerical analysis," *Fusion Engineering and Design*, vol. 173, p. 112795, 2021.
- [11] Mistrangelo, C., Bühler, L., Alberghi, C., Bassini, S., Candido, L., Courtessole, C., Tassone, A., Ugorri, F. R. and Zikanov, O.; "MHD R&D activities for liquid metal blankets," *Energies*, vol. 14, p. 6640, 2021.



Group: Severe Accident Research

## SAR/ITES research activities in 2021

*B. Fluhrer, X. Gaus-Liu, T. Cron, R. Stängle, Th. Wenz and M. Vervoortz*

In 2021, the research activities of ITES/SAR were mainly focused on tasks within the EU HORIZON 2020 ESFR-SMART project. One of the aim of this European project is to improve the understanding and to provide quantitative estimation on the heat transfer of corium after relocation to an in-vessel core catcher in a Sodium Fast Reactor (SFR) to ensure the safety criteria in the long term.

In-vessel core catcher is one safety design feature of European type Sodium-Cooled Fast Reactor (ESFR) to guarantee the reactor integrity during a postulated core-melt accident. The core catcher has the function to collect the relocated melt derived from the upper core area and to prevent the recriticality in the core. The thermodynamics of the melt with decay heat and its heat transfer at the core catcher boundaries are studied experimentally at KIT by the SAR group and numerically at CEA, France.

The work was focused on the finalization of the construction of the new LIVE facility ESFR-LIVE and the performance and analysis of experiments in this new test facility, which is a 3-dimensional model of a core catcher of a SFR in a diameter scale 1:10. The lower part of the vessel is a truncated cone and the upper part is a cylinder with 1 m in diameter. The height of the truncated cone is 0.08 m, and the polar angle of the inclined wall is 20°, corresponding to 1:1 scale of the prototype geometry. The whole height of the test vessel inner cavity is 0.38 m. The cooling of liquid Na at all boundaries is simulated by a water cooling channel enclosing the test vessel and a cooling lid at the upper surface of the simulated core melt. Four planes of resistance heaters with a total power of up to 86 kW simulate the decay

power. The heaters are individually controllable and the two upper heating planes can be removed individually to enable the variation of the height of the core melt and the shapes of the melt pool. The distribution of bulk temperature, boundary temperature, wall temperatures and heat flux can be measured or determined. The simulant of core melt is the eutectic  $\text{NaNO}_3\text{-KNO}_3$  mixture, which is representative for the character of the general liquid oxide melt. With the similar pool height as in the prototypical core catcher, the EFSR-LIVE facility can well capture the dimensionless heat transfer features, e.g. Ra and Nu.

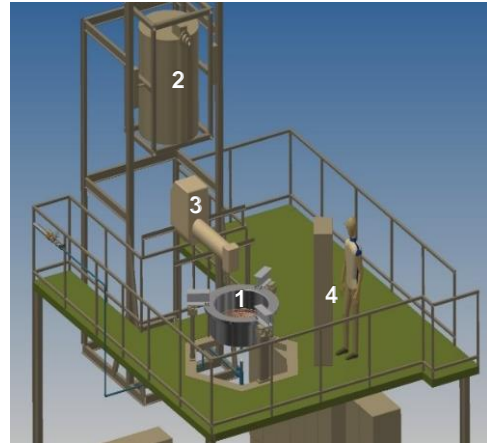


Fig.1. LIVE experimental platform with ESFR-LIVE facility. 1- ESFR test vessel, 2 - heating furnace for melt preparation, 3 - pouring spout, 4 - instrumentation board.

Two test series, LIVE-CC1 and LIVE-CC2, have been carried out in August and September 2021 respectively.

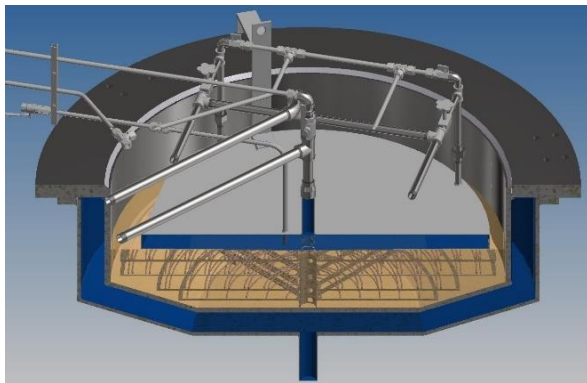


Fig.2. ESFR-LIVE test vessel with all boundary cooling systems.

In LIVE-CC1, the pool height was above the highest heater. In three different test phases, the lower part of the melt pool geometry have been varied by shutdown the lowest heating planes and the second lowest heating plane subsequently. The liquid melt below the operating heaters was solidified due to the bottom cooling and very low downward heat transfer rate. Therefore, the liquid pool height in the truncated cone varied from 80 mm to 50 mm to 0 mm. Several power levels have been performed for each test phase with different pool geometry to obtain the heat transfer characteristics under a large range of Ra numbers and heat flux. In all test phases, all boundaries were cooled (wall and top surface).

In LIVE-CC2, the melt was only filled in the truncated cone part. Therefore, the upper two heating planes have been removed to enable the cooling lid at a lower position. Two different test phases have been performed: in the first test phase, only the upper heating plane was switched on and in the second test phase both heating planes were in operation. For both test phases, several heating power level have been realized. In all test phases, all boundaries were cooled except for the last heating phase in which the cooling lid has been removed and an insulation lid has been placed on the top of the test vessel.

In the following two figures, the thermal balances of the two test series are shown. The heating power dissipated in the melt was transferred through the top surface and the test vessel wall boundaries and was removed by the cooling water. The heat transfer by the cooling lid ( $Q_{lid}$ ) is nearly twice as high as the heat transfer by the external cooling of the test vessel ( $Q_{wall}/Q_{ext}$ ) in LIVE-CC1. In LIVE-CC2, the heat transfer by the cooling lid is even higher than in LIVE-CC1. Therefore, a high efficiency of upper surface cooling was observed.

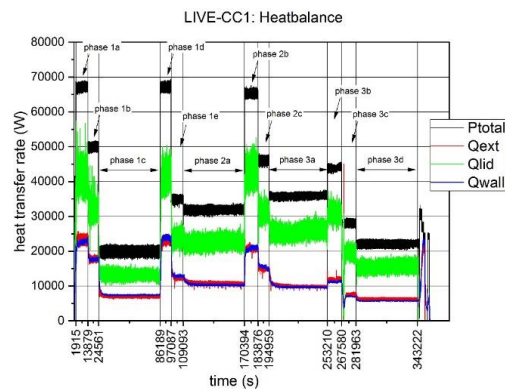


Fig. 3. Thermal balance of LIVE-CC1.

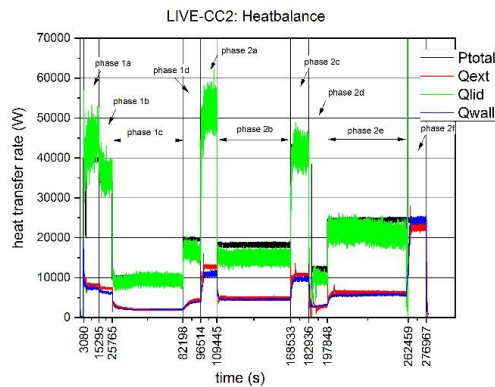


Fig. 4. Thermal balance of LIVE-CC2.

The heat fluxes at steady state over the vessel height are shown in the next two figures. The heat fluxes at the bottom are very low and are increasing along the vessel wall height. The last heat flux values are the heat fluxes through the cooling lid. The heat flux

at the cylindrical wall is about half of the heat flux at the top surface.

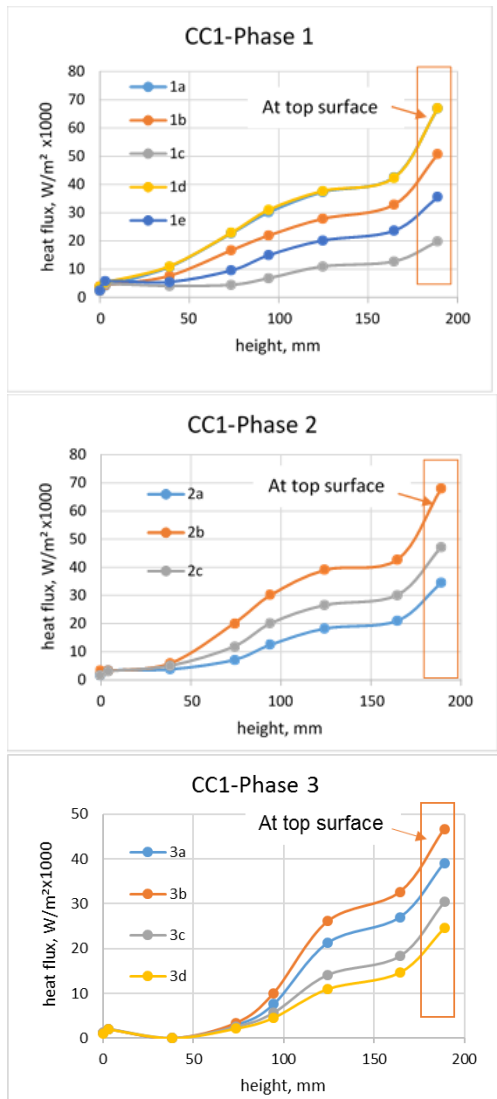


Fig. 5. Steady state heat fluxes for LIVE-CC1.

In LIVE-CC2 in test phase 2f, the cooling lid has been removed and the power input remained at the same power as in test phase 2e. The heat flux through the vessel wall is therefore increasing significantly and all the power input to the melt is transferred through the vessel wall to the external cooling water.

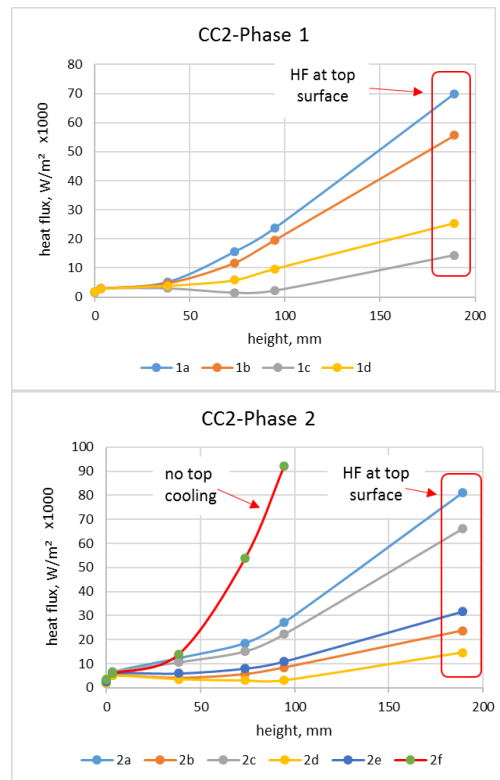


Fig. 6. Steady state heat fluxes for LIVE-CC2.

One main conclusion from the LIVE-CC1 and LIVE-CC2 test series is that the cooling at the melt upper surface can immensely relieve the thermal load on the core catcher sidewall.

Further analytical analysis including calculation of Nu and Rayleigh numbers is done at KIT and numerical calculations are performed by CEA.

### Some Publications

- [1] Gaus-Liu, X., Cron, T., Fluhrer, B., Wenz, T., "Experimental study and analytical analysis on the global heat transfer of stratified corium in LWR lower head", Nuclear Engineering and Design, 372, 2021
- [2] Fluhrer, B., Gaus-Liu, X., Cron, T., Stängle, R., Vervoortz, M., Wenz, T., "LIVE-BWR Experiments to Study the Effect of

CRGT Cooling on In-Vessel Melt Retention Strategy”, 19th International Topical Meeting on Nuclear Reactor Thermal Hydraulics (NURETH-19), Brussels, Belgium, March 6 - 11, 2022

[3] Gaus-Liu, X., Cron, T., Bottomley, D., Fluhrer, B., “MCCI on Siliceous and LCS Concrete with Oxide and Metallic Melt: Re-Evaluation of MOCKA Experiments”, 19th International Topical Meeting on Nuclear Reactor Thermal Hydraulics (NURETH-19), Brussels, Belgium, March 6 - 11, 2022

[4] Madokoro, H., Gaus-Liu, X., et.al., “LIVE-J1 Experiment on Debris Melting Behavior Toward Understanding Late In-Vessel Accident Progression of the Fukushima Daiichi Nuclear Power Station”, 19th International Topical Meeting on Nuclear Reactor Thermal Hydraulics (NURETH-19), Brussels, Belgium, March 6 - 11, 2022

[5] Gaus-Liu, X., Bigot, B., Journeau, C., Payot, F., Cron, T., Clavier, R., Peybernes, M., Angeli, P. E., Fluhrer, B., “Experiment and Numerical Simulations on SFR Core-catcher Safety Analysis after Relocation of Corium”, CN291-IC336, #FR22, International Conference on Fast Reactors and Related Fuel Cycles Fr22: Sustainable Clean Energy for the Future (CN-291), 25-28 April 2022, Beijing, China.

[6] Tromm, W., Gaus-Liu, X., “KIT-JMEC Experiments to Investigate Jet Impingement on the Ablation of Core Catcher Bottom”, 30th International Conference Nuclear Energy for New Europe (NENE 2021), Veldes, Slowenien, 06.09.2021 – 09.09.2021

Group: Multiphase Flow

## **Multiphase flows with heat transfer- subcooled boiling water flows up to boiling crisis**

*Stephan Gabriel, Giancarlo Albrecht, Wilson Heiler, Felix Heineken, Stelios Michaelides (IATF)*

### **Introduction**

Two-phase flows with heat transfer are used in numerous technical systems of power engineering, they also occur in other fields of technology. By using evaporation and condensation in heat transfer, very high heat flux can be realized. Applications are found in reactor technology but also in water-cooled systems of fusion power plants. They are also conceivable, for example, in solar thermal power plants with direct evaporation.

The complex physical processes in the two-phase flows during flow boiling up to the boiling crisis are still challenging. Instabilities and the strong dependencies of the main influencing variables pressure, temperature (inlet subcooling), mass flow and heat exchanger geometry and material on the transferable heat output offer room for innovative research projects.

In 2021, the main activities of the multiphase flow group focused on experimental research work within the framework of the McSAFER (EU) and KEK/SIMA (GRS) projects. In McSAFER, essential steps were completed at the high-pressure circuit COSMOS-H to set up the test section and the test facility. At the low-pressure circuit COSMOS-L, several test series were carried out in cooperation with the Institute of Applied Thermofluidics (IATF) as part of the KEK/SIMA project. In addition, to modernize the 428 pilot plant building used by the group, a current model replaced the building's overhead crane, which has now reached the end of its life cycle.

### **COSMOS-L**

At the low-pressure test facility COSMOS-L, the group has already been collaborating with the IATF in the KEK/SIMA project since spring 2019 on experiments to investigate critical heat flux density under periodically fluctuating mass flows. Scenarios like these are relevant in emergency systems for in vessel retention (IVR) by external reactor vessel cooling (ERVIC). In the previous years, an optically accessible test section densely instrumented with thermocouples was designed with a powerful planar heater and was already commissioned at the end of 2020. In 2021, extensive measurements were carried out with variation of the following key parameters [2, 3]:

- Pressure
- Fluid temperature respectively inlet subcooling
- Mass flow (constant, periodically fluctuating with amplitude and period time)
- Test section orientation (0° vertical, 45°, 90° horizontal)

Figure 1 shows the test section with flexible power supply and tilting mechanism. A measurement matrix with 14 different measurement points in total was created. The tests with horizontal test section were started in 2021 and are expected to be completed in the first quarter of 2022.

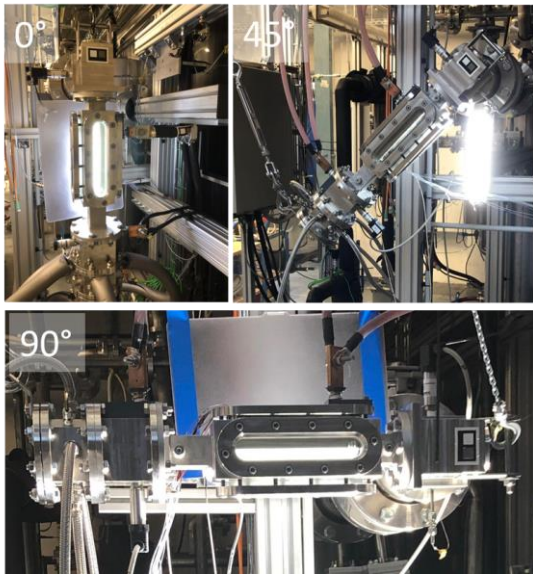


Figure 1: Test track with swivel mechanism in three different angles of attack

The results of the test series at  $0^\circ$  and  $45^\circ$  as well as the first results of the tests at  $90^\circ$  show a strong dependence of the flow morphology and the critical power on the inclination of the heater. It can be seen that the buoyancy force acting on the steam bubbles has a significant influence. It is directed at the heater at  $45^\circ$  and  $90^\circ$  and leads to an increase of the void at the heater with increasing inclination angle and reduces the critical thermal power considerably.

In the next step, additional measurements were performed at periodically oscillating mass flows of different period durations and amplitudes as expected in an IVR-EVC scenario. The mass flow was thereby set into a sinusoidal oscillation by the high-speed valves upstream of the test section and test section bypass. The period  $T$  was chosen at 10 s and 50 s. The oscillation amplitude was 30 % and 70 %. It turns out that the critical thermal power at several measuring points - not at all measuring points, as initially expected - is lower than at constant mass flow. As Figure 2 shows, with an average mass flow of  $400 \text{ kg/m}^2\text{s}$ , an amplitude of  $\pm 30\%$  and a period of 50 s, the critical heat flow of the reference point was exceeded even without oscillation. The evaluation of the

tests shows that there is a significant dependence on the inlet subcooling even after considering all measurement uncertainties.

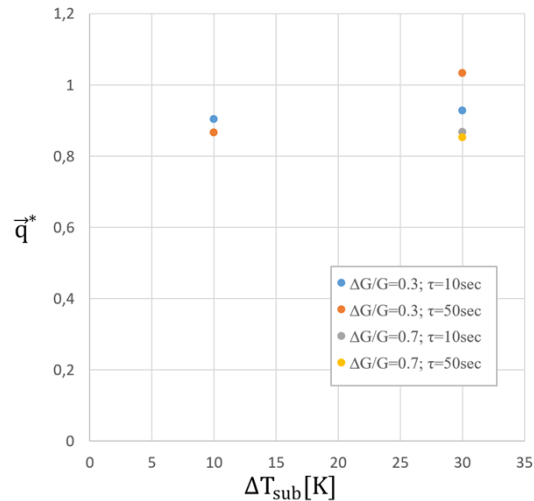


Figure 2: Dimensionless critical heat flux as a function of Inlet Sub-Cooling ( $G = 400 \frac{\text{kg}}{\text{m}^2\text{s}}$ ,  $\theta = 45^\circ$ ).

Initially, it would be expected intuitively that the boiling crisis occurs exactly at the minimum for a decreasing mass flow. In fact, however, the measurements shown indicate that the critical heat flux density can even increase at higher inlet subcooling, since the heat transport at the high point of the mass flow oscillation cools the heater so intensively that the thermal inertia of the heater at the minimum is sufficient to prevent a boiling crisis from occurring.

In addition to the measurements of the boundary conditions and the temperature and pressure distribution in the test section, high-speed recordings of the flow were made at all measurement points. The recordings taken at 3 kfps were triggered to capture the heater approximately 2.5 seconds before and 0.5 seconds after boiling crisis. As Figure 3 exemplifies, the boiling crisis could thus be observed in the form of a bubble or vapor film permanently standing at the surface. The temperature excursion at the temperature measuring site T6 (vertical position of the measuring site is

marked in the figure) clearly confirms the connection between the emerging film boiling of this site and the upcoming boiling crisis.

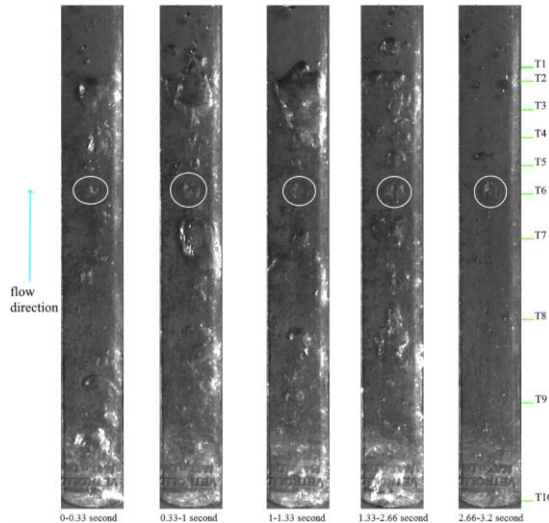


Figure 3: Optical observations of the boiling crisis at  $G = 185 \frac{\text{kg}}{\text{m}^2\text{s}}$ ,  $\Delta T_{\text{sub}} = 45 \text{ K}$ ,  $p = 1200 \text{ mbar}$

At the end of 2021, the BMWi project MESA was acquired together with the Framatome Professional School (FPS) group, in which the behavior of accident tolerant fuels materials (ATF) [5] such as Crome Coatet Zircaloy, FECRAL and ceramic materials are to be investigated in normal operation up to boiling point. The project will start in 2022 and includes experiments with a new rod bundle test section at COSMOS-L as well as CFD calculations.

### COSMOS-H

In the EU project McSAFER [4], the measurement matrix was created in 2020 and a corresponding test track was designed to investigate the thermohydraulic behavior of several selected concepts of small modular reactors (SMR) [1]. In 2021, the test setup was started and the adaptation of the facility to the test section was planned and already mostly implemented.

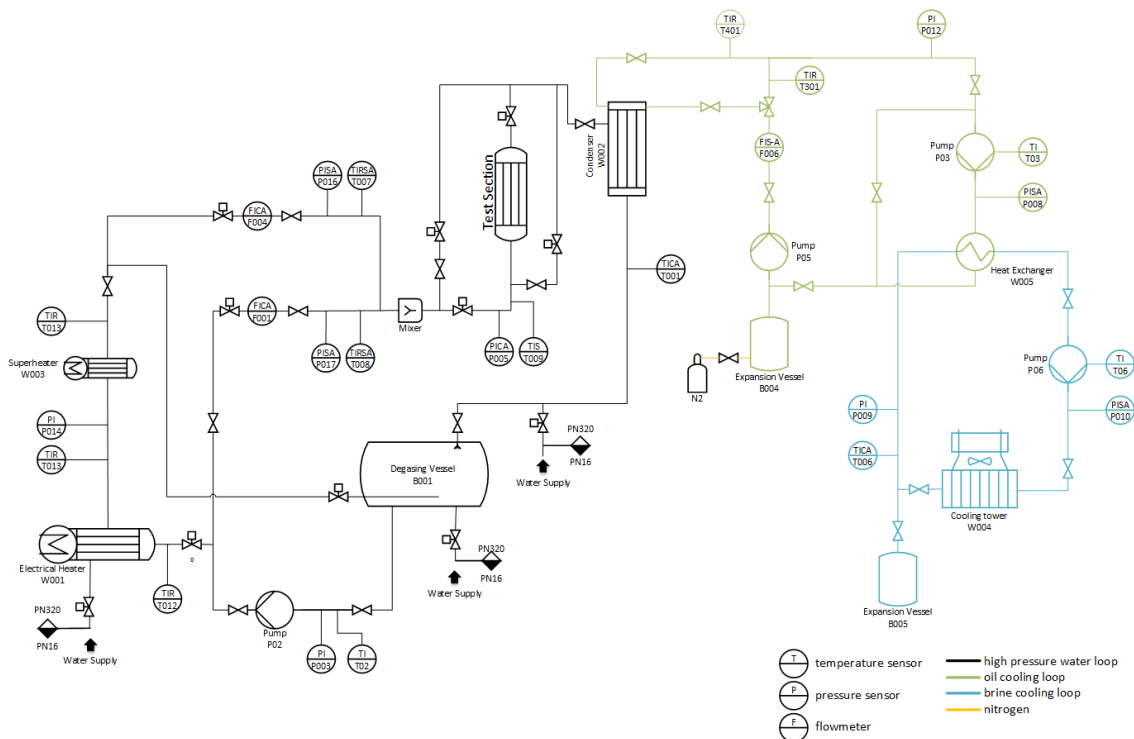


Figure 4: Simplified P&ID of COSMOS-H

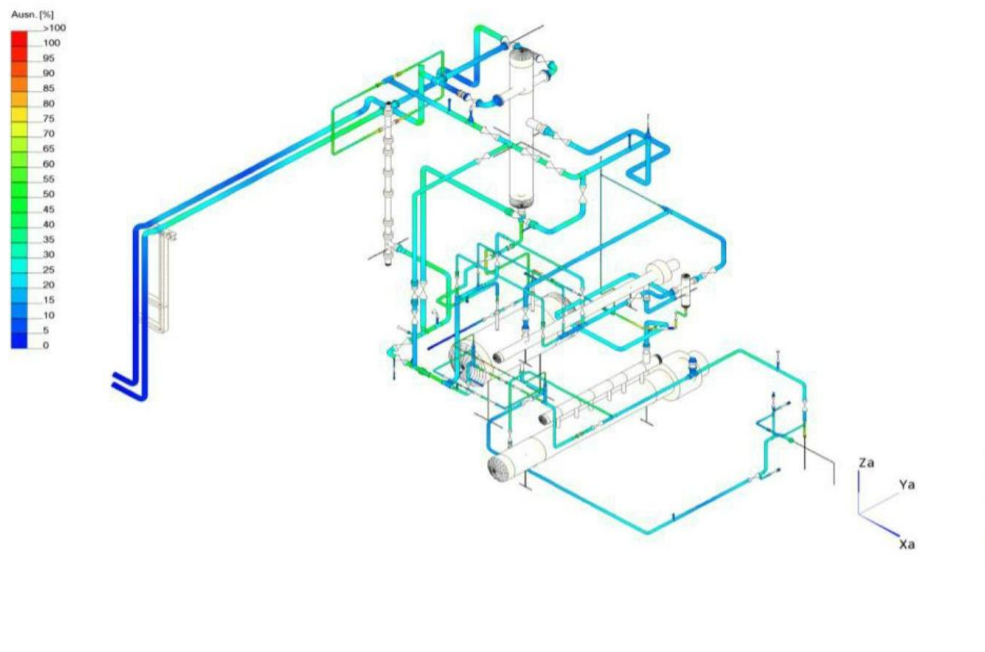


Figure 5: 3D isometry with maximum mechanical load in operation

As an important step, equipment and piping construction in the high-pressure loop were completed in 2021. This also includes the steel construction and the complex mounting of piping and equipment. Prior to this, in cooperation with an engineering firm specializing in thermal-mechanical load analyses, proof had been provided that the plant could withstand the loads occurring in trial operation with the required number of cycles and transients. In addition to processes such as startup and shutdown, this also includes the experiments planned for McSAFER to determine the critical heat flow density under conditions typical of SMR. As the necessary verifications were available, steel construction, piping construction and pipe supports were realized by the end of the year. Now all circuits of the plant are mechanically completed. The legally required acceptance tests, instrumentation, thermal insulation and (after approval) commissioning of the plant will follow in 2022.

After the test loop had been adapted to all project requirements, the test section and the multi-stage safety system required for it were also completed, including the external control

room. For the first time, the pressure hull of the test section was completely assembled and installed in the plant.

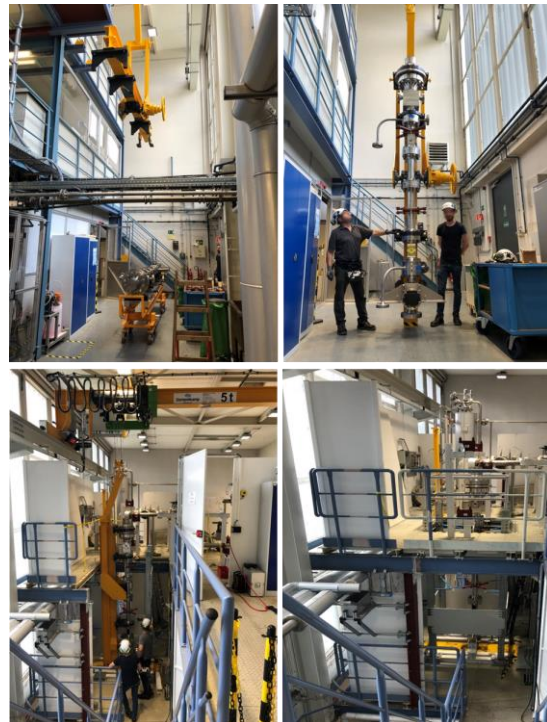


Figure 6: First test section moc-up for McSAFER

Due to the central importance of the high pressure sight glasses for the instrumentation of the test section for McSAFER, testing of the high pressure sight glasses was started in 2021. For this purpose, an improvised small-scale test rig consisting of a heated pressure vessel with safety equipment and redundant pressure and temperature sensors was installed. The vessel has a volume of about 2.5 liters. It can be operated up to a pressure of 17 MPa and a temperature of 360°C. The small-scale facility also has a safety system based on the COSMOS-H system.

In preparation for the McSAFER tests, commercially available sight glasses were first tested. It was found that they could not withstand the pressure, temperature and transient requirements imposed during the experiments. As a result, a new 25 mm sight glass was designed and extensively tested. So far, this design has shown no failures in testing and will be usable in experimental operation at least up to 10 MPa and 310°C. Further testing in 2022 will show whether the sight glass can also be used under higher pressure and temperature conditions.



Figure 7: Previous (left) and new (right) high-pressure sight glass for the COSMOS-H test section.

## Outlook

In the upcoming year, the experimental work on the KEK/SIMA project will be largely completed. Afterwards, the group will start together with the ITES group FPS the 2021 jointly acquired project KEK/MESA. The project involves experimental and simulative investigation of ATF cladding materials in normal operation. The experiments will be carried out at the low-pressure test facility COSMOS-L and the simulations will be supervised by FPS.

At the COSMOS-H test facility, the final construction phases, such as the installation of the external measuring station, will be completed in 2022. The plant itself will undergo the prescribed tests prior to commissioning, approval and instrumentation. Once commissioning is completed, the first tests on the facility are planned as part of the McSAFER project.

## Acknowledgements

We would like to thank Prof. Xu Cheng for the fruitful cooperation in the project KEK-SIMA (FKZ1501577). Furthermore, we would like to thank Victor Sanchez for his support and the good cooperation in Project McSAFER (GA No 945063). We are looking forward to future cooperation with Framatome Professional School in the KEK/MESA project.

## References

- [1] Reitsma, F., Subki, M.H., Luque-Gutierrez, J.C., Bouchet, S.; Advances in Small Modular Reactor Technology Developments, A Supplement to: IAEA Advanced Reactors Information System (ARIS) 2020 Edition; <http://aris.iaea.org>
- [2] Kaiser, F., Gabriel, S., Albrecht, G.; Investigation of the Critical Heat Flux in an Annular Gap and a Rod Bundle Configuration under low Pressure Conditions. ProcessNet-Fachgruppe Wärme- und Stoffübertragung, Bruchsal, 16.-17. Februar 2017
- [3] Kaiser, F.; Dietrich, B.; Gabriel, S.; Wetzel, T.: Experimentelle Ermittlung von kritischen Wärmestromdichten bei reaktortypischen Bedingungen als Validierungsdaten, Final Report Project NUBEKS (BMW 1501473B, 27.02.2019)
- [4] Sanchez-Espinoza, V.H.; Gabriel, S.; Suikkanen, H.; Telkkä, J.; Valtavirta, V.; Benčík, M.; Kliem, S.; Qeral, C.; Farda, A.;

Abéguié, F.; Smith, P.; Uffelen, P.V.; Ammirabile, L.; Seidl, M.; Schneidesch, C.; Grishchenko, D.; Lestani, H.; The H2020 McSAFER Project: Main Goals, Technical Work Program, and Status. *Energies* 2021, 14, 6348. <https://doi.org/10.3390/en14196348>

[5] INTERNATIONAL ATOMIC ENERGY AGENCY, Accident Tolerant Fuel Concepts for Light Water Reactors, IAEA-TECDOC-1797, IAEA, Vienna (2016)

[6] Michaelides, S., Cheng, X., Heiler, W., Gabriel, S. LOW PRESSURE, HIGH FLOW BOILING CRISIS EXPERIMENTS IN A RECTANGULAR CHANNEL UNDER OSCILLATING MASS FLUX (NURETH-19) Log nr.: 36358 Brussels, Belgium, March 6 - 11, 2022

Group: Karlsruhe Liquid metal Laboratory (KALLA)

## Liquid Metal Technology for Energy Conversion, Storage and Process Technology

*Markus Daubner, Benjamin Dietrich, Ines Duran, Frank Fellmoser, Christoph Hofberger, Marta Kamienowska, Ralf Krumholz, Tim Laube, Karsten Litfin, Martin Lux, Franziska Müller-Trefzer, Klarissa Niedermeier, Leonid Stoppel, Neele Uhlenbruck, Thomas Wetzel, Kurt Wittemann*

### Introduction KALLA

Research at Karlsruhe Liquid Metal Laboratory (KALLA) follows a strategic approach, focused on three main areas: 1) Thermal fluid dynamics of liquid metals, 2) Liquid metal based thermal storage and 3) Liquid metal based process technology.

The common foundations of all our work lie in combining experimental and modelling approaches and in the long standing liquid metal engineering experience at KALLA. Again we were able to add another exciting year to this. Our loop facilities, reactor setups, instrumentation, components as well as process control and data acquisition systems define the state of the art in liquid metal technology in our international environment and community.

Based on this, we try to provide advancement in the scientific foundations of liquid metal technology and support innovation in our focus areas. High temperature heat storage is a key technology for a post-fossil industrial society. High temperature processes are a complementary step to storage, but their innovative power goes far beyond. Direct dehydrogenation of methanol and direct thermal decomposition of methane for example, are long known, yet never industrially realized processes with huge potential benefit compared to their established counterparts. Liquid metal technology is now acting as an enabler to their further development. The intense and still increasing interest by several major industrial partners as well as startup companies in cooperating with us in these areas are encouraging.

Fundamental scientific contributions to heat transfer in tubes and tube bundles with complex thermal boundary conditions and geometric details have again been achieved in sophisticated experiments. Unique data sets, correlations and considerations will be and have been brought to the community by contributions journals and conferences. We remain grateful for the exciting and strong partnership with our research partners across Europe and worldwide.

All our work aims at enabling technologies and new ideas for the energy transition and the fight against global warming, with their challenges not only for the energy sector, but for chemistry, transport and the society as a whole. We look forward to working with YOU in future, so if you find an interesting point on the next pages, do not hesitate to get in touch.

### Thermal fluid dynamics of liquid metals

#### GALINKA

In a current DFG project (WE 4672/4-1), the influence of an azimuthally inhomogeneous thermal boundary condition on the heat transfer in a turbulent liquid metal tube flow is under investigation. This type of boundary condition can be found in concentrating solar power plants. For this purpose, a test section was developed to realize either an azimuthally homogeneous (OH) or inhomogeneous (IH) heat flux distribution, i.e. heating over half of the circumference of the tube. The experimental setup is

explained more in detail in the work of Laube et al. [1].

The experimental data for the azimuthally averaged Nusselt number  $\langle Nu \rangle$  as a function of the Péclet number  $Pe$  for both boundary conditions are given on the left side of Figure 1. The data show no significant influence of the boundary condition on  $\langle Nu \rangle$  and correspond well with the correlation by Skupinski et al. [2], developed for turbulent liquid metal tube flows.

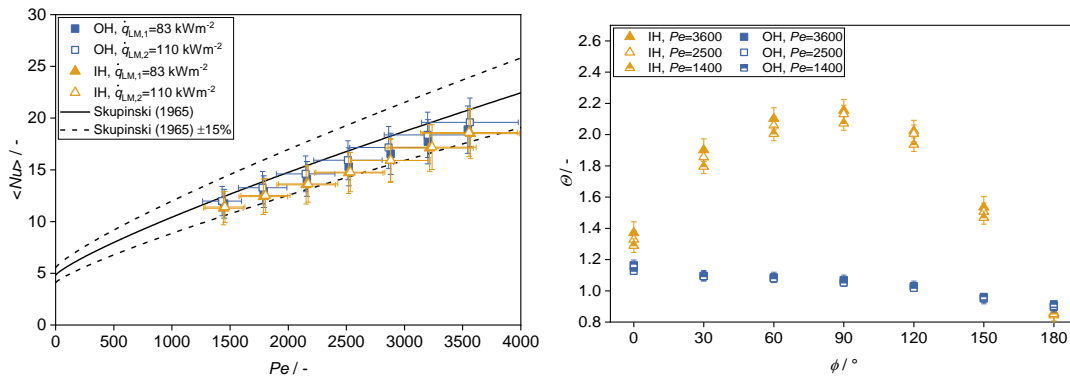


Figure 1:  $\langle Nu \rangle$  vs.  $Pe$  for a liquid metal flow for OH and IH [1] (left),  $\theta$  on the heated side of the tube wall as function of angular position  $\phi$  for OH and IH at different  $Pe$  [1] (right).

In order to study the temperature distribution of the tube wall for both boundary conditions, a non-dimensional temperature,

$$\theta = \frac{T_w(\phi) - T_b}{\langle T_w(\phi) \rangle - T_b},$$

is used.  $\theta$  corresponds to the local excess temperature of the tube wall over the mean value. The distribution of  $\theta$  on the heated arc of the tube wall as a function of the angular position  $\phi$  for different  $Pe$  is given on the right side of Figure for OH and IH. For the homogeneous heated case (OH)  $\theta$  is close to unity, as it was expected. For the azimuthally inhomogeneously heated case (IH)  $\theta > 1$  and increases for higher  $Pe$ . Therefore, the local excess to the mean temperature of the tube wall increases for higher values of the convective heat transfer coefficient.

### Fuel assembly experiments in Heavy liquid metal flows

For the design and operation of modern nuclear reactors like the research reactor MYRRHA (Multi-purpose hYbrid Research Reactor for High-tech Applications) or Gen IV reactors, heavy liquid metal is one of the proposed coolants. For the reliable operation of a fuel assembly in the reactor core, the knowledge of the heat transfer to the coolant is essential. Moreover, during the lifecycle of the assembly its geometry can be deformed by

swelling, creeping and mechanical defects or blocked by debris. As a consequence, locally reduced cooling and hot spots are expected.

A set of two different experiments and accompanying CFD is planned in support of safety studies for heavy liquid metal cooled fast reactor systems in the EU-Projects PATRICIA (Partitioning And Transmuter Research Initiative in a Collaborative Innovation Action) and PASCAL (Proof of Augmented Safety Conditions in Advanced Liquid-metal-cooled systems) which were launched in 2020.

In a first study, the effect of a well-defined porous blockage in a wire spaced 19-pin rod bundle will be investigated. Following the EU-Project MAXSIMA [3-6], where a total blockage has been studied experimentally and numerically, the effect of a more realistic sintered blockage with well-defined porosity will be investigated in PATRICIA. A detailed blockage

made of  $ZrO_2$  has been designed and constructed by means of 3d-printing and will be inserted into the rod bundle and investigated in the THEADES LBE loop of KALLA. Detailed instrumentation will give insights about local hot spots as well as recirculation patterns, which will be used for the validation of numerical models in house by the Framatome Professional School (FPS) Group of the ITES and external partners in the framework of the EU-project.

In a second experimental study, the effect of deformations in a rod bundle on the local flow and temperature field in a wire spaced 7-pin rod bundle will be studied. The rod bundle contains a rotating central rod and bendable outer pins to simulate wire displacement and bended rods in a rod bundle. This experiment will be performed in the THESYS LBE loop of KALLA.

In the framework of EU-Project PASCAL, a water rod bundle experiment is under construction at the Karman Institute for Fluid Dynamics (VKI), Brussels. The detailed design of the experiment and the blockage is supported by KALLA team and post experimental CFD will be performed by FPS.

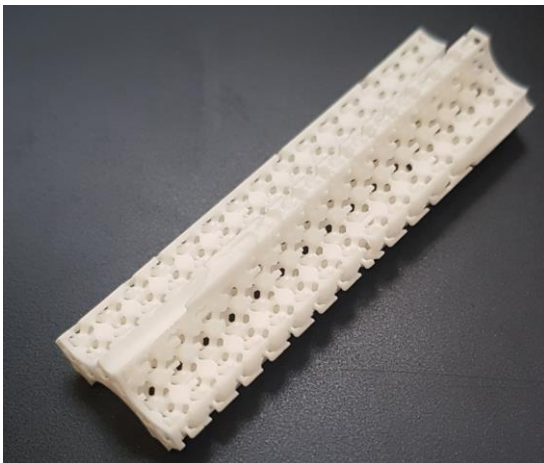


Figure 2: Blockage element with well-defined porosity made of 3d printed  $ZrO_2$ .

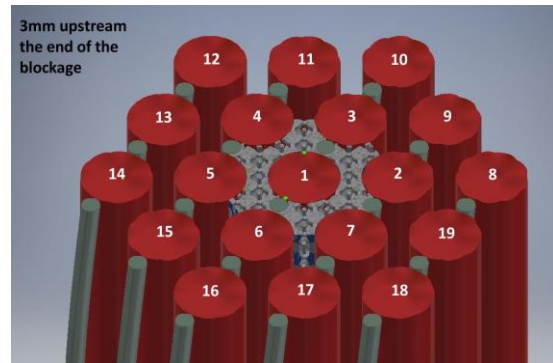


Figure 3: Placement of the blockage in the rod bundle.

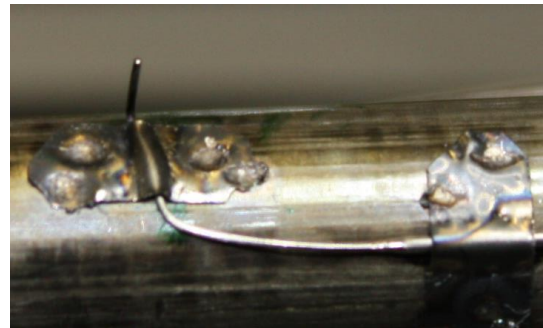


Figure 4: Instrumentation of one sub-channel with a 0.5mm Thermocouple (rod diameter is 8.2mm).

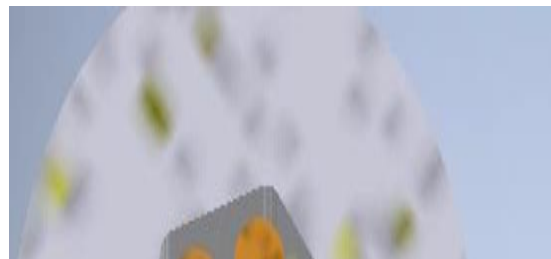


Figure 5: Construction detail for the planned rod bundle deformation experiment in EU-Project PATRICIA.

## Liquid metal based thermal energy storage

### Lab to Pilot Scaling of Dual-Media Storage

Liquid metals have been proposed as heat transfer fluids in thermal energy storage systems because of their high operating temperature range and their excellent heat transfer capabilities [7]. A dual-media configuration with filler material has been proposed and numerically analysed [8,9]. In 2020 and 2021, a lab-scale storage system (VESPA) with a thermal storage capacity of 1 kWh was successfully demonstrated [10].

The lab-scale (VESPA) experiments were run with liquid lead-bismuth eutectic as heat transfer fluid and spherical ceramic particles (zirconium silicate) as filler material at temperatures from 180°C to 380°C. The results showed that the stratification as well as the storage capacity in the tank and, thus, the performance of the storage system can be improved by using a solid filler compared with lead-bismuth eutectic only. Additionally, different modes of operation such as charging, discharging and standby, and varying mass flow and inlet temperature were tested [11].

Based on the results of the lab-scale experiment, a pilot-scale set-up (DUO-LIM) with a thermal storage capacity of 100 kWh is under construction. The dual-media storage will be inserted into one of the test sections of the THEADES loop at KALLA (Figure 6). As the lab-scale results showed that a constant and instantly high inlet temperature into the tank (during charging) is one of the crucial aspects for the temperature distribution in the tank, the inlet mixing region was designed with low liquid volume.

### **LIMELISA - Development of a High Temperature Liquid Metal Loop for Testing Future Process Engineering Key Components**

In the frame of the BMWK funded project LIMELISA a high temperature liquid lead loop will be designed, constructed and operated at the Karlsruhe Liquid Metal Laboratory (KALLA) at ITES [12]. The aim is to test future process engineering key components like valves and a radial pump provided by the company KSB. Needed vessels have to be designed, suitable

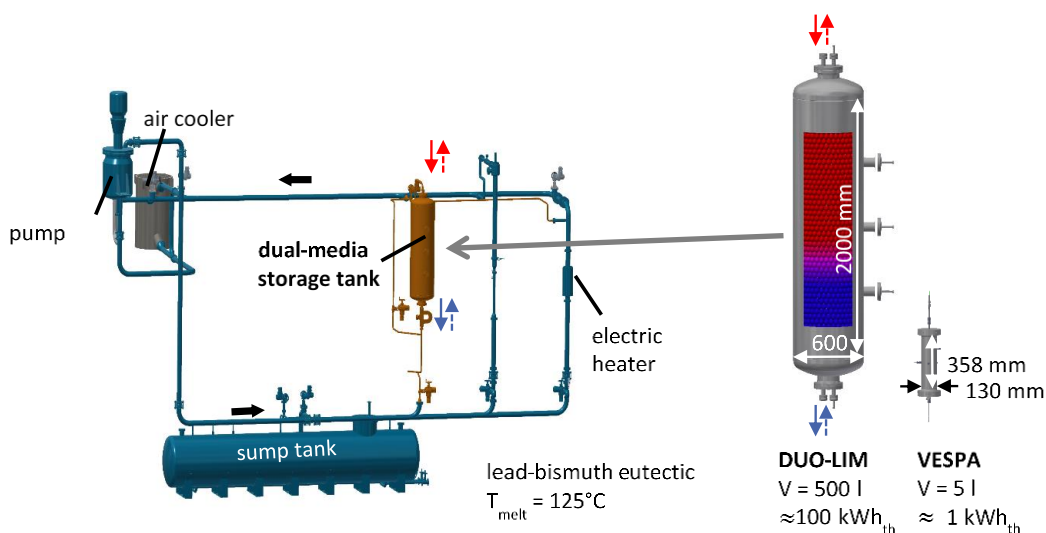


Figure 6: Left: Implementation of the DUO-LIM heat storage in the THEADES loop; right: comparison of the dimensions and thermal storage capacities of the planned DUO-LIM storage and the lab-scale experiment VESPA.

loop material selected, custom flange connections and gaskets calculated as well as respective measurement technique for pressure, pressure loss, flow, level, vibration and temperature defined and implemented in a process control system. The piping system of the high temperature liquid lead loop and the key components are wrapped by trace heating and covered by isolation material to be able to heat up the loop above the melting point of lead and to keep it in a liquid state. The components will be tested up to temperatures of 700°C. For the piping system, the material Alloy800H with an alumina protection layer will be used. The loop will have a connection to a vacuum system for filling the loop and an Argon cover gas system. For safety reasons the pipes are inclined so that in case of an emergency the molten lead can flow through the dedicated drain valve into the sump tank by gravity(Figure 7).

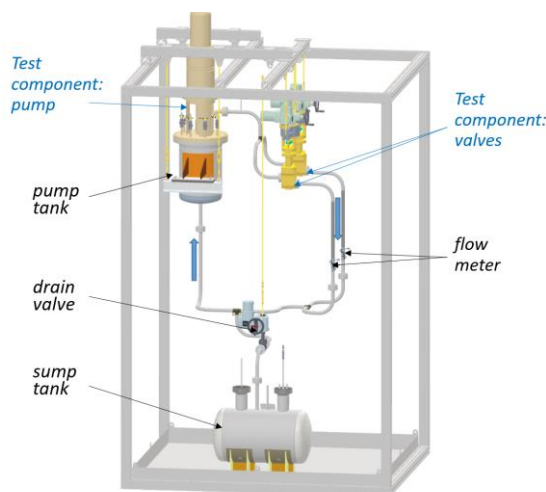


Figure 7: 3D layout of the high temperature liquid metal loop of LIMELISA.

## Liquid metal based process technology

### DECAGAS<sup>LM</sup> - Decarbonisation of nature gas in liquid metal

Hydrogen technology has significant potential to enable a successful energy transition. In June 2020, the German government adopted

the national hydrogen strategy [13]. These extensive measures and investment packages are intended to establish hydrogen as a predominant energy carrier in the foreseeable future.

Since 2012, intensive work has been carried out at KALLA on a continuously operable process for direct thermal methane pyrolysis as a viable process to produce hydrogen and solid carbon from methane and – perspective – biogas and natural gas. In the process, the extensive experience with liquid metals, established at KALLA, could be transferred into successful lab-scale experiments, which to date have repeatedly proven the possibility to reach high methane conversion rates and their dependency on operation parameters like temperature [14, 15].

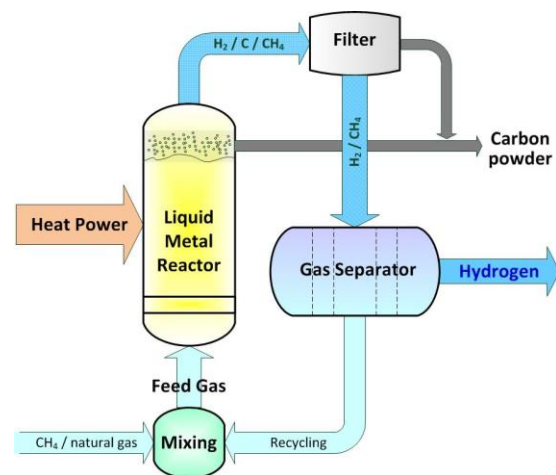


Figure 8: Process flow diagram of methane pyrolysis. [15]

Together with the industrial partner Wintershall Dea [16], the technique is now being further developed for the use on an industrial scale. The basis is the pyrolysis of methane in a liquid metal bubble column reactor (see Figure 8). In this process, methane gas is passed through liquid tin heated to a temperature of 950 °C to 1200 °C. Due to the temperature conditions, the methane is split into two components, solid powdered carbon and gaseous hydrogen.

Since the solid carbon has a much lower density than the liquid tin, it accumulates on the surface of the liquid metal and can be removed from the reactor. The gas phase, containing a mixture of hydrogen and unreacted methane, will be further processed according to the requirements of the final application. Unreacted methane and other hydrocarbons can be fed back into the reactor.

In the year 2021, pyrolysis experiments were prepared and carried out on both pure methane and real natural gas. At the same time, these experiments evaluated the performance of various technical solutions in reactor design. In parallel as part of this project, various materials and coatings were considered and investigated for use in the reactor.

### **MTET InnoPool Solar H<sub>2</sub>**

In the framework of the Innovationspool Project "Solar Hydrogen - Highly Pure and Compressed", an assessment of the use of solar energy to produce hydrogen by direct thermal pyrolysis of methane based on liquid metal technology is being conducted.

In a bubble column reactor filled with liquid tin, methane is split into its elementary components: hydrogen and solid carbon, so that no CO<sub>2</sub> is released in the process. To achieve technically relevant CH<sub>4</sub> conversion rates, temperatures of around 1000 °C are required. In order to make the process completely CO<sub>2</sub>-free, the necessary pyrolysis reaction heat could be provided by a renewable energy source such as solar thermal energy or electrical energy from photovoltaics.

The research carried out in 2021 during the initial phase of the project consisted of a thorough literature review of the state-of-the-art of solar reactors for the production of hydrogen from methane. The main advantages and limitations of different types of solar reactors were evaluated. In addition, the current status of Concentrated Solar Power (CSP) technology

as a possible renewable source of high-temperature heat was investigated.

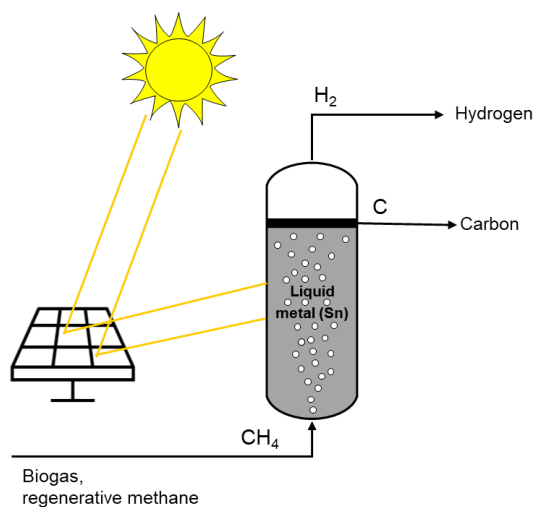


Figure 9: Concept of solar pyrolysis of regenerative methane/biogas to produce H<sub>2</sub> and carbon.

Future work will involve the development of the process concept of the solar heated reactor starting with the analysis of different scenarios. It is foreseen to comprise the elaboration of experimental, constructional and instrumentation plans of the laboratory test facility including safety aspects.

Another interesting topic to be theoretically analyzed is the effect of CO<sub>2</sub> on methane pyrolysis as a key factor in the use of biogas (a renewable energy source, mainly composed of methane and carbon dioxide) as a reactant. In addition, the influence of pressurized operation on system efficiency and the purity of the product obtained will be further investigated.

### **NAMOSYN - Anhydrous formaldehyde production with sodium vapours as the catalyst**

With the aim of reducing global warming to an acceptable level, emissions of the greenhouse gas carbon dioxide (CO<sub>2</sub>) must be significantly reduced worldwide. For that reason the

NAMOSYN (Nachhaltige Mobilität mit synthetischen Kraftstoffen) project funded by BMBF started in 2019 [17]. The project's primary goal is to develop and test eco-friendly synthetic fuels for diesel and petrol engines. Formaldehyde, one of the most important industrial chemicals, may be used as an intermediate to synthesise a promising alternative to diesel – oligomeric oxymethylene dimethyl ethers (OMEs,  $\text{CH}_3\text{-[O-CH}_2\text{]}_n\text{-O-CH}_3$ ) [18,19].

As part of the NAMOSYN project, the MEDENA (methanol dehydrogenation with sodium (Na) catalyst) plant was designed and constructed (Figure 10). The MEDENA setup intends to prove that vaporised elemental sodium homogeneously catalyses the reaction of methanol to anhydrous formaldehyde. In order to create a suitable catalyst dosing method, a designated sodium evaporation and condensation system was designed. The evaporation and condensation experiments proved that sodium could be dosed as a catalyst. The next objectives are to optimise the crucial parameters in the reactor, e.g. temperature, pressure, methanol molar fraction and residence time.



Figure 10: MEDENA mini-plant for the dehydrogenation of methanol to anhydrous formaldehyde at KALLA (Photo: M. Kamienowska)

### **NECOC - Negative Emissions by Carbon Synthesis from Atmospheric CO<sub>2</sub>**

The BMWK funded project NECOC aims at creating negative emissions by synthesizing

solid carbon materials from atmospheric CO<sub>2</sub> in a three-step process. In collaboration with the two start-ups Climeworks Germany GmbH and INERATEC GmbH, a group of researchers from the Karlsruhe Liquid Metal Laboratory (KALLA) and the Institute of Thermal Process Engineering (TVT) is building an innovative demonstration plant.

Atmospheric CO<sub>2</sub> is separated from the air via a direct air capture (DAC) facility developed by Climeworks. The second process step, operated by INERATEC, is the catalytic methanation of CO<sub>2</sub> using microstructured reactor concepts in order to overcome the challenge of the high thermal stability of the CO<sub>2</sub> molecule. In a third step the thermal dissociation of methane, also known as methane pyrolysis, takes place in a liquid metal bubble column reactor developed at KALLA. The innovative technology using liquid tin as heat transport medium prevents the pyrolysis reactor from clogging as the solid carbon produced by methane pyrolysis rises to the liquid metal surface as a powder due to its lower density compared to tin.

During the past months, the demonstration plant was set up successfully and currently the project partners are launching the individual processes and running first tests. The process steps are going to be joined to synthesize carbon from atmospheric CO<sub>2</sub> in late summer. A detailed characterization of the thus obtained carbon products is going to follow later this year in order to determine their potential for various industrial applications.

NECOC was selected as part of the KIT booth at Hannover Messe 2022 where the project was met with lots of interest, from both industry and individuals.

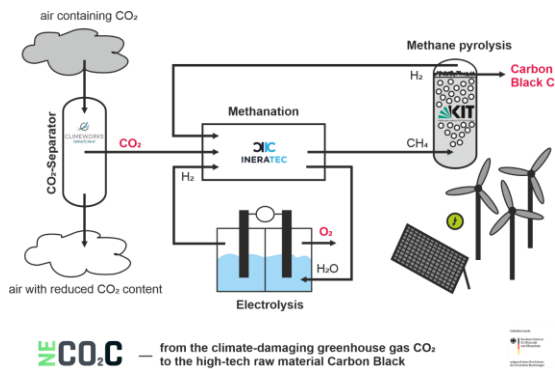


Figure 11: Schematic of the process for converting the greenhouse gas CO<sub>2</sub> into economically usable carbon materials, which has recently been set up at KIT in a plant.



Figure 12: Demonstration plant built at KALLA: detailed picture of the methane pyrolysis set-up.



Figure 13: Demonstration plant built at KALLA: view of the entire plant: from left to right, the pyrolysis reactor with the container plants from INERATEC and Climeworks.

## References

- [1] Laube, T., Dietrich, B., Marocco, L., Wetzel, Th.; Turbulent heat transfer in a liquid metal tube flow with azimuthally inhomogeneous heat flux, *International Journal of Heat and Mass Transfer*, 189 (2022), 122734.
- [2] Skupinski, E., Tortel, J., Vautre, L., Determination des coefficients de convection d'un alliage sodium-potassium dans un tube circulaire, *International Journal of Heat and Mass Transfer*, 8 (1965), 937-951.
- [3] Pacio, J., Daubner, M., Fellmoser, F., Litfin, K., Wetzel, T.; Heat Transfer Experiment in a Partially (Internally) Blocked 19-Rod Bundle with Wire Spacers Cooled by LBE, *Nuclear Engineering and Design*, 330 (2018), 225-240
- [4] Pacio, J., Daubner, M., Wetzel, T.; Local Blockages in a Rod Bundle with Wire Spacers: Heat Transfer in LBE for the Safety Assessment of MYRRHA, *Advances in Thermal Hydraulics (ATH 2018) 2018 ANS Winter Meeting, Orlando, Florida, November 11-15, 2018*
- [5] Batta, A., Class, A. G.; Thermalhydraulic CFD Validation for Liquid Metal Cooled 19-Pin Hexagonal Wire Wrapped Rod Bundle, *8th International Topical Meeting on Nuclear Reactor Thermal Hydraulics (NURETH-18), Portland, Oregon, USA, August 18-23, 2019*
- [6] Batta, A., Class, A. G., Pacio, J.; Numerical analysis of a LBE-cooled blocked 19-pin Hexagonal wire wrapped rod bundle experiment carried out at KIT-KALLA within EC FP7 Project MAXSIMA, *The 8th European Review Meeting on Severe Accident Research (ERMSAR), Warsaw, Poland, May 16-18, 2017*
- [7] Niedermeier, K.; Numerical Investigation of a Thermal Storage System Using Sodium as Heat Transfer Fluid (PhD thesis), KIT Scientific Publishing, KIT-SR 7755, 2019.
- [8] Laube, T., Marocco, L., Niedermeier, K., Pacio, J., Wetzel, T.; Thermodynamic Analysis

- of High-Temperature Energy Storage Concepts Based on Liquid Metal Technology, *Energy technology*, 8 (3) (2020), 1900908.
- [9] Niedermeier, K., Müller-Trefzer, F., Marocco, L.; Parametric study of filler size and properties for a liquid-metal thermal energy storage, *Applied Thermal Engineering*, 212 (2022), 118568.
- [10] Müller-Trefzer, F., Niedermeier, K., Daubner, M., Wetzel, T.; Experimental investigations of a dual-media thermal energy storage system with liquid metals. 15th International Conference on Renewable Energy Storage (IRES 2021), Online, 16.–18. March 2021.
- [11] Müller-Trefzer, F., Niedermeier, K., Daubner, M., Wetzel, T.; Experimental investigations on the design of a dual-media thermal energy storage with liquid metal, *Applied Thermal Engineering*, 213 (2022), 118619.
- [12] Heidelberger, M. (2021); Renewable Energy Sources: On the Way towards Large-scale Thermal Storage Systems. KIT press release 034/2021.
- [13] Die nationale Wasserstoffstrategie. BMWi, 2020. <https://www.bmw.de/Redaktion/DE/Publikationen/Energie/die-nationale-wasserstoffstrategie.pdf>
- [14] Geißler, T.; Methan-Pyrolyse in einem Flüssigmetall-Blasensäulenreaktor. Dissertation. Karlsruher Institut für Technologie. 2017.
- [15] Stoppel, L., Fehling, T., Geißler, T., Baake, E., Wetzel, T.; Carbon dioxide free production of hydrogen, *IOP Conference Series: Materials Science and Engineering*, 228 (2017), 012016
- [16] Presseinformation 141/2019. Wasserstoff aus Erdgas ohne CO<sub>2</sub>-Emissionen. [https://www.kit.edu/kit/pi\\_2019\\_wasserstoff-aus-erdgas-ohne-co2-emissionen.php](https://www.kit.edu/kit/pi_2019_wasserstoff-aus-erdgas-ohne-co2-emissionen.php)
- [17] Project website: <http://namosyn.de/>
- [18] Reuss, G., Disteldorf, W., Gamer, A. O., Hilt, A.; in *Ulmann's Encyclopedia of Industrial Chemistry*, Wiley-VCH Verlag GmbH & Co, Weinheim, (2011), 671–692.
- [19] Oestreich, D., Lautenschütz, L., Arnold, U., Sauer, J.; Reaction kinetics and equilibrium parameters for the production of oxymethylene dimethyl ethers (OME) from methanol and formaldehyde, *Chemical Engineering Science*, 163 (2017), 92-104



Group: Accident Management Systems

## **Key Advancements in the Research Area of Energy System Resilience and Crisis Management in 2021**

*S.S. Ottenburger, N. Chavan, T. Makumbi, and W. Raskob*

### **Introduction**

The Department 'Resilient and Smart Infrastructure Systems' of ITES performs research in three Helmholtz programmes, namely Energy System Design (ESD), FUSION and Nuclear Waste Management, Safety and Radiation Research (NUSAFE).

In the ESD program, ITES represents the topics of resilience, systemic risks, and uncertainties in connection with sustainable energy systems, and addresses issues that link topological degrees of freedom with the avoidance of outages and flexible operation of energy systems. In addition, early warning systems are developed to predict critical situations in different contexts.

In FUSION, ITES performed dose assessments to the population for the DEMO reactor. Calculations are performed for a generic site and in a probabilistic mode. The 95% percentile is provided as endpoint at different distances from the DEMO site. This allows to evaluate the consequences of potential accident sequences, allowing to adjust safety options to reduce the consequences where necessary.

In NUSAFE, work focused on the improvement of the Decision Support System (DSS) JRODOS (Java based Real-time Online Decision Support) for nuclear and radiological emergencies. An advanced atmospheric dispersion model (FLEXPART) was implemented allowing to perform long-range calculations around the world as well as assessing the potential location of unknown sources via inverse modelling. Furthermore, generic decision support approaches related to nuclear and non-nuclear

smart dynamic crisis management are developed within HGF Portfolio Security.

### **Resilient and Sustainable Energy Systems**

Not least because of the UN Sustainable Development Goals (SDGs) - in particular SDG 11 (Sustainable Cities and Communities) and SDG 13 (Climate Action) - and the UN Sendai Framework for Disaster Risk Reduction (e.g. Priority 3: Investing in Disaster Risk Reduction and Resilience), resilience and system transformations must be considered interrelatedly if sustainability developments are to be a long-term success story.

In resilience engineering and in the context of utility infrastructure, the term resilience often neglects the negative consequences of failures in terms of cascading effects, which extend beyond the defined system boundaries. In this context, resilience is defined as the inherent ability of an organization or system to avoid major system failures after a disruption occurs by achieving as stable, albeit reduced, a state as possible and restoring normal operations as quickly as possible.

However, the resilience of a society or a city, i.e., community or urban resilience, is multidimensional and depends not only on the resilience and physical robustness of individual delivery systems within their own boundaries. It also depends on whether it is still possible to maintain an acceptable basic supply of various critical services during a critical phase or whether a blackout will occur instead - what an urban population perceives as an acceptable

basic supply is not clear per se. With increasing digitalization and automation, the importance of a continuous energy supply for the functioning of modern societies will further grow.

In the context of critical urban functions, we interpret a city's performance as the fulfilment of these functions. In this chapter, we focus on the overall security of supply with respect to all urban critical functions that depend on the timely inflow of energy. Therefore, we assign a specific value to an infrastructure that describes the degree of degradation in overall urban supply security that would be caused by a reduction in the supply of power to that specific infrastructure. In addition to safety factors and system hardening measures to improve the resilience of infrastructures, the development of response and recovery strategies is also part of the portfolio of much-discussed resilience measures - furthermore, emerging smart technologies provide opportunities for the development of new effective measures.

In general, resilience-enhancing measures are motivated by clearly defined risks that are no longer acceptable. In other words, if we have appropriately specified risks caused by, for example, recurring natural hazards such as hurricanes or typhoons, then efficient integrated resource and resilience planning can be designed alongside specified hardening measures to mitigate the impacts for the corresponding known threats. However, estimating future supply risks related to infrastructures that are transforming into digital and intelligent systems (e.g., energy system), have expanded attack surfaces and vulnerabilities, and exist in a world with changing boundary conditions is not possible or feasible in a meaningful way. For example, climate change may lead to a drastic increase in energy consumption that causes extreme peak loads. As a drastic and rough conclusion, we do not have a clear picture of weather-dependent energy generation profiles and the nature of novel cascading effects within complex interconnected grids, nor do we know future energy consumption patterns, as these depend on climate variables

and diffusion parameters related to energy consuming technologies, among others. With respect to the latter aspect, problems would already arise at the distribution level if, for example, 3 or 4 electric vehicles were charged simultaneously with 20 kW power.

In this context, publications summarizing foundational findings and forming a base for future in-depth research on resilient grid design are the following: [1,1-4].

### **Artificial Intelligence for predicting Critical Supply States**

Critical infrastructure systems are characterized by strong interdependencies, and the development of urban areas into smart cities further increases the underlying complexity due to increasing automation and networking. A system of highly interconnected components is particularly vulnerable to systemic risk, making concepts of resilience correspondingly important. One way to survive stressful situations, maintain security of supply, and promote adaptive and anticipatory capacity is to build early warning systems. Because cities are complex and rather chaotic socio-technical systems governed by randomness, the resulting parametric uncertainties pose a challenge for modelling approaches designed to support robust decision making. Sophisticated artificial intelligence-based methods can play an essential role in this case, as they perform well in highly complex environments and with large amounts of data.

One work [5] focuses on the predictability of critical supply states. To study urban utility states, a selected urban area was divided into zones, where the state of that city was determined by the state of those zones, and the state of a zone is characterized by the criticality of the infrastructures housed there. Considering criticality as an atomic building block for urban performance evaluations, we proposed a zone-based state prediction method using deep convolutional neural networks to learn

the state evolution, which is influenced by non-linear demand dynamics. To this end, we presented a case study that applies agent-based simulations Figure 1 (top) and highlights the relevance of deep learning approaches for smart city early warning systems Figure 1 (bottom).

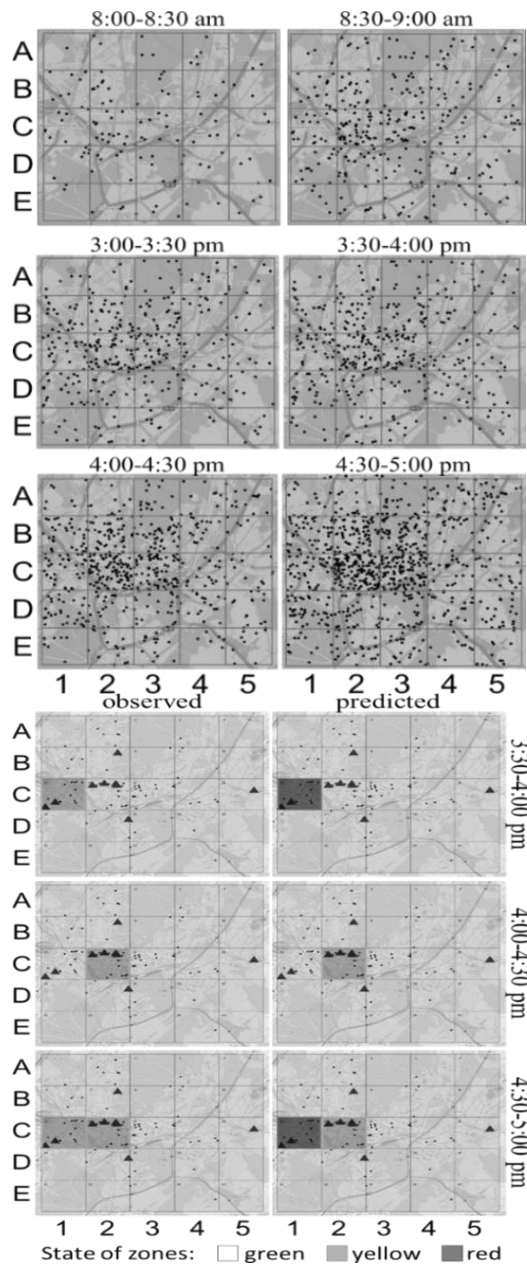


Figure 1 top: Generated demand agents for different time slots. Zones C1 and C2 experience state deteriorations during the day. Bottom: Observed (simulated) vs. predicted states. The triangles illustrate disrupted service providers, the circles non-disrupted providers.

### Integration of FLEXPART into JRODOS

The Lagrangian particle dispersion model FLEXPART (FLEXible PARTicle) is an open-source mathematical model able to simulate the transport and turbulent mixing of gases and particles in the atmosphere. FLEXPART has a strong supporting community further developing the code. However, the usability is limited due to missing graphical user interfaces. JRODOS on the other hand has user friendly input means and is used in more than 40 countries world-wide for operational use. However, JRODOS is lacking the functionality of inverse modelling. To overcome that gap, the Federal Ministry for the Environment, Nature Conservation, Nuclear Safety and Consumer Protection (BMUV) decided to ask KIT to integrate FLEXPART into JRODOS.

This was realised as part of the project "Integration of the atmospheric dispersion model FLEXPART into JRODOS to extend the possibilities of inverse modelling for source location and source term determination based on measured data". The work included the creation of a uniform database for FLEXPART, the coupling to the meteorological forecast data of the German Weather Service and the development of a graphical user interface for FLEXPART as part of the JRODOS system. A direct integration of FLEXPART was not possible because of the GNU licence. Therefore, a method was developed that allows the user to integrate the application on his own. Since FLEXPART only calculates activity concentrations but not doses, special modules were developed to provide dose information, like all other atmospheric transport and dispersion models in JRODOS. Furthermore, FLEXPART was coupled with the food chain module FDMT of JRODOS. Finally, a special module for estimating the impact of a nuclear explosion was integrated.

The following highlights some of the key functionalities that were achieved in the project. With FLEXPART, European-wide or worldwide atmospheric dispersion modelling is possible

with a state-of-the-art model Figure 2 shows the gamma dose rate from a release in Finland.

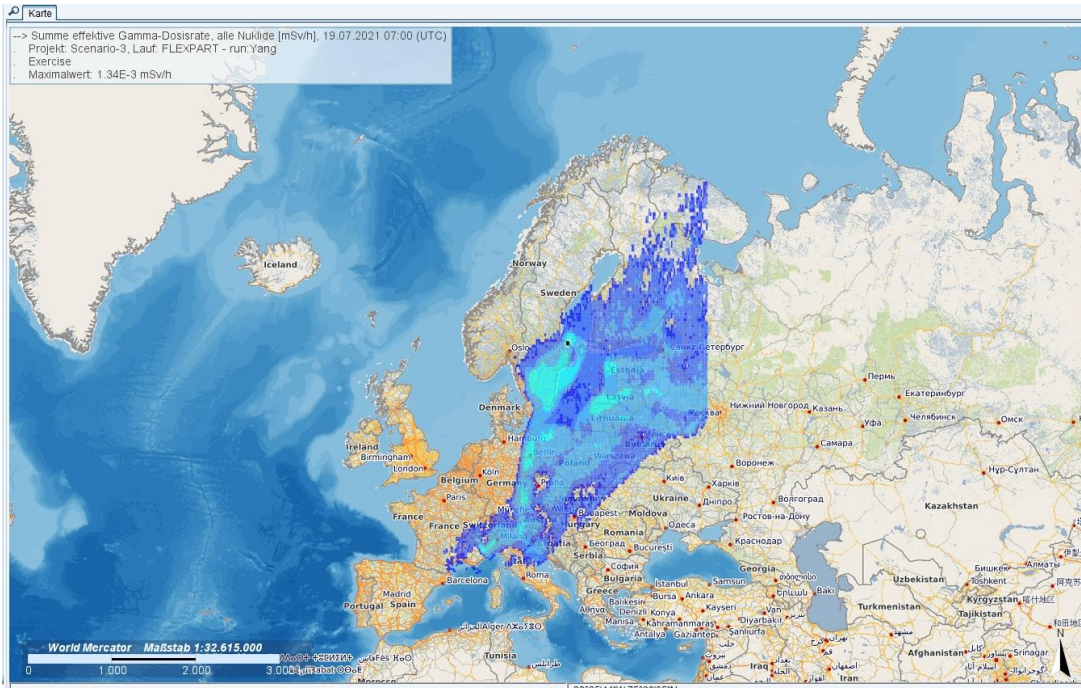


Figure 2 Dose rate map from a large-scale dispersion simulation.

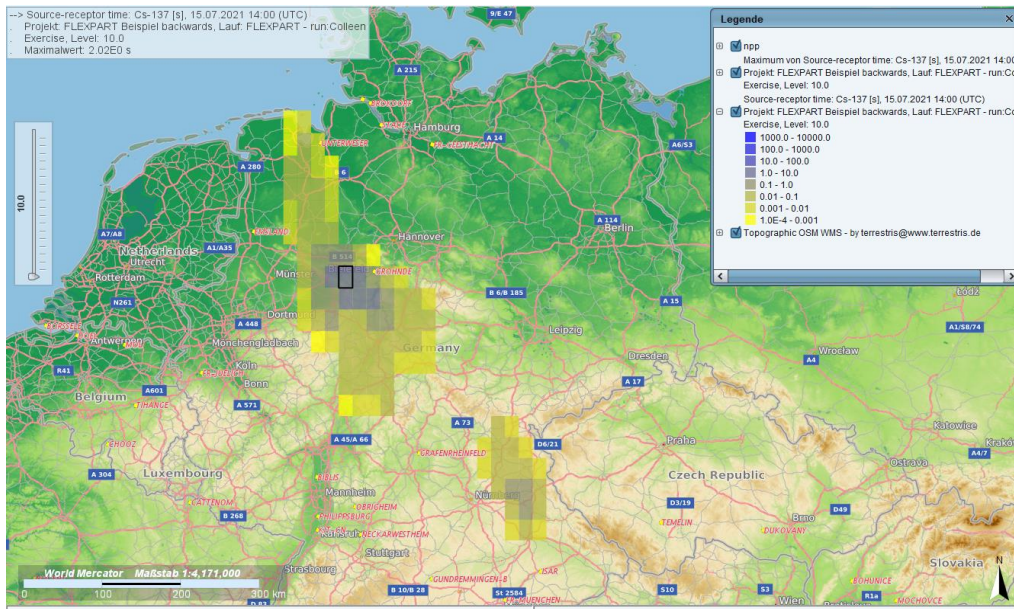


Figure 3 Probability map of the origin of a release location – darker colours mean higher probability.

Figure 3 shows the result of a backward run. This functionality allows to estimate the probability of a release location that is unknown – inverse modelling. Starting point is the detection of concentrations at particular locations. These locations are input to an inverse computer run with FLEXPART resulting in probability maps for possible release points. In a forward calculation, the possible release locations can be tested and checked whether a release from that location hits the monitoring station. This is of particular importance if an accident, that is not known but monitoring networks record some impact.

With FLEXPART, it was also possible to implement a nuclear explosion module. The nuclear explosion is characterized by six boxes, three of them for the stem and three for the mushroom from the explosion. The size and content are set dependent on the amount of explosive in kilo tons (KT). The database was derived for an explosion of 10 KT, but can be scaled between 0.1 KT and 1 MT. The database is not appropriate for larger missiles in the MT area. Our simulations do not consider the effect of the explosion as such or the direct radiation

and flash, but concentrate on the radiation dose from radioactive plume. As the plume reaches high in the atmosphere, dispersion and transport of radioactive particles may reach far, however, the largest part of the particles is rather big and deposition concentrates typically on the near range. Figure 4 shows the areas of the highest contamination from a hypothetical explosion of 10 KT at CN of KIT. Zone I require immediate evacuation, whereas in zone II, also sheltering might be possible. However, decision making for these events is still not much elaborated in Germany.

### Assessment of uncertainties affecting dosimetric calculations for Intake of Radon and NORM

This research aims at developing a software tool that will be used to better understand and quantify uncertainties in doses to humans calculated from the intake of radon and other naturally occurring radionuclides in their body. It is part of the European project RadoNorm (Managing risk from radon and NORM).

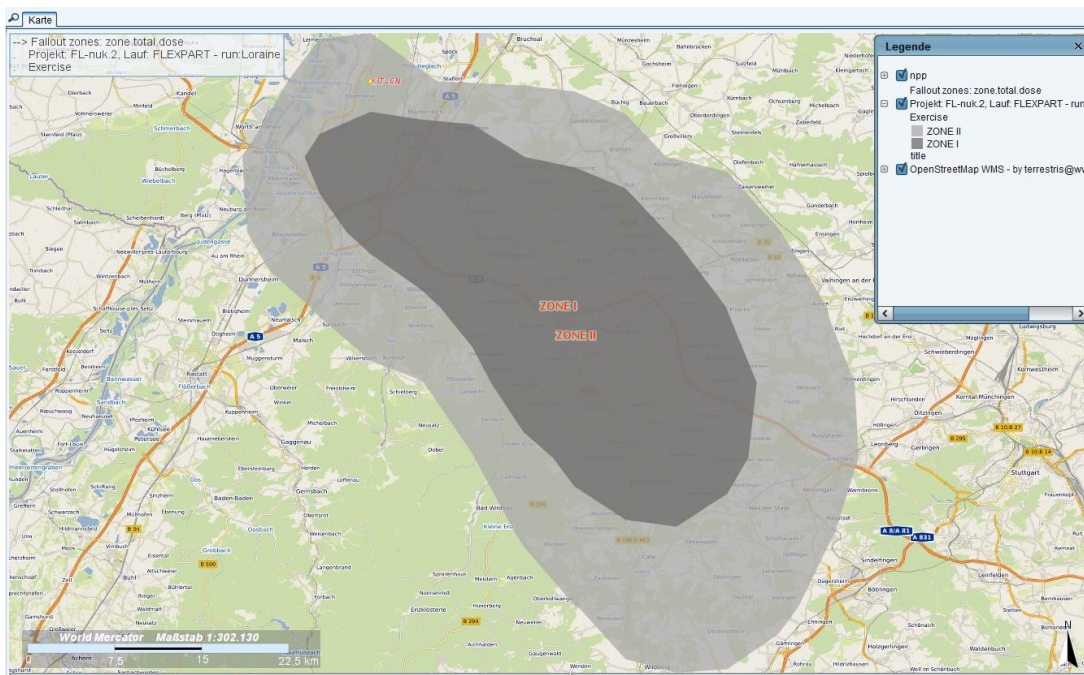


Figure 4 Zones with highest contamination important for defining early countermeasures.

As a first step, a literature study was performed. The literature reviewed focused on the International Commission on Radiological Protection (ICRP) biokinetic and dosimetric models, their model parameters, the ICRP methodology for internal dosimetry and the sources of uncertainty in internal dosimetry. Based on the findings, a first version of the software tool that implements the ICRP methodology for internal dosimetry has been developed using R studio software<sup>1</sup>. This software includes code for both biokinetics and dosimetry. The software has been successfully tested and applied to calculate doses from the intake of radionuclides such as I-131, Co-60, S-35, Ba-133, Pu-239 and Am-241 via inhalation, ingestion and injection. The tool was later successfully validated using data taken from ICRP Occupational Intake of Radionuclides (OIR) data viewer and the results were in agreement with ICRP data with a percentage deviation of less than 1% in the calculated doses.

The first version of the software has been extended and is currently being tested on the implementation of a decay chain starting with Ra-223 and Ra-226. Tests on these radionuclides were successful and the calculated doses are in agreement with ICRP values (less than 1% deviation). In future, the software will be further extended to perform uncertainty and sensitivity analysis on calculated doses to humans and will be tested on Radon and its progeny as well as other radionuclides such as Uranium and Thorium under typical exposure scenarios. Figure 5 shows the plot of the retention of activity in body organs from inhalation of Pu-239 using both simulated and ICRP data. The black circles depict the trend of ICRP OIR data while the lines represent simulated data and HATM stands for the human alimentary tract. From the plot, it is evident that the simulated data agrees well with ICRP data. This demonstrated

that the simulation approach implemented performs as anticipated.

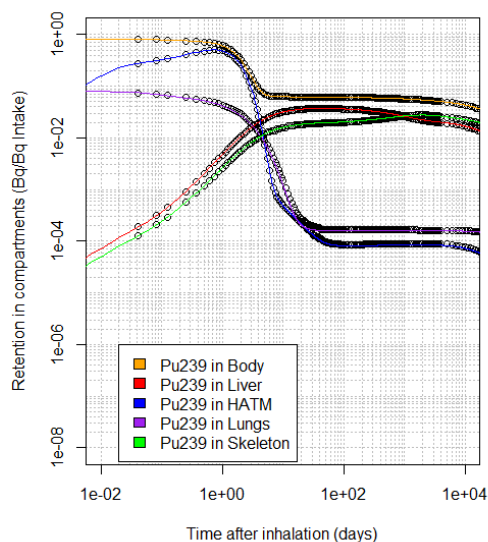


Figure 5: Plot of retention functions with time for inhalation of Pu-239 for both simulated and ICRP data

### Modelling the biokinetic behaviour of Americium in the human body with and without the presence of decorporating agents

This research activity is part of the BMBF project RADEKOR (Speciation and transfer of radionuclides in the human organism especially taking into account decorporation agents) and aims at developing a mathematical model describing the behavior of Americium in the human body. Internal exposure of the Americium can be harmful to Humans. Before treatment, it is necessary to calculate the dose received by the body. Once internalized, most of the Americium is removed from body via urine and faeces. The remaining Americium gets depos-

<sup>1</sup> RStudio Team (2021). RStudio: Integrated Development Environment for R. RStudio, PBC, Boston, MA URL <http://www.rstudio.com/>.

ited in different organs of the body. The biokinetic modelling of the Americium helps us to simulate the amount of Americium deposited in the individual organs of the body. The current biokinetic model is based on the available data from experiments performed on Humans, rats, baboons and dogs. In some cases, data from chemical analogous of Americium is also used. However, this Biokinetic model does not explain the speciation of Americium in the tissue or cells. The first part of the project involves improving the accuracy of the current Biokinetic and Dosimetric model developed for Americium. Moreover, the second part of the project is to understand the biochemistry of Americium in the body as well as study how decorporation agents such as DTPA enhance the removal rate of Americium from the body. Figure 6 shows the representation of the internal organs for the modelling.

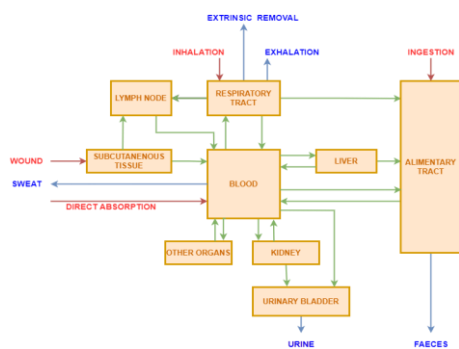


Figure 6 Flowchart representing the biokinetic of Americium inside the human body

## References

- [1] Kropp, C.; Ley, A.; Ottenburger, S.S.; Ufer, U. Making Intelligent Cities in Europe Climate-Neutral: About the Necessity to Integrate Technical and Socio-Cultural Innovations. *TATuP* 2021, 30, 11–16, doi:10.14512/tatup.30.1.11.
- [2] Ottenburger, S.S. Criticality-Based Designs of Power Distribution Systems: Metrics for Identifying Urban Resilient Smart Grids. 2021, *Information Technology Applications for Crisis Response and Management*. Ed.: J. Beard, 150–175, doi:10.4018/978-1-7998-7210-8.ch008.

[3] Hanselka, H.; Ottenburger, S.S.; Raskob, W.; Hagenmeyer, V.; Orphal, J. Resilience by Design: Erneuerbare Energiesysteme Nachhaltig Gestalten.

[4] Ottenburger, S.S.; Raskob, W. Smart Grid Resilience - The Role of Future Power Systems in Critical Infrastructure Protection 2021.

[5] Möhrle, S.; Ottenburger, S.S.; Müller, T.O.; Trybushnyi, D.; Deines, E.; Raskob, W. Strengthening Resilience in Critical Infrastructure Systems: A Deep Learning Approach for Smart Early Warning of Critical States. 2021, *Proceedings of the 31st European Safety and Reliability Conference (ESREL 2021)*. Hrsg.: B. Castanier, doi:10.3850/978-981-18-2016-8\_239-cd.



Group: Hydrogen

## **Fundamental Behaviour of Hydrogen to Applied Accident Consequence Analysis for Hydrogen as a Safe Energy Carrier**

*Abhiram Chavali, Andrei Denkevits, Andreas Friedrich, Joachim Grune, Guang Hu, Olaf Jedicke, Thomas Jordan, Birgit Kaup, Alexei Kotchourko, Mike Kuznetsov, Alexander Lelyakin, Gottfried Necker, Marco Ordonez, Frank Prestel, Jeremy Rietz, Torsten Schuler, Karsten Sempert, Maria Stassen, Jianjun Xiao, Zhanjie Xu, Fangnian Wang*

### **Introduction**

The Hydrogen Group continued to develop models and in-house specialized reactive CFD codes (GASFLOW and COM3D) and conducted an extensive experimental program to deepen the understanding of the behavior of hydrogen in postulated accident. Accidents in tunnels were addressed via the participation in the HyTunnel-CS project and the behavior of cryogenic hydrogen via several industry projects.

Members of the group are actively transferring their insights and expertise into the standards developing organizations ISO (TC 197) and CEN/CENELEC (TC 6) and are contributing to the activities of the European Hydrogen Safety Panel.

However, this report focusses on three activities related to the further development and application of our in-house specialized CFD codes, GASFLOW and COM3D. Firstly, GASFLOW simulations supporting the development of the KIT Aerobuster, a special anti-Coronavirus filtering devices developed by several groups of KIT<sup>1</sup> are shown. Although not directly related to hydrogen, the aerosol transport model of GASFLOW could be applied successfully for transport and determination of infection hazards. GASFLOW showed

excellent performance for those kind of problems. Then again GASFLOW was used for modelling and simulation of filters and membranes for purifying hydrogen. This work has been organized as a part of the Helmholtz Innopool Project "Solar Hydrogen". Finally, COM3D developments and applications are shown for simulating the dynamics of high-pressure hydrogen injection into a combustion chamber and assessing the propensity for spontaneous shock diffusion ignition.

### **Quantitative Corona Infection Risk Assessment**

The Conronavirus-laden droplets can be exhaled by humans or expelled during speaking, sneezing or coughing. Depending on the surrounding air temperature and relative humidity, droplets with diameters less than 50  $\mu\text{m}$  may shrink quickly due to the evaporation, and become the so-called "droplet nuclei" that is smaller than 5  $\mu\text{m}$ . Indoor environment has been known as the place where most transmission of SARS-CoV-2 caused COVID-19 occurs [1]. Virus-laden aerosols in poorly ventilated indoor environments with low humidity and high temperature might result in an infectious dose over time [2]. These airborne droplet nuclei may remain suspended in the air for several hours, and can be widely dispersed by the turbulent gas flow. Evidences have pointed to a

---

<sup>1</sup> [https://www.kit.edu/kit/pi\\_2020\\_100\\_aerobuster-jagt-herumfliegende-corona-viren.php](https://www.kit.edu/kit/pi_2020_100_aerobuster-jagt-herumfliegende-corona-viren.php)

dominant role of airborne transmission of the SARS CoV-2 virus, adequate control measures shall be taken to prevent airborne transmission in indoor environment [3].

The 3-D CFD code GASFLOW has been further developed to enable the simulation capabilities for the multi-phase flows with multi-class, multi-size particles, droplets and dusts. The code incorporates the physics to model the transport, deposition and entrainment, turbulent diffusion, heat and mass transfer, chemical reaction of the discrete aerosol particles, water droplets and dusts. The discrete particles are evenly distributed on each CPU processor and can efficiently exchange information with the continuous conveying fluid. The parallelization approach allows millions of simulation particles that represent billions to trillions of real particles, and in the meanwhile ensures a decent parallel scalability.

A GASFLOW-based systematic step-by-step procedure has been developed to model the airborne transmission of Coronavirus-laden aerosol particles, to perform quantitative infection risk assessment, and to evaluate the efficiency of the mitigation devices, as shown in Figure 1. The innovative method can be subdivided into three main parts: infectious aerosol transport, infection risk assessment, and optimization of control measures.

GASFLOW includes two kinds of computing methods: fast running approximate 0-D point models and 3-D CFD simulation for space resolved applications. This is a unique, complementary modelling approach for calculating infection risks in confined and /or vented spaces. The 0-D point models can evaluate space averaged infection probabilities for a given vented room and exposure scenario. They can describe the effect of mitigation measures like improved ventilation, face masks, reduction of exposure time, limitation of person number, vaccination, and others. Point models allow fast risk evaluation for given room without and with protection measures to compare residual risk to commonly accepted risk criteria. In the space resolved 3-D GASFLOW simulations,

Lagrangian approach is used for aerosol behaviors (transport, turbulent diffusion, deposition and removal) in air flow in 3-D space with random aerosol injection sources. The following analysis results can be obtained: particle parameters, such as number density and mass fraction, in arbitrary user-defined boxes, accurate prediction of intake dose of the exposed agent, quantitative infection risk assessment under a given intake dose, aerosol removal efficiency and infection risk mitigation.

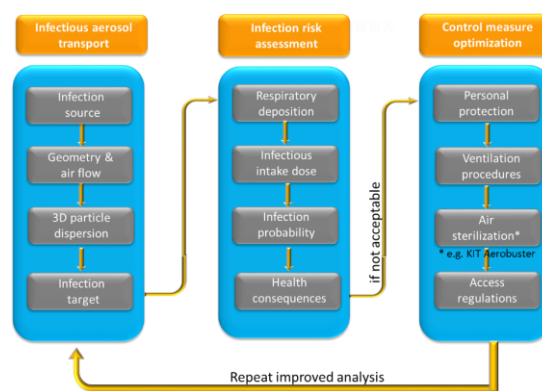


Figure 1. GASFLOW-based analysis procedure

As part of the KIT Innovation Fund - Technology Transfer Project "Aerobuster" (TT Project N076 Aerobuster) in the field of control and remove virus-laden aerosols, the parties, including INT, ITES, IPE and ISTM, strived for the joint development of an Aerobuster up to a near-market prototype/readiness for pilot production. Three milestones have been achieved in 2021: 1) determination of the functional parameters in indoor environment; 2) efficacy demonstrated in laboratory conditions with model viruses; and 3) efficacy with Corona-viruses confirmed in the laboratory and numerical studies.

GASFLOW has been used to simulate the Coronavirus-laden aerosol transmission and perform quantitative infection risk assessment in indoor environments, such as classrooms and offices. The Aerobuster were modeled to

remove the Coronavirus-laden aerosol particles. Furthermore, the effectiveness was experimentally and numerically evaluated by changing the numbers and locations of the Aerobuster devices.

Coronavirus-laden aerosol transport and removal in a classroom with an infected teacher and 20 healthy students has been simulated using GASFLOW (see Figure 2). The calculations impressively show how quickly the Virus-laden aerosol particles disperse in the closed room when the infected teacher keeps on talking loudly. The results also show that the optimized Aerobuster system can significantly reduce the aerosol concentration and the risk of infection through continuous disinfection/sterilization of the room air.

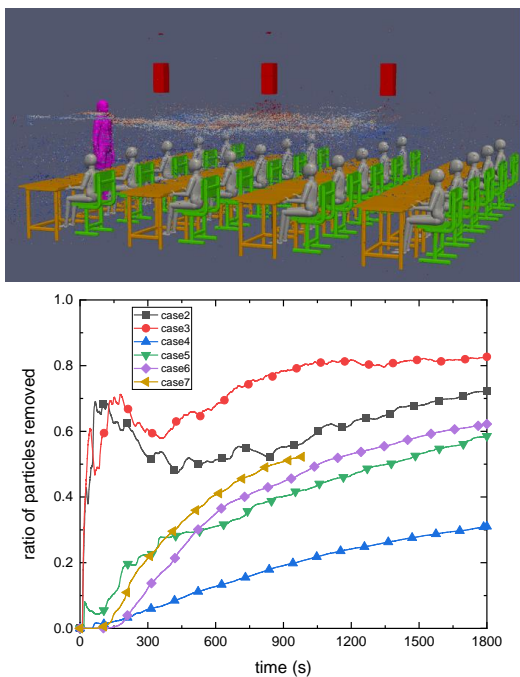


Figure 2. GASFLOW simulations of Coronavirus-laden aerosol removal in a classroom

As a successful outcome of the Technology Transfer Project “Aerobuster”, a license agreement has been signed between KIT and TENNECO GmbH. During the cooperation with TENNECO GmbH, Coronavirus-laden aerosol concentration, venting strategy, Aerobuster efficiency and infection risk have been studied.

The volume of the office room is  $48.6 \text{ m}^3$  with two persons. It is conservatively assumed that the room is closed and the infected person releases virus-laden droplets continuously.

The 3-D GASFLOW calculation results are shown in Figure 3. The aerosol particle location, concentration, velocity and the flow field of the carrier phase can be calculated. The infection probability is roughly 10% at one hour even without any measures. This is mainly due to the distance ( $> 3 \text{ m}$ ) between the two persons and the protection of the monitor screens. The infection probability can be effectively reduced with the optimized Aerobuster system. It is expected that the infection probability will be increased dramatically when the two persons are sitting less than the safety distance and there is no obstacle between the persons. Therefore, mitigation measures to remove virus aerosol shall be taken in the closed indoor environment.

Venting strategy and infection probability in the office room has also been studied using the point model, as shown in Figure 4. It is assumed the office is closed for 60 min, then vented for 30 min with three different ways. The calculated infection probability at the first hour is 18% which is higher than the one calculated in the 3-D simulation. This is because the more diffusive CO<sub>2</sub> instead of discrete particles is used in the point model which leads to a higher local virus concentration near the healthy person. Consequently, more viral RNA copies are inhaled. The infection probability is dependent on the accumulated intake dose and the critical infective dose. The calculation results show that the infection probability increases continuously with the time even though the door and windows open for 30 minutes every one hour. The infection probability reaches 75 % after 330 min. It indicates that Coronavirus removal system, such as Aerobuster, is a good option to reduce the overall virus concentration and infection probability without too frequent venting.

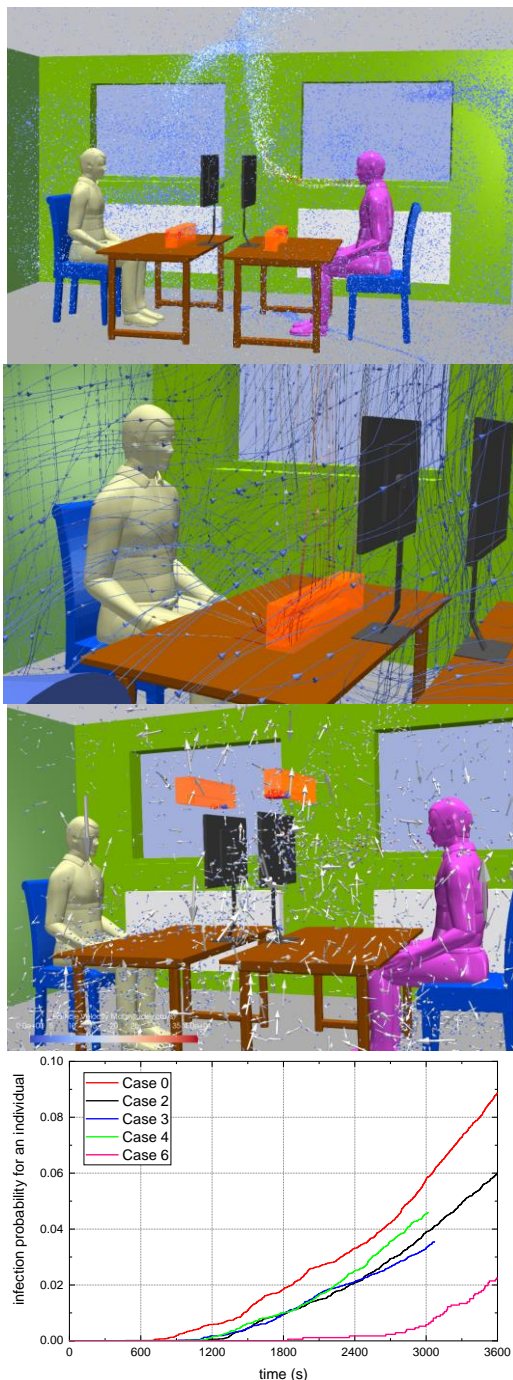


Figure 3. GASFLOW analysis of Coronavirus-laden aerosol removal and infection risk in a closed room



Figure 4. Analysis of venting strategy and infection probability using the point model

### Contributions to the Innopool Project “Solar Hydrogen”

The “Solar Hydrogen” innovation pool project aims to provide essential scientific knowledge and viable technologies for converting solar energy into hydrogen with the highest possible value for a sustainable energy system in Germany and worldwide [5]. The technologies pursued in the project are therefore characterized by the fact that they enable the generation of solar hydrogen with high purity and high pressure. Solar hydrogen, which has these properties, can be used to in particularly high-quality applications (e.g. operation of a hydrogen fuel cell in cars). In this way, new technologies that can use solar energy to provide high-purity and compressed hydrogen at very low cost in the future make a special contribution to combining effective climate protection, security of supply and economic efficiency.

In the Helmholtz Association, the topic of “solar hydrogen” is pursued with different, complementary, innovative technological approaches at the highest scientific level [5]. The participating scientists expect a particularly intensive scientific exchange of research approaches and process concepts from each other, a joint evaluation of the technologies for the production of solar hydrogen and the quality and suitability of the hydrogen provided with regard to the relevant applications.

A very advancing technology to produce solar hydrogen is the methane pyrolysis in liquid metal [6]. Two groups of ITES are involved in

the development of this technology. One group is conducting the relevant experiments in order to improving the solar hydrogen converting effectiveness for instance. The hydrogen group is responsible for the solar hydrogen purification and the safety issues. In the solar hydrogen purification work, the left methane and carbon particles will be separated from hydrogen by the membrane and porous media in the purification system, in order to fulfill the requirements [7]. Our tasks are to develop physical models and perform high fidelity direct numerical simulations of the hydrogen purification process and analyze the potential safety issues.

The solar hydrogen purification work, e.g. the filtering the carbon particles via porous media, involves the dynamics of the gas phase (hydrogen and methane, etc.) and the solid phase (carbon particles) in the complex geometry filled (porous media). Therefore, the underlying theory adopted in the project is the Continuum

Mechanics, which specifically is the computational fluid dynamics. The objective of the numerical modeling of purification and safety of solar hydrogen consists of developing the purification model for filtering the carbon particles and separating the left methane in the production, meanwhile ensuring the system running safely. The goal consists of the computations of the flows of the gases (hydrogen and methane) and the carbon particles.

The main theory adopted in the project is the computational fluid dynamics so that the mathematical model is Navier-Stokes-Equations with turbulence model and porous media model. In addition, the particle transport, deposition, and even entrainment governing equations are solved independently of the fluid flow equations with one-way coupled particle model. The numerical method is a scalable finite volume method with multigrid on structured hexahedron grids, which is used to solve the transient, three-dimensional (3D) and compressible Navier-Stokes equations for multiple

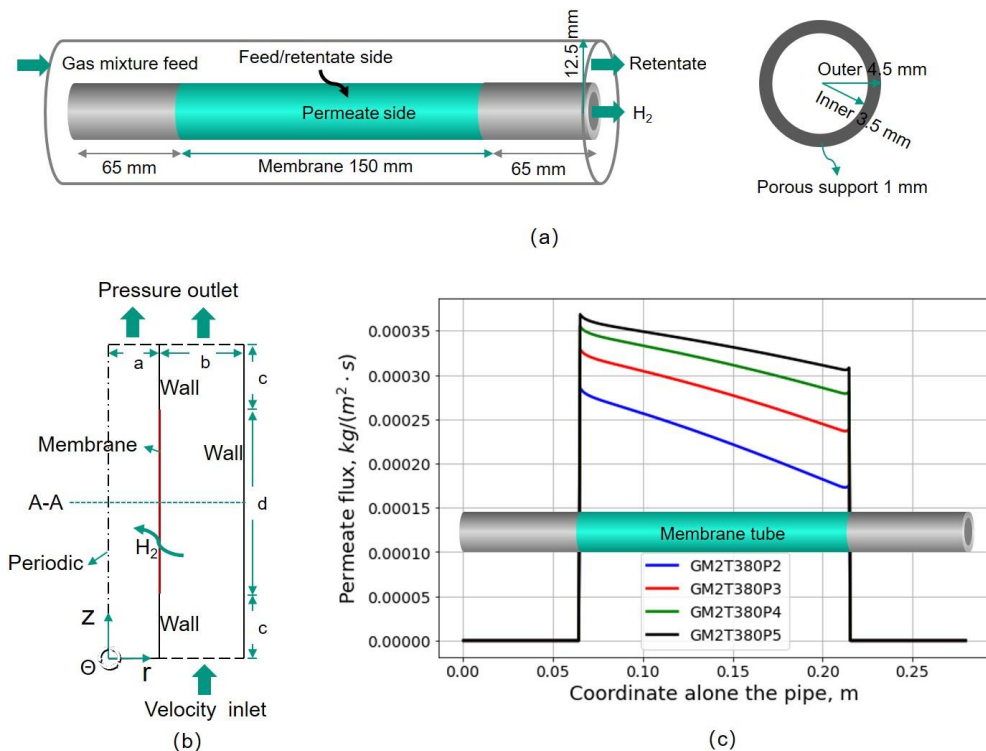


Figure 5. Membrane experiment tube, the corresponding CFD modelling, and the hydrogen permeate flux along the tube

gas species [8]. The linearized ICE'd ALE algorithm provides the basis of the computational method to integrate the equations in time and space.

During the reporting period, it is the beginning of our project. Therefore, a simulation of an experimental membrane tube is performed for validating/testing the code. The geometry model is set-up with the boundary conditions, as seen in Fig. 5 (a) and (b) respectively. For the testing calculation, only 1-2 nodes (namely 16-32 processors) are utilized since the cell number is 150-500 thousand. The CPU consuming time is less than one day.

The calculation results of hydrogen permeate flux along the membrane pipe is shown in Fig. 5 (c). There is no uniform permeate flux since the hydrogen distributes in the feed side of the membrane tube, as seen in Figure 6. When we model the membrane tube bundle in a hydrogen membrane separator, the hydrogen concentrations could be more polarized. That is quite important for evaluating the membrane performance and the hydrogen recovery. Therefore, the need of more nodes for the further calculations is of existence. The complex CFD modelling is planned for the later study.

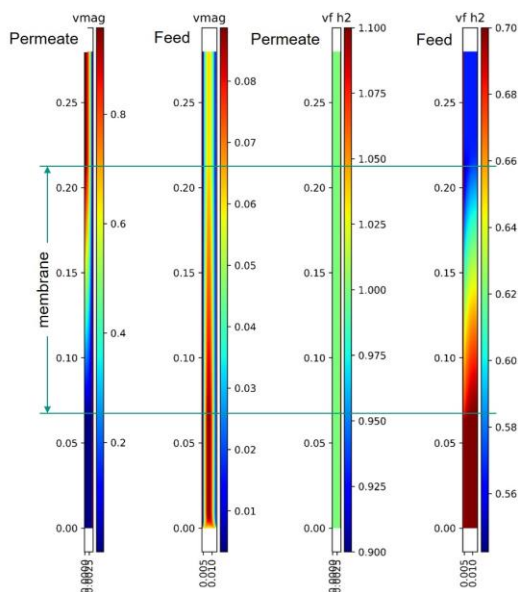


Figure 6. CFD contours of the velocity and hydrogen concentration in the feed and permeate sides

### Simulation of High Pressure Hydrogen Injection

The current work was aimed to perform the test of the possibility to predict unexpected ignition during hydrogen injection into combustion chamber of the prototypical internal combustion engine.

The simulations were performed using the real geometry of the test facility part (Figure 7) containing of the lower compartment of injecting hydrogen supply channel with the valve rod and the upper compartment of the combustion chamber with the hood forwarding injected mixture from the valve.

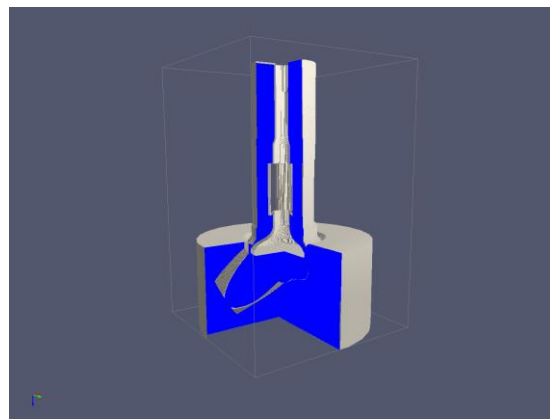


Figure 7. COM3D representation (calculation domain and discretization mesh) of the test facility part. The quarter of the model is removed to demonstrate internal details of the model.

The conditions of the simulations were corresponding to the test conditions:

- Pressure in the supply was 10.2 bar, pressure in the combustion chamber was 1.8 bar;
- Pressure in the valve cap area was near 3 bar;
- Velocity of the valve was ~ 1 m/s during moving phase;
- Mass flow rate by the opened valve was ~ 10 m/s.

For the simulations a COM3D module which allows to reproduce moving boundary was used. The moving boundary conditions were applied to the valve cap and the short section of the valve rod above the cap. To minimize the computational efforts, only the components near the moving interface were included into the test simulations (see Figure 8).

The mesh size in the mentioned case is  $40\ \mu\text{m}$ . The initial state was selected by the beginning of the opening phase. The supplying duct is filled with pure hydrogen at 3 bar pressure, the combustion chamber is air ( $\text{O}_2 + 3.76\ \text{N}_2$ ) at 1.7 bar. The initial gap between the valve cap and the valve seat is about 1 mesh cell.

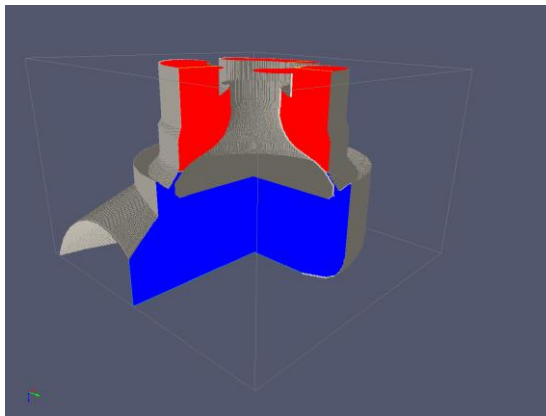


Figure 8. The initial state of the test simulation. Hydrogen is shown by red color, air is in blue.

The simulation started with valve cap moving downwards with velocity of 1 m/s. Since the spatial details were resolved with high accuracy, no macroscopic models as for instance models for turbulence, were used. The mass transfer model in the Navier-Stokes equation is based on the natural diffusion coefficients. The observed hydrogen inflow speed is quite high, as it could be expected in narrows it can achieve choked conditions with the local values of sound speed in pure hydrogen, and soon after modeling start, the noticeable amount of the combustible mixture was identified below the valve cap. In Figure 9, hydrogen distribution after  $24.9\ \mu\text{s}$  is shown. The observed tongues are partially mixed with clearly

seeing pockets of the  $\text{H}_2$  concentration near 30% vol. The temperature distribution (see Figure 10) shows that in the areas of the burnable composition, the conditions correspond to the setting of the auto-ignition state.

In the future work, an application of the chemical reaction accounting is planned. The detailed chemistry model for the  $\text{H}_2$ -air mixture is available in the COM3D code and its inclusion in the simulation is straightforward. Note, that for the trustworthy application of the chemical model, most likely further refinement of the geometry can be required.

On the basis of the obtained results, one can conclude that the proposed approach can be useful for the obtaining of the detailed information on the possibility of the unforeseen ignition during

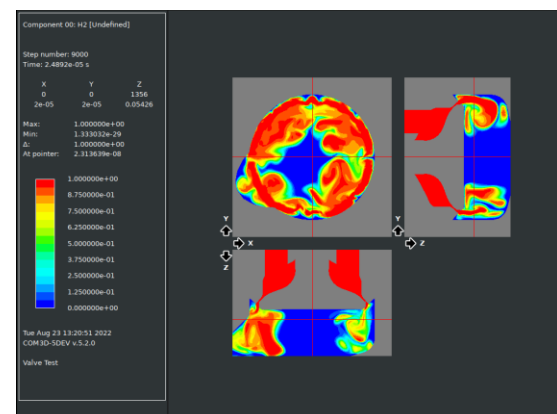


Figure 9. Hydrogen concentration distribution after  $24.9\ \mu\text{s}$  after opening beginning.

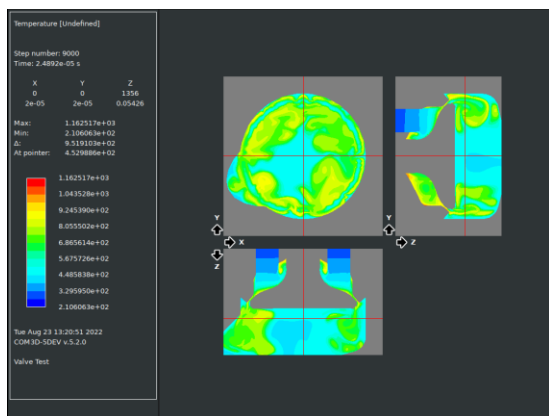


Figure 10. Temperature distribution after 24.9  $\mu$ s.

## References

- [1] Morawska, L., et al., "How can airborne transmission of COVID-19 indoors be minimised?", *Environ. Int.*, vol. 142, no. April, 2020.
- [2] Lowen, A. C., et al., "Influenza virus transmission is dependent on relative humidity and temperature", *PLoS Pathog.*, vol. 3, no. 10, pp. 1470–1476, 2007.
- [3] Morawska, L., et al., "It Is Time to Address Airborne Transmission of Coronavirus Disease 2019 (COVID-19)", *Clin. Infect. Dis.*, vol. 2019, no. 9, pp. 2311–2313, 2020.
- [4] Xiao, J., et al., *GASFLOW-MPI: A Scalable Computational Fluid Dynamics Code, VOLUME 1: Theory and Computational Model, Revision 1.0*, KIT Scientific Report Nr. 7710, KIT Scientific Publishing, Karlsruhe, ISBN: 9783731504481, April, 2016.
- [5] Innovationspool-Projekt 2021-2023 des FB Energie – Programm MTET Zukunftsthema „Solarer Wasserstoff – hochrein und komprimiert (Solarer Wasserstoff)“, FB Energie – Innovationspool 2021 – 2023: Zukunftsthema „Solarer Wasserstoff“, 15th, May, 2020.
- [6] Geißler, T., Abánades, A., Heinzl, A., Mehravaran, K., Müller, G., Rathnam, R.K., Rubbia, C., Salmieri, D., Stoppel, L., Stückrad, S. and Weisenburger, A., 2016. Hydrogen production via methane pyrolysis in a liquid metal bubble column reactor with a packed bed. *Chemical Engineering Journal*, 299, pp.192-200.
- [7] Ohi, J.M., Vanderborgh, N., Consultants, G.V., Ahmed, S. and Kumar, R., 2016. Hydrogen fuel quality specifications for polymer electrolyte fuel cells in road vehicles. Office of Energy Efficiency and Renewable Energy: Washington, DC, USA.
- [8] Xiao, J., Breitung, W., Kuznetsov, M., Zhang, H., Travis, J.R., Redlinger, R. and Jordan, T., 2017. GASFLOW-MPI: A new 3-D parallel all-speed CFD code for turbulent dispersion and combustion simulations: Part I: Models, verification and validation. *International journal of hydrogen energy*, 42(12), pp.8346-8368.

Group: Energy and Process Engineering

## First experimental results of a supercritical Organic Rankine cycle turbine using propane as working fluid

Joaquin Mardon Perez, Julia Filipe, Hans-Joachim Wiemer

For industrial waste heat applications the heat of 100-200°C has a great potential. One way to tap this energy potential is to convert it into electrical power via a thermodynamic cycle process. Electricity generation for these low-temperature cycles is nowadays usually realized via an ORC process (Organic Rankine Cycle).

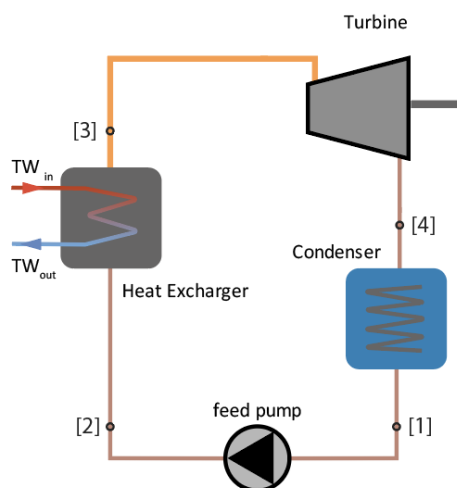


Fig. 1: ORC process

The variation of the boundary conditions and the working fluids used has a large influence on the net electricity yield and thus on the economic efficiency of a waste heat application.

The approach followed by the ITES-EVT group is to maximize electricity production by selecting a heat transfer fluid suitable for the site-specific boundary conditions in Europe and a supercritical live steam pressure. In previous

studies [1], [3] Vetter et al. have shown that significant performance improvements are possible at supercritical conditions.

The working fluid selection has taken into account environmental and operational criteria, such as high thermal conductivity, low specific volume, high chemical stability, low corrosiveness, low flammability, toxicity, low Ozone Depletion Potential (ODP) and Global Warming Potential (GWP) [2].

In order to optimize and validate this simulation model we built a supercritical ORC (MoNiKa).

### The MoNiKa power plant

MoNiKa (Modular low-temperature cycle Karlsruhe) is a facility built at KIT campus north with the idea of studying and optimizing the ORC process. This installation is a small and compact power plant. It was designed as a modular installation to allow the study and investigation of different components and operational parameter for the research of waste heat power generation from low-temperature heat sources.

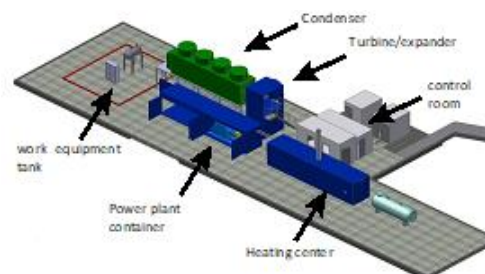


Fig. 2: MoNiKa -ORC power plant

In one Master thesis we mainly investigate the experimental results of the turbine operation with the focus to the load range between 40-100%.

The second work involved the creation of a transient Simulink model of the two main power plant components, turbine and condenser. The focus was on the combination of these two components and the implementation of a turbine efficiency model obtained from experimental data.

### Components description

The pumping system is compound by two pumps. The main pump is a LEWA triplex M514US G3G. It is a piston pump with a maximum mass flow of 3.6 kg/s and a design pressure of 6.5 MPa (in this will be referenced as main pump).

The heat exchanger manufactured by Gesmex, is the connection between both cycles, (water and organic). It is a counter-flow plate heat exchanger designed to work in a supercritical regime. The design thermal power installed is 1000 kW for full load operation.

The condenser manufactured by KÜHLTURMKARLSRUHE has a support sub frame with 3.5 m of height. It is located between the exit of the turbine (or throttling valve), and the propane tank. However, the condenser is prepared to work with water spray. The heat exchange areas are built symmetrically in "V" configuration. They include three chambers. Each one is equipped with a vertical fan (impeller and diffusor) of 2.5m diameter. The power consumption of each motor is max.13 kW at 322 RPM and a maximum volume flow rate of 44 m<sup>3</sup>/s each and in total 39 kW - 132 m<sup>3</sup>/s.



Fig. 3:Propane tank und Condenser

The last component of the circuit is the turbine.



Fig. 4: Turbine with gearbox and generator

In Fig.5 the axial four-stage propane turbine with constant stage pressure (impulse design) with a nominal rotational speed of 9996 1/min. It is a welded construction made by M+M TURBINE-TECHNIK [10]

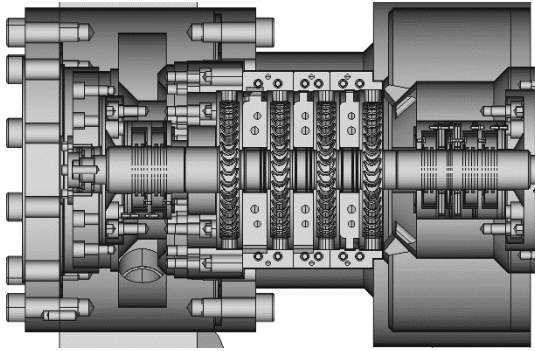


Fig. 5: Turbine cross-section

The axial bearing is made in the steam inlet. Sealing to the outside is achieved by means of carbon seals. The vapor inlet area (front side) is of closed design and has a leakage gas discharge, which is led to the exhaust vapor. In the area of the shaft passage at the coupling connection (gear side), a closed design is not possible. Here, nitrogen is supplied behind the first seal and the nitrogen-propane mixture is discharged behind the second seal. Behind the third seal, atmospheric conditions prevail.

The 150 MVA synchronous generator is connected to the turbine with a gearbox.

The generator made by MarelliMotori has a control system provided by DEIF, which work in temperatures between  $-20\text{ }^{\circ}\text{C}$  and  $70\text{ }^{\circ}\text{C}$ . The measuring voltage is from 100 to 690 V AC ( $\pm 20\%$ ), and the measuring current is  $-1$  or  $-5$  A AC. The current overload is  $4xI_n$  in continuous,  $20xI_n$  in 10 s ( $\max\{75A\}$ ),  $80xI_n$  in 1 s ( $\max 300A$ ) and the measuring frequency is 30 to 70 Hz. To connect the generator with the KIT grid, a Janizta UMG 512 is used as a measurement system.

In addition to these main components, the following auxiliary units are also important for the power plant operation.

Support pump from Grundfos, which ensures the upstream pressure to the main pump.

Propane separator from Borsig which separates the nitrogen propane mixture from the

purge gas of the turbine shaft seal. The separated propane can be returned to the propane tank.

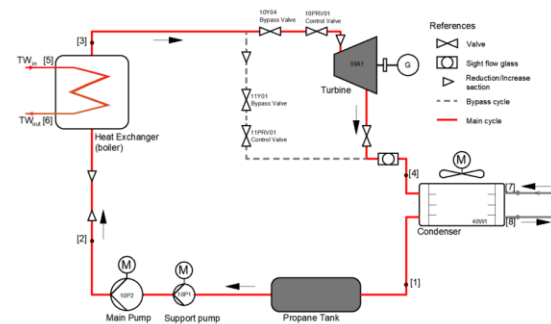


Fig.6: Scheme of the power plant MoNiKa

Propane tank with a volume of  $2.4\text{ m}^3$ , also an additional storage tank for refilling propane.

Furthermore, we have a  $7\text{-m}^3$  fuel oil storage tank to supply the water heating station.

The control and regulation technology container with a redundant S7-416 PLC and the SIEMENS power plant software T3000.

The Control room container include two workstations for power plant monitoring and control. One additional PC manage the data storage for the scientific instrumentation.

Additionally installed scientific measuring points are used for the acquisition of additional parameters such as ambient temperature and humidity, pressure difference condenser, temperature and velocity field condenser as well as an optical access to the propane circuit for flow characterization.

## Instrumentation

The sensor technology installed in MoNiKa fulfills two requirements: the first for power plant control and regulation, the second as a platform for scientific studies conducted in the plant. Therefore, the plant is much more extensively instrumented than in a normal power

plant. For balancing purposes, sensors for temperature and pressure are installed along the entire cycle, i.e., at the inlet and outlet of each component.

The mass flow rate and density of the working fluid are measured between the outlet of the main pump and the inlet of the heat exchanger using an E+H Promass 83F sensor. This sensor uses Coriolis forces and resonance frequency to provide a direct measurement of mass flow, velocity and density.

A WIKA TR34 Class A-PT100 is used to measure temperatures at all points in the system. These sensors are connected as 4-wire resistance thermometers and have an operating range of -50 to 250 °C. These thermometers are characterized by a compact design, are resistant to vibration and have a fast time response for operating measuring points. Type K thermocouples are used in areas with increased time requirements.

For pressure measurements at the MoNiKa plant we use the Vegabar 81 and 82. These pressure transmitters are universally applicable for the measurement of gases, vapors and liquids. They have a ceramic measuring cell, which allows the sensor to behave well in corrosive and hot environments. The main difference between purchased sensors is the temperature range in which they can operate. In addition, the pressure range in which they operate is different within the ORC cycle, resulting in pressure measurements in the low-pressure section having higher absolute accuracy than in the high-pressure section.

The sensors are in direct contact with the liquid (propane and water). There is no sleeve or cap between them. This direct contact allows better measurement of the fluid properties, but makes it impossible to remove the sensor from the pipeline for maintenance reasons without draining it first. For this purpose, MoNiKa's measurement system is designed with redundancy, which means that two or three sensors of the same type are installed at each measurement point. This redundant configuration

makes it possible to increase the availability of the measurement technology, which on the one hand increases safety during operation and on the other hand helps to detect systematic errors.

To measure the environmental conditions, the system is equipped with one pressure, humidity and temperature sensor. In addition, a set of type k thermocouples and a pressure sensor is installed in each chamber of the condenser.

Tab. 1: List of Sensors used for this master's thesis

Facility code	Model	Signal type
PS10-02	VEGABAR 81	4-20 mA
PI10-03	VEGABAR 81	4-20 mA
PS10-03	VEGABAR 81	4-20 mA
PI10-12	VEGABAR 82	4-20 mA
TS10-02	TR34 Class A	TR300(4-20mA)
TI10-02	TR34 Class A	TR300(4-20mA)
FI10-02	PROMASS 83F	Profibus DP
10P1*	SINAMICS G180	AC
10P2**	CRN20-04 E-FGJ-G-E	PI controller

### Simulation Software GESI

GESI (Geothermal Simulation) Vers.2.3.6c [5] is an in-house program that has been developed in MATLAB by the ITES (Institute for Thermal Energy Technology and Safety) for studying and optimizing the thermodynamic process of the Organic Rankine Cycle (ORC). The software use the physical property data taken from REFPROP 9.0, from the National Institute of Standards and Technology [6].

This tool solve the energy and mass balance of the ORC Power Plant in stationary regime. As an input the definition of the thermal water values, selection of the operational points, the

ambient characteristic and the equipment is necessary. The tool provides as a result the major values of the whole process and delivers diagrams e.g. temperature- and entropy diagram.

The results of the simulation allows to validate the power plant model and to determine the efficiency of the pump and turbine in full- and part load operation.

### **Experimental results in turbine operation**

The tests runs were performed in November 2021, in turbine operation. The focus of these tests was to investigate the turbine characteristic and to measure the turbine efficiency.

It should be noted that the plant has certain limitations, either with respect to plant safety or thermodynamic values that cannot be reached, which prevent some values planned through the GESI software from being addressed experimentally.

Safety limitations:

- Quality factor at turbine outlet (4) should never be less than  $X < 0.80$ . in case of occurrence, the formation of droplets inside the blades may cause damage to the blades.
- When the boiler temperature exceeds  $160^{\circ}\text{C}$ , for its own safety, the heating station immediately shuts down.

Thermodynamics limits:

- The power plant, due to some problems with the manufacturing of the heat exchanger (boiler), cannot reach a temperature at the inlet of the turbine (3) of more than  $113^{\circ}\text{C}$  for  $\dot{m}_T < 2.2 \text{ kg/s}$  and  $109^{\circ}\text{C}$  for  $\dot{m}_T > 2.6 \text{ kg/s}$  at given constrains. For comparison, the design point at the inlet of the turbine is  $117^{\circ}\text{C}$ .

The experiment started on the first day with a slow warm-up when the cycle starts in bypass

mode and the boiler is prepared. The warmup concludes when the main pump head temperature is less than  $0.5^{\circ}\text{C}$  for at least 30 minutes, and all the process takes around 4 hours. After warming up, the load points were processed with an average time of 30 minutes each, and once the seven load points were completed, the experimental day ended with the regular shutdown.

The purpose of the second day was a sensibility experiment with the opening of the turbine control valve. As on the first day, the experiment started with a warm-up, which lasted 4 hours. Then by changing the opening of the turbine control valve (*10PRV01* see Fig. 7), i.e., opening for each run, the ORCs pressure started to modify.

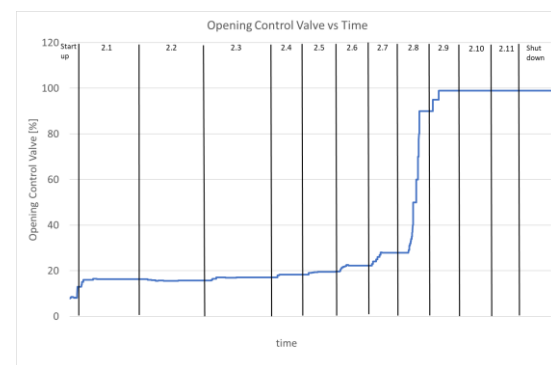


Fig. 7: Test run results 2<sup>nd</sup> day, opening of control valve

When the load is above 40% and the turbine control valve has fixed position, e.g., fully open, and the propane temperature is constant, the propane pressure will change proportional to the mass flow according to Stodola's law. This regime is preferred at load above 40% Fig.8. The next figure shows the two different regimes in MoNiKa power plant when the bypass valve is fully closed during the warm-up. The minimum mass flow rate at which the plant can be operated properly is  $\dot{m}_T = 2.3 \text{ kg/s}$  which corresponds to ca. 80% of the design mass flow.

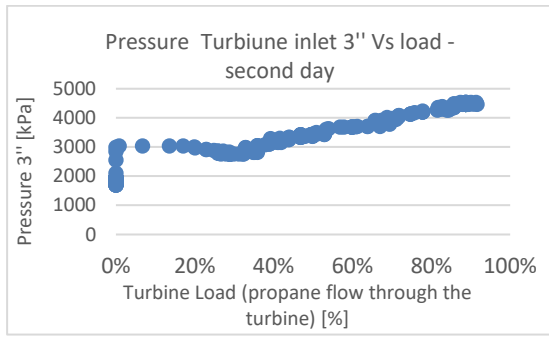


Fig. 8: Test run results 2<sup>nd</sup> day fixed and sliding pressure operation

Experimental work on turbine sensitivity was also planned for the last day, but in this case related to the ORCs mass flow increase. It started with a  $\dot{m}_T = 2.1 \text{ kg/s}$  and after that it was increased by  $0.1 \text{ kg/s}$  until a turbine mass flow rate of  $2.8 \frac{\text{kg}}{\text{s}}$  was reached. As during the previous days, the day started with a slow warm-up but with an issue in the middle of the process: The boiler surpasses  $160^\circ\text{C}$ , so automatically the control system tripped the boiler. Once, the boiler worked more stable, the warm-up finally ended properly.

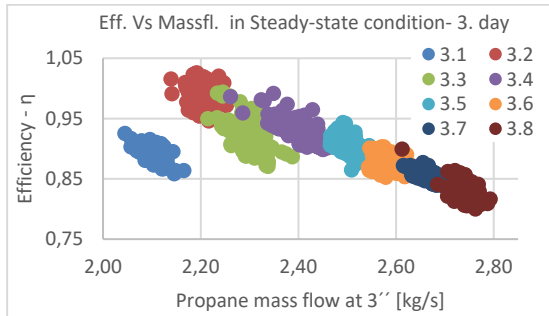


Fig. 9: Test run (3.6) results 3<sup>rd</sup> day turbine efficiency vs. mass flow

Here can be observed the efficiency increase with decreasing turbine mass flow rates. In particular, run 3.1 has a different behavior because pressure and temperature at point 3'' are quite close to the critical point, which means a bigger error in the calculation of the enthalpy and entropy with REFPROP. Additionally, it is important to remark that run 3.2

surpasses the maximum value possible of efficiency, that is greater than 1 (Fig 9). The main reason for this behavior is that the temperature values at point 3''(cal. turbine inlet) is very close to the critical point, where the enthalpy calculation has very high systematic errors. The range of this error in all day was higher in the points 3.1, 3.2 and 3.3 (2,4%, 3,5% and 5,5% respectively) and in the range of 1,6% for the other runs.

### Stodola's law

The aim of this section is correct the Stodola's law due to the real behaviour of the turbine compared with the ideal equation 1.

$$\left(\frac{\dot{m}_T}{\dot{m}_{T,0}}\right)^2 = \frac{p_{T1}^2 - p_{T2}^2}{p_{T1,0}^2 - p_{T2,0}^2} \frac{T_{T1,0}}{T_{T1}} \quad (1)$$

In addition, the equation (1) could be rearranged as,

$$\dot{m}_T = C * \sqrt{F} \cdot \sqrt{\frac{p_{3''}^2 - p_4^2}{T_{3''}}} + C' \quad (2)$$

The missing coefficients are determined with the experimental data to:

- $C = 1.5442$
- $C' = -1.3352 \text{ kg/s}$

This equation only valid in the following limits:

- Mass flow:  $1.88 < \dot{m}_T < 2.74 \text{ [kg/s]}$
- Pressure:  $3860 < p_{3''} < 4900 \text{ [kPa]}$
- Temperature:  $363.5 < T_{3''} < 376.5 \text{ [K]}$

### Simulink model of Turbine and Condenser

The second master thesis from Julia Filipe use the Stodola equation and the correction coefficients from J.Mardon Perez [7] to develop a Simulink model of the turbine. She add the existing model of the condenser which was developed by M. Fossati [9] to her turbine model. One of the main objectives was to create a model that is consistent in its outputs, and to obtain results that reflect the real measurements over a wide operating range. In line with this, another objective is to analyze the turbine efficiency and its dependence with the inputs to the model. Finally, the model is intended to describe and aid the understanding of the phenomena related to the supercritical operation, and to allow the definition of the fluid state at the inlet of the turbine.

The Figure 10 shows the flow chart of the turbine model.

Afterwards, the Stodola block modelled was coupled to the condenser model, by performing the modifications needed in the inputs and outputs of the blocks. Once this was completed, the energy balance modelling began. At this point, the model gained complexity because of the need for data acquisition provided by the REFPROP database, used to retrieve the intermediate values of enthalpy and entropy that allow the calculus of the turbine outlet enthalpy. Therefore, the indirect connection of REFPROP with Simulink through Lookup tables was implemented, following the methodology described by M.J. Fossati in his thesis.

The validation of the Stationary model is done by comparing the simulated results with the averaged measurements related to the same run.

The relevant outputs discussed are the turbine power ( $P_t$ ), the turbine inlet pressure ( $p_{t,in}$ ) and inlet temperature ( $T_{t,in}$ ). The comparison between measured and simulated results is also reflected in the percentual difference of the simulated value over the measured value.

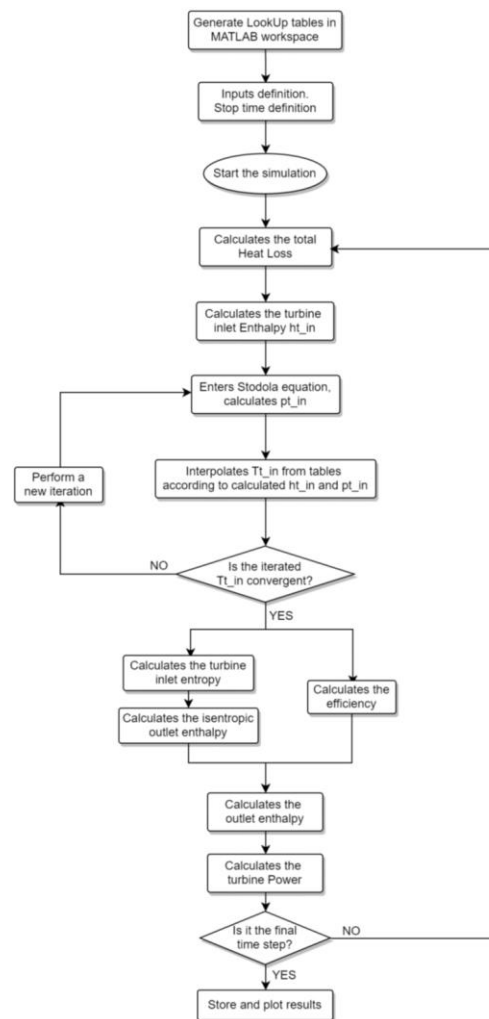


Fig. 10: Flow chart of the Simulink model

In Figure 11, the values corresponding to the turbine power can be seen. Firstly, it should be pointed out the fact that the variable actually being measured is the electric power, while the comparison is made against the shaft power. Having said that, the calculated shaft power can be taken as a reliable value whose rate to the measured electric power (related to the efficiencies of the generator and the gear box) is maintained almost constant.

The majority of the simulated power values obtained present a percentual difference of less than 5% against the real values. However, the runs corresponding to the 3<sup>rd</sup> day show a tendency to increase this difference. This could be

explained by the fact that the 3<sup>rd</sup> day also presents high overall parameters fluctuation due to a malfunction of the boiler during the operation of the plant. Therefore, the employment of averaged data in such conditions produces low quality results, and the prediction can be expected to be inconsistent and ambiguous.

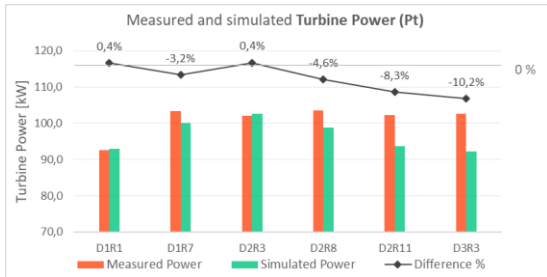


Fig. 11: Test run (3.6) results 3<sup>rd</sup> day turbine efficiency vs. mass flow

**Transient results**

Regarding the turbine inlet pressure and temperature as seen in Figure 12 and Figure 13, it can be observed a good coupling between the measurement curve and the simulated variable during the incremental period and in the stabilization region too. Both outcomes look consistent. However, the T simulation is 2 K approx. higher with respect to the measured values, both in the Simulink output and in GESI result. In these two cases the advantage over GESI is clear, as the program is unable of simulating transient conditions.

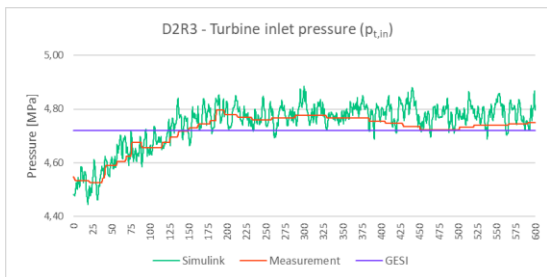


Fig. 12: Turbine inlet pressure simulation result

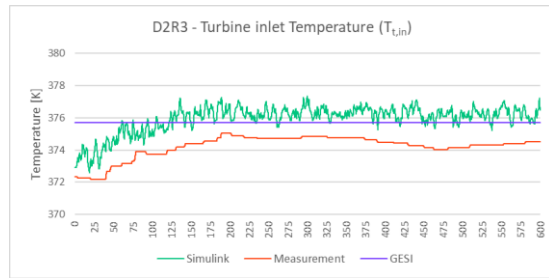


Fig. 13: Turbine inlet temperature simulation result

There it can be observed a progressive increment in the measured power during the first 150 s approx. After that, the power values seem to stabilize around 100 kW (Fig.14). The simulated power tightly follows this increase, thus performing an overall good prediction. However, the model is not able to follow the fluctuation of the signal. With respect to GESI, the simulated constant power is relatively far from the measured power, presenting a difference of near 40 kW above the real values.

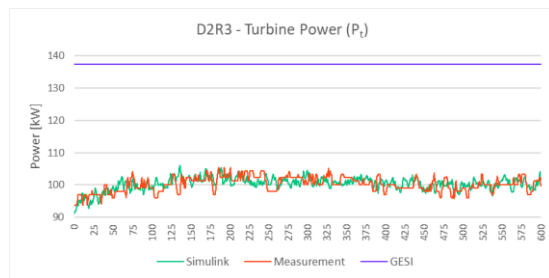


Fig. 14: Turbine outlet power simulation result

**Summary**

For that matter, the temperature and pressure were iteratively found by employing enthalpy values and working with LookUp tables. This way of modelling proved to be successful and brought versatility to the model, making possible to achieve fluid definition results at the turbine inlet, which are close to the measurements. However, it should be pointed out that these calculations still need refinement in order to lower the error against the real values.

Apart from that, when considering the temporal behavior of the test runs, the model is consistent in simulating stationary conditions, and is capable of predicting progressive and relatively slow transient conditions. Since the model is based in Stodola's equation, which is only applicable to stationary conditions, it is not suitable for simulation of fast variations such as the transient conditions encountered during the warm-up and shutdown of the turbine.

The simulated results show some marked tendencies on each of the variables. In general, the model predicts power results consistently below the measured values. With respect to the turbine inlet temperature, it is observed a sustained prediction of values approx. 2 K above the measured data. In the case of the pressure, the results show accuracy and fluctuate 0,1 MPa approx. around the measured pressure values.

Based on this work, a relevant future study would be to further analyze and understand the relation between the variables that compose the plant, trying to set correlations between coupled effects from the different elements, which are part of the cycle. Furthermore, a logical next step would be to develop a one-dimensional model of the turbine that considers the variation of the parameters progressively inside it.

## References

- [1] Vetter, C., Wiemer, H.-J. and Kuhn, D.: Comparison of sub- and supercritical Organic Rankine Cycles for power generation from low-temperature/low-enthalpy geothermal wells, considering specific net power output and efficiency. *Applied Thermal Engineering* 51 (2013) 1-2, S. 871–879
- [2] DiPippo, R.: *Geothermal power plants. Principles, applications, case studies and environmental impact* / Ronald DiPippo. Amsterdam: Butterworth-Heinemann 2015
- [3] Vetter, C., Wiemer, H.-J: *Dynamic Simulation of a Supercritical ORC using Low-Temperature Geothermal Heat*. Melbourne, Australia (2015)
- [4] Vetter, C., *Parameterstudie zur Simulation von Niedertemperatur-Kreisprozessen* (KIT scientific reports) 2011, ISBN 978-3866446731
- [5] ITES Institute for Thermal Energy Technology and Safety: *GESI. Geothermal Simulation*. 2018
- [6] REFPROP. *Reference Fluid Thermodynamic and Transport Properties Database*. NIST National Institute of Standards and Technology (2018)
- [7] Mardon Pérez, J., *Experimental examination of the MONIKA-ORC Turbine and comparison of the results with thermodynamical calculation*, Master Thesis 2022, KIT-ITES
- [8] Filipe, J., *Design of a MoNiKa-ORC-turbine model in Simulink and comparison with experimental results*, Master Thesis 2022, KIT-ITES
- [9] Fossati, M., *Transient Simulation and Validation of a Condenser for a Supercritical Organic Rankine Cycle*, 2020, KIT-ITES
- [10] M+M Turbinen-Technik GmbH. *GT 120-4 Turbine Datasheet*.



Group: Framatome Professional School

## Introduction Framatome Professional School (FPS)

The FPS is strongly involved in higher education activities. In 2021 numerous master's thesis were supervised with topics from energy technology including the GWh-scale Carnot battery system BattMarines, and energy topics relevant for countries in South America or industries including Siemens Energy GmbH. Some of the PhD studies in the FPS are presented in separate sections of this article.

Furthermore, Andreas Class is the programme director of the EIT InnoEnergy Master School's double-degree programme "MSc Energy Technologies" offering an English-taught broad-based higher education in a variety of key energy engineering disciplines, from renewable energy to decentralized power supply, energy economics and more. Next to mastering the latest technologies in energy, students gain an in-depth understanding of the role of innovation and entrepreneurship in the future of this industry.

Within the programme the business partner UnternehmerTUM teaches the Innovation and Entrepreneurship Journey providing a thorough education on the role and the basics of I&E in engineering. Industry challenges and in particular the Siemens-Energy New Energy Challenge give students the opportunity to develop innovative approaches and pitch them in front of innovation managers at leading companies in the energy sector. In the Industry Applied Project and the Innovative Project students work hands-on at problems which are developed and monitored together with industrial partners. The programme is run by a consortium of 4 European universities: KIT; Uppsala University, Sweden; Instituto Superior Técnico, Portugal and Grenoble INP-UGA, France.

Karsten Litfin is involved in nuclear competence preservation at the "Fortbildungszentrum für Technik und Umwelt" (FTU) of KIT where courses for the introduction in nuclear reactor technology and IAEA Safeguards Traineeship are provided. Other educational activities include courses in physics at the Duale Hochschule Baden-Württemberg (DHBW) in Karlsruhe.

### CFD Validation

*Abdalla Batta, Karsten Litfin, Andreas G. Class*

Validation of CFD models takes important part of our work at the FPS. An example of recent validation work can be found in [1]. There, numerical validation for temperature measurements in a blocked 19-pin hexagonal wire wrapped rod bundle experiment carried out by the Karlsruhe Liquid Metal Laboratory (KALLA) of the Institute within the EC-FP7 project MAXSIMA "Methodology, Analysis and eXperiments for the Safety In MYRRHA Assessment" is presented. The recent study considers validation by using temperature values measured downstream of the side upper blockage E1 shown in Figure 1. Here, temperature results at interface between rods and wire wraps and fluid for the blocked case 145 with a flow rate of  $18.7\text{kg}\cdot\text{s}^{-1}$  and a heat load of 394kW is presented. The wireframe in this figure represents the measurements layer 3.

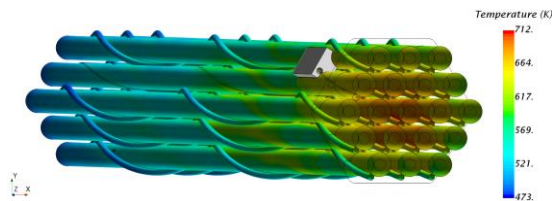


Figure 1. Temperature at interface between rods and wire wraps and fluid case 145, wireframe represents ML3.

It was concluded in [1] that a strong impact of the blockage on the local temperature values surrounding the blockage just downstream of the blockage level was found both numerically and experimentally. However, the results show different locations for the highest impact in the considered cases. In the validation, we define the error as the difference of numerical values to experimental values. Acceptable agreement is found for all thermocouples far from the edge channels. Near the edge channels, bigger errors were observed even for the none-blocked case 24. This indicates that the thermal behavior is influenced by effects not considered in the simulation. These may include physical effects such as conjugate heat transfer to the fuel bundle casing and potential nonhomogeneous inlet conditions in the experiment as well as the well-known deficiencies of RANS turbulence models for low Prandtl number fluids which are under continuous consideration

## References

- [1] Batta, A.: Class, A., CFD Validation For Partially Blocked Wire-Wrapped Liquid-Metal Cooled 19-Pin Hexagonal Rod Bundle Carried Out At KIT-KALLA Paper ID 36240, Nureth 19, Brussels, Belgium, 2022

## Reduced Order Model (ROM) of Standard K- $\epsilon$ Turbulence Model

Jorge Yanez, Andreas G. Class

Development of previous nuclear reactors heavily exploited experiments ensuring that thermal hydraulics is predicted under design and off-design conditions. Today's development of energy technology relies much stronger on numerical predictions. With the heavy usage of computational fluid dynamics (CFD) it becomes mandatory to not only predict the results for the exact cases considered in the CFD but also to provide information on the sensitivity on parameters, initial and boundary conditions. A promising strategy seems to be post-processing of CFD results yielding a very fast-running surrogate model and finally assessing the sensitivity of the results by running the surrogate model for numerous varying cases. In particular, we investigate surrogate models for the standard k- $\epsilon$  model the workhorse for turbulent flow simulation.

The completion of so many calculations –hundreds or even thousands of them– is a task that requires a highly efficient methodology reported in [1-3]. The proposed POD-Galerkin ROM consists of computing an initial value problem with a *High Fidelity Solver*, store a set of solutions (snapshots) and post process them finding a reduced base employing POD. Finally, the governing equations are rewritten in this new coordinate system and resolved. However, the creation of a POD-Galerkin model of the standard k- $\epsilon$  model is complex due to the non-linearities of k- $\epsilon$  equations which are  $|u|, \nu_t = c_\mu k^2 / \epsilon$  and  $\epsilon / k$ . Those are analysed utilizing the Discrete Empirical Interpolation Method (DEIM), Firstly, we calculate CFD snapshots of the non-linear magnitudes and create reduced basis of the non-linear variables. Next, we calculate the values of the variables in a set of selected points, the so-called *magic points*. Magic points are usually calculated utilizing a Greedy algorithm (to get optimal points). In our study, we will utilize point oversampling with a random distribution

strategy. In the computation of the nonlinearities rational functions are computed involving both  $k$  and  $\epsilon$  which are strictly positive and exhibit very large variation. Our strategy to overcome resulting severe deficiency is to identify domains where the error is high in the snapshots themselves. Then, exclude these domains from the reduced basis generation. Technical details of the procedure can be found in [3].

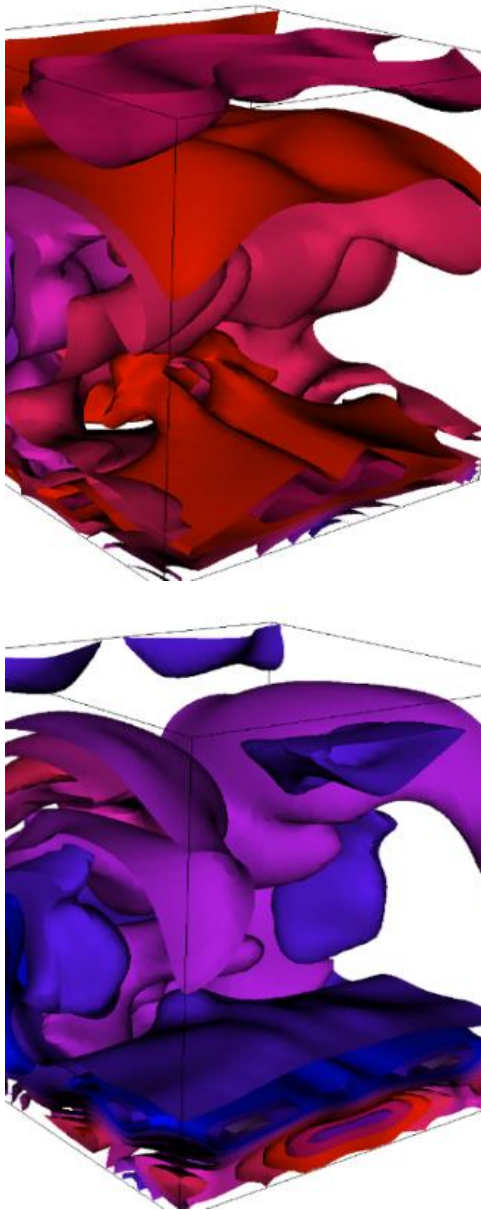


Figure 1: Two DEIM modes for  $\epsilon/k$  nonlinearity.

Applying our methodology results in a ROM with small complexity, which can be evaluated several orders faster the original high fidelity model. Projecting the high fidelity CFD results into the reduced basis allows direct comparison. Velocities, temperatures and turbulent kinetic energy are very well predicted. Even the turbulent dissipation reproduced acceptably, so that the ROM is suitable to investigate sensitivity.

## References

- [1] Yanez, J., Class, A. G., Analysis of the accuracy of residual heat removal in gen-IV reactors, *Nuclear Engineering and Design* 376 (2021) 111102.
- [2] Yanez, J., Class, A. G., Analysis of the accuracy of residual heat removal and natural convection transients in reactor pools, *Nuclear Engineering and Design* 378 (2021) 111151
- [3] Yanez, J., Class, A.G., Reduced order model of standard  $k$ - $\epsilon$  turbulence model, submitted to *Computers and fluids*, in review.

## Weak curvature asymptotics for Debye layers as electrohydrodynamic discontinuities

*Philipp Marthaler, Andreas G. Class*

Electric effects in fluid dynamics are particularly important for microscale systems and thus for biological systems, such as cells and vesicles, and technical systems like micropumps. In the field of electrohydrodynamics, a widely accepted approach is the simplification that the electric and the fluid mechanic problems are just weakly coupled via Smoluchowski-type boundary conditions. However, our understanding to date is limited on a range of full electrokinetic problems that can only be explained considering a strong coupling between electrostatics and fluid flow.

The FPS research group pursues numerical and analytical approaches to reach a deeper understanding of full electrokinetic systems. Current numerical examinations focus on the development and optimization of electrokinetic micropumps [1]. Previously, a number of analytical studies with applications in biomechanics have been published. Important aims are for instance the understanding of varying surface potentials (compare figure 1) or the influence of complex surface geometries as highlighted in the following paragraph. [2,3,4,5]

Important microfluidic phenomena, such as droplet deformation and cell motion, are impacted by the formation of Debye layers at charged interfaces. Previous studies examined interface problems with leaky dielectrics or the formation of diffuse charge layers. In most cases, the results are derived for weakly curved spherical geometries. Moreover, many studies of streaming-potential phenomena at fluid-solid interfaces lack a macroscale description of effects that are higher than first order. An asymptotic methodology capturing both complex surface geometries and an accurate description of higher-order phenomena is presented in this study (compare figures 2 and 3). For this purpose, we consider a generic streaming-potential problem. As a result, the complex three-dimensional electrohydrodynamics in the Debye layer are entailed in two-dimensional discontinuity conditions. The latter contain a free parameter, the layer thickness, which mathematically represents the discontinuity position within the Debye layer. It can be used to derive an alternative definition of the Debye thickness capturing the influence of the  $\zeta$ -potential. We introduce a virtual particle whose outer boundary envelopes the solid particle plus a fraction of the Debye layer. It interacts with the macroscopic flow while incorporating the detailed electrohydrodynamics inside the layer. [4]

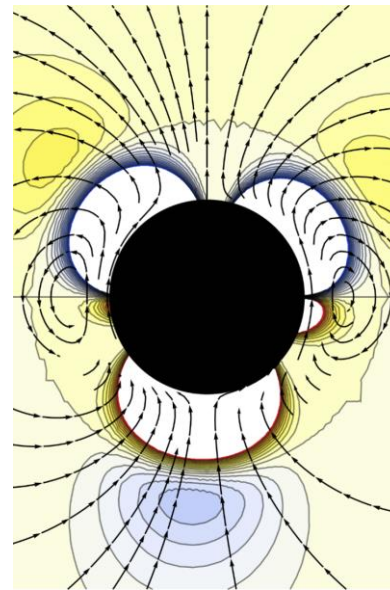


Figure 1. Electrohydrodynamic flow around a sedimenting particle with time-varying zeta-potential. Streamlines in black, high pressure in red and low pressure in blue colors. [5]

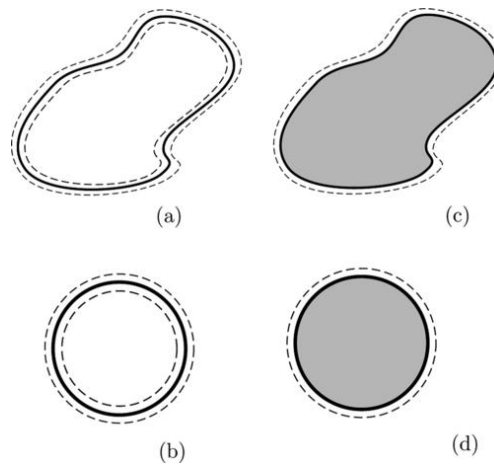


Figure 2. Electrically charged solid particles and vesicles (fluid-fluid interface systems) that can be investigated with our model. (a) Liquid-liquid bilayer model, (b) spherical liquid-liquid bilayer model, (c) liquid-solid model, and (d) spherical liquid-solid model. [4]

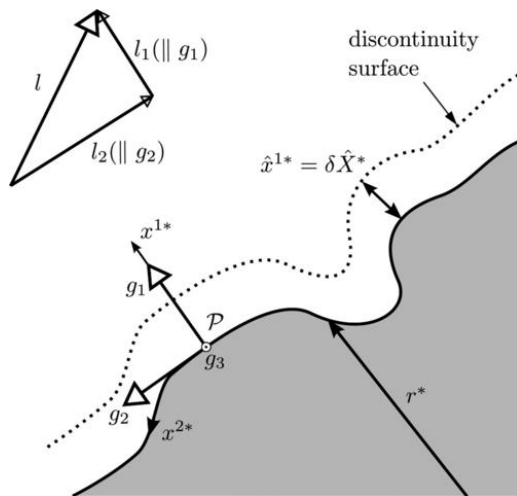


Figure 3. Geometrical modeling of curved interfaces in the asymptotic model.

## References

- [1] Marthaler, P., Simon, M. (2020): Interview with the nominees of the NEULAND Innovation Contest, KIT Research to Business Online Portal (<https://www.kit-technology.de/en/blog/interview-nominees-of-the-neuland-innovation-contest>, 26.04.2021, 16:10)
- [2] Marthaler, P. G. and Class, A. G., Integral effects of the Debyelayer on a sedimenting particle with zeta-potential variations. PAMM, 21(1):e202100209, 2021a.
- [3] Marthaler, P. G. and Class, A. G., Integral jump conditions for singular problems - applied to Debye-layer phenomena. PAMM, 20(1): e202000044, 2021b.
- [4] Marthaler, P. G. and Class, A. G., Weak curvature asymptotics for Debye layers as electrohydrodynamic discontinuities. Physical Review E, 105(3):035106, March 2022.
- [5] Marthaler, P. G. and Class, A. G., Integral jump conditions for time-dependent Debye layer phenomena, 73rd Annual Meeting of the APS Division of Fluid Dynamics, Chicago (virtual), November 2020.

## Analysis of Flow Blockages in a Typical Fuel Assembly of a Liquid Metal Cooled Reactor employing CFD, Coarse Grid-CFD and POD-ROM methodologies

Shenhui Ruan, Andreas G. Class

Flow blockage of coolant channels in Liquid metal cooled fast reactors (LMFRs), which leads to increasing of cladding temperature and possibly results in failure of cladding, is a severe risk to the safety of reactors. Recently, many experiments and simulations have been conducted to analyse the heat transfer and flow characteristics in flow blockage regions. Some experiments (Fontana, et al. 1973; Pacio, et al. 2018) show that small partial blockage has insignificant effect on pressure drop and flow rate of assemblies. Computational fluid dynamics (CFD) is also applied to analyze the effect of some factors including blockages properties and boundary conditions (Chai, X, et al. 2019).

Compared to conventional CFD method, the Reduced Order Models (ROM) could dramatically accelerate the simulation speed and produce acceptable results (Yanez, J, & Andreas C. 2021). Therefore, our group plans to develop a ROM method which is based on Coarse Grid-CFD and Proper Orthogonal Decomposition (POD)-Galerkin projection method to simulate the flow blockage phenomenon.

The typical fuel assembly contains many repeating geometrical blocks and the flow behavior in the blocks is similar. Hence, the dominant flow patterns, named spatial POD modes, could be obtained after post processing a series of conventional CFD simulations of a typical LMFR assembly. Then a ROM will be created by projecting governing equations onto the dominant modes. The flow and heat transfer in each block could be predicted by the ROM combined with a method to minimize the discontinuities between block interfaces. The comparison between CFD and ROM simulations will be carried out to verify the ROM. Fi-

nally, the influence of blockage geometric factors and coolant flow conditions will also be simulated and summarized.

To perform POD of variable fields in blocks, the mesh topology and cell number in repeating blocks for high resolution CFD simulations should be the same. Hence, a meshing method based on mirroring and copying is carried out. Figure 1 shows the mesh of repeating blocks which is applied to perform high resolution CFD simulations.

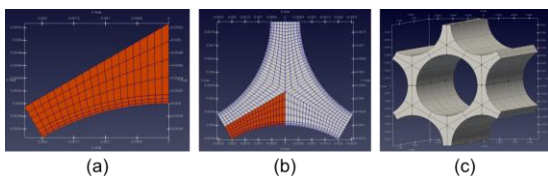


Figure 1: Mesh of subchannels in LMFR, (a) mesh of an individual block; (b) mesh of a typical sub-channel; (c) mesh of several subchannels.

Dominant modes of different variable fields and the number of modes considered for Galerkin projection could be obtained by conducting POD on variable fields. Figure 2 shows dominant modes and normalized eigenvalue of velocity field for a case with porous blockages in 2 blocks.

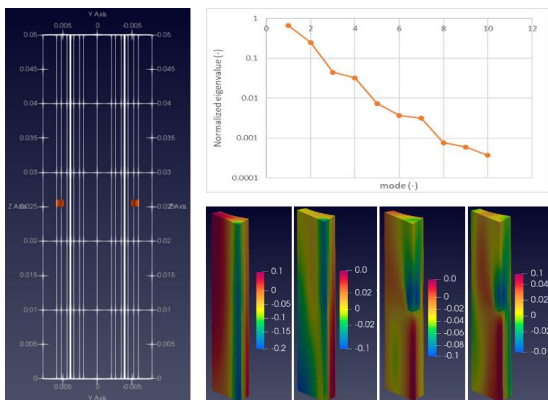


Figure 2: Dominant modes of velocity for a case with porous blockages in 2 blocks

## References

- [1] Fontana, M. H., Kress, T. S., et, al. (1973). Effect of partial blockages in simulated LMFBR fuel assemblies (No. ORNL-TM-4324). Oak Ridge National Lab.(ORNL), Oak Ridge, TN (United States).
- [2] Pacio, J., Daubner, M., Fellmoser, F., Litfin, K., & Wetzal, T. (2018). Heat transfer experiment in a partially (internally) blocked 19-rod bundle with wire spacers cooled by LBE. Nuclear Engineering and Design, 330, 225-240.
- [3] Chai, X., Liu, X., Xiong, J., & Cheng, X. (2019). CFD analysis of flow blockage phenomena in a LBE-cooled 19-pin wire-wrapped rod bundle. Nuclear Engineering and Design, 344, 107-121.
- [4] Yanez, J, & Andreas C. (2021). Analysis of the Accuracy of Residual Heat Removal in Gen-IV Reactors. Nuclear Engineering and Design 376: 111102.

## PDF Methods for Two-Phase flows

*Lorenz Weber, Andreas Class*

A deeper understanding of phenomena in two-phase flows can be applied to many fields in engineering and science. Cavitating flows or condensation and boiling processes are found for example in power plants, pumps, or heat pumps. For numerical simulations of two-phase flows, a stochastic approach [1], [3] is further developed in the present work focusing on phase-change and heat-transfer problems. Since decades PDF methods in CFD are successfully used in the field of reactive flows to handle their highly non-linear behavior [2].

The present study is evaluating the use of Voronoi diagrams in combination with a constrained K-Means clustering in the postprocessing of bubble distributions for improved histograms in space. Developed methods are

tested and validated with the institute's experimental data. Insights into the improved analysis of PDF fields are enabling the development of an enhanced statistical field method for two-phase flows.

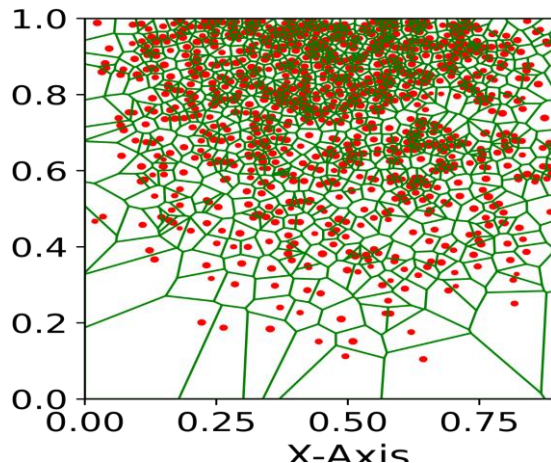


Figure 1: Voronoi-diagram applied to a random bubble distribution

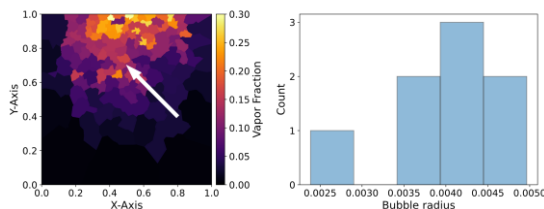


Figure 2: Instantaneous vapor fraction based on Voronoi diagram grouped in clusters of 8 bubbles with histogram of the bubble size distribution at an example location (white arrow).

## References

- [1] Dumond, J., F. Magagnato und A. Class (2013). „Stochastic-field cavitation model“. In: *Physics of Fluids* 25.7, S. 073302. doi: 10.1063/1.4813813. eprint: <https://doi.org/10.1063/1.4813813>.
- [2] Pope, S. (1985). „PDF methods for turbulent reactive flows“. In: *Progress in Energy and Combustion Science* 11.2, S. 119–192.

issn: 0360-1285. doi: [https://doi.org/10.1016/0360-1285\(85\)90002-4](https://doi.org/10.1016/0360-1285(85)90002-4).

[3] Raquet, M. R. (2019). „Stochastische Euler-Euler-PDF-Methodik für das Zwei-Fluid-Modell und Anwendung auf kavitierende Strömungen der Automobilindustrie“. 32.02.01; LK 01. Diss. Karlsruher Institut für Technologie (KIT). 152 S. doi: 10.5445/IR/1000096827.15

## Measurement and modeling of the boiling crisis in a rod bundle on Accident Tolerant Fuel (ATF) cladding materials

Nicolas Wefers, Stephan Gabriel, Andreas Class

The boiling crisis in rod bundles has been studied for long time, yet the critical heat flux density (CHF) and especially the mechanism of local film boiling Departure from nucleate Boiling (DNB) has so far eluded simulative prediction. This is due to the complexity of the flow and the limited observability of the phenomenon with available measurement technology. The complexity also stems from the fact that the material properties of the boiling surface have a direct effect on the critical heat flux density [1,2,3].

Within the scope of the project, new cladding tube materials for rod bundles will be investigated experimentally at the Multiphase Flow Group (MPF) and with accompanying simulations at the Framatome Professional School (FPS), for their suitability for the regular operation of nuclear power plants. For this purpose, accident-tolerant fuel materials (ATFs) optimized for beyond-design-basis events, such as chromium-coated Zircaloy-4 and CrFeAl, will be compared with a classical rod bundle made of Zircaloy-4. In particular, the influence of cladding materials on CHF and the mechanism of DNB, which have not been previously considered in lock-up tables for determining CHF, are investigated [4]. The planned work packages of the project include:

Since, according to previous investigations, the occurrence of DNB does not seem to exhibit a discrete threshold value, but rather a frequency distribution, simulation calculations are to be carried out in the project at the FPS to better delimit the finite measurement accuracy and the statistical behavior of the flow. For this purpose, a CFD model of the test section is to be built and verified with own preliminary test data. Furthermore, simulations are to be used to find the essential parameters and a setup for the subsequent tests, which are to provide meaningful data. Experiments at the COSMOS-L facility of the MPF in figure 1 are planned to characterize the measuring section and provide validation data for the CFD simulation.



Figure 1: Critical-heat-flux On Smooth and Modified Surfaces – Low pressure loop (Test Facility COSMOS-L)

In the main experiments, boiling or CHF in the reference Zircaloy-4 rod bundle as well as the two ATF rod bundles will be investigated with the optimized experimental setup and design from the preliminary experiments and pre-test simulations. For this purpose, measurements will be performed on the boiling cladding tubes

up to CHF. The parameter studies shall include pressure, inlet temperature, mass flow and, if necessary, other important influencing variables. It shall be investigated how the expected differences of the CHF values, can be assigned to the different material properties of the cladding tubes.

While the pre-test simulations are intended to support the test execution, the post-test analyses are used to interpret and evaluate the error limits of the measured data. In particular, the heat transfer conditions when the CHF phenomenon occurs depend very much on the parameters of the heat transfer relations used. The goal of the evaluations is to identify the main influencing parameters for the different ATFs. Furthermore, the experimental/numerical results will be used to provide a database for the validation of further developments of CHF simulation codes and system codes, with reference to the boiling crisis.

## References

- [1] Haas, C., Critical Heat Flux for Flow Boiling of Water at Low Pressure on Smooth and Micro-Structured Zircaloy Tube Surfaces, Dissertation, KIT Scientific Reports 7627
- [2] Haas, C., Kaiser, F., Schulenberg, T., Wetzel, T., Critical heat flux for flow boiling of water on micro-structured Zircaloy tube surfaces, International Journal of Heat and Mass Transfer, Volume 120, May 2018, Pages 793-806
- [3] Kaiser, F., Dietrich, B., Gabriel, S., Wetzel, T., Schlussbericht zum Verbundprojekt „Experimentelle Ermittlung von kritischen Wärmestromdichten bei reaktortypischen Bedingungen als Validierungsdaten“, Arbeitspaket 3.1.12, (Förderkennzeichen GRS 1501473B)
- [4] Groeneveld, D.C., et.al. The 2005 CHF Look-up Table, Nuclear Technology Vol. 152 2005

## List of Publications

- [1] Asselt, E. D. van; Twenhöfel, C. J. W.; Duranova, T.; Smetsers, R. C. G. M.; Bohunova, J.; Müller, T., Facilitating the Decision-Making Process After a Nuclear Accident : Case Studies in the Netherlands and Slovakia, Integrated environmental assessment and management, 17 (2), 376–387 doi:10.1002/ieam.4375
- [2] Ba, Q.; Xiao, J.; Jordan, T., Measurements and Modeling on Hydrogen Jet an Combustion from a Pressurized Vessel [in press], Proceedings of the 9th International Conference on Hydrogen Safety (ICHS2021), 432–441, Paper ID56
- [3] Ba, Q.; Xiao, J.; Jordan, T., Measurement and Modeling on Hydrogen Jet and Combustion from a Pressurized Vessel International Conference on Hydrogen Safety (ICHS 2021), Online, 21.–24. September 2021
- [4] Ba, Q.; Denkevits, A.; Hu, G.; Jedicke, O.; Jiang, F.; Jordan, T.; Kaup, B.; Kotchourko, A.; Kuznetsov, M.; Lelyakin, A.; Mohacsi, J.; Prestel, F.; Stassen, M.; Xiao, J.; Xu, Z.; Zhang, Y.; Zhang, Z., Fundamental Behaviour of Hydrogen to Applied Accident Consequence Analysis for Hydrogen as a Safe Energy Carrier, Annual Report 2019 of the Institute for Nuclear and Energy Technologies, 49–55, Karlsruher Institut für Technologie (KIT)
- [5] Batta, A.; Class, A. G., CFD validation of heavy liquid metal thermal-hydraulic in bare rod bundles, International Congress on Advances in Nuclear Power Plants (ICAPP 2021), Online, 16.–20. Oktober 2021
- [6] Batta, A.; Class, A. G., CFD validation of heavy liquid metal thermal-hydraulic in bare rod bundles, Proceedings of ICAPP 2021, International Congress on Advances in Nuclear Power Plants (ICAPP 2021), Online, 16.–20. Oktober 2021, Paper 21414
- [7] Baur, S.; Neuberger, A.-K.; Kuhn, D.; Seibt, A., Measurements on Fluid-Rock-Interaction of Thermal Water-Inhibitor-Mixtures with the HydRA Facility, Proceedings of the World Geothermal Congress 2020+1, Reykjavik, Iceland, April - October 2021
- [8] Baur, S.; Seibt, A.; Buse, C.; Stern, G.; Kuhn, D., Versuche an der Gesteins-Durchströmungsanlage HydRA zum Einfluss eines Inhibitors zur Verhinderung von Calcit ausfällungen im Molassebecken, Der Geothermiekongress (DGK 2021), Essen, Deutschland, 30. November–2. Dezember 2021
- [9] Brenneis, B.; Gordeev, S.; Ruck, S.; Stoppel, L., Höhenprofilmessung einer offenen Kanalströmung mit Blick auf das Flüssigmetalltarget in DONES, Experimentelle Strömungsmechanik : 28. Fachtagung, 7.-9. September 2021, Bremen. Hrsg.: A. Fischer, Article: 27, Deutsche Gesellschaft für Laser-Anemometrie - German Association for Laser Anemometry GALA e.V
- [10] Brenneis, B.; Gordeev, S.; Ruck, S.; Stoppel, L.; Hering, W., Wake Shape and Height Profile Measurements in a Concave Open Channel Flow Regarding the Target in DONES, Energies, 14 (20), Art.-Nr.: 6506. doi:10.3390/en14206506
- [11] Broda, B.; Köhl, B.; Eichinger, F.; Iannotta, J.; Kuhn, D.; Seibt, A., Roadmap to prevent calcium carbonate precipitations in medium enthalpy hydrogeothermal projects in the South German Molasse Basin- From EvA-M to EvA-M 2.0. project, Der Geothermiekongress (DGK 2021), Essen, Deutschland, 30. November–2. Dezember 2021
- [12] Bühler, L.; Brinkmann, H.-J.; Courtessole, C.; Klüber, V.; Köhly, C.; Mistrangelo, C., Magnetohydrodynamics for liquid-metal blankets, Annual Report 2019 of the Institute for Nuclear and Energy Technologies, 7–16, Karlsruher Institut für Technologie (KIT)
- [13] Bühler, L.; Lyu, B.; Brinkmann, H.-J.; Mistrangelo, C., Reconstruction of 3D MHD liquid metal velocity from measurements of electric potential on the external surface of a thick-walled pipe, Fusion Engineering and Design,

168, Art.-Nr.: 112590.[doi:10.1016/j.fusengdes.2021.112590](https://doi.org/10.1016/j.fusengdes.2021.112590)

[14] Champouillon, M.; Schröder, E.; Kuhn, D., Study of a liquid air energy storage system, Annual Report 2019 of the Institute for Nuclear and Energy Technologies, 57–62, Karlsruhe Institut für Technologie (KIT)

[15] Chen, X.-N.; Rineiski, A., 3-D Simulation of Fuel Assembly Blockage in MYRRHA, Annual Report 2019 of the Institute for Nuclear and Energy Technologies, 17–22, Karlsruhe Institut für Technologie (KIT)

[16] Cirrone, D.; Makarov, D.; Kuznetsov, M.; Friedrich, A.; Molkov, V., Effect of Heat Transfer Through the Release Pipe on Simulations of Cryogenic Hydrogen Jet Fires and Hazard Distances [in press], Proceedings of the 9th International Conference on Hydrogen Safety (ICHS2021), 838–852, Paper ID75

[17] Cirrone, D.; Makarov, D.; Kuznetsov, M.; Friedrich, A.; Molkov, V., Effect of Heat Transfer Through the Release Pipe on Simulations of Cryogenic Hydrogen Jet Fires and Hazard Distances, International Conference on Hydrogen Safety (ICHS 2021), Online, 21.–24. September 2021

[18] Eichinger, F.; Seibt, A.; Iannotta, J.; Würdemann, H.; Otten, C.; Kuhn, D., New approaches for the evaluation of scaling inhibitors for hydrothermal applications, Der Geothermiekongress (DGK 2021), Essen, Deutschland, 30. November–2. Dezember 2021

[19] Erdogan, S.; Schulenberg, T.; Deutschmann, O.; Wörner, M., Evaluation of models for bubble-induced turbulence by DNS and utilization in two-fluid model computations of an industrial pilot-scale bubble column, Chemical Engineering Research and Design, 175, 283–295. [doi:10.1016/j.cherd.2021.09.012](https://doi.org/10.1016/j.cherd.2021.09.012)

[20] Fellmoser, F.; Flesch, J.; Daubner, M.; Müller-Trefzer, F.; Pacio, J.; Niedermeier, K.; Stoppel, L.; Piecha, H.; Uhlenbruck, N.; Wittemann, K.; Wetzels, T., Concentrating Solar Power with Liquid Metals as Heat Transfer Fluids, Annual Report 2019 of the Institute for Nuclear and Energy Technologies, 35–37, Karlsruhe Institut für Technologie (KIT)

[21] Friedrich, A.; Necker, G.; Vesper, A.; Grune, J.; Kuznetsov, M.; Jordan, T., Experimental investigation on the burning behavior of homogeneous H<sub>2</sub>-CO-air mixtures in an obstructed, semiconfined channel, Proceedings of the 9th International Conference on Hydrogen Safety (ICHS2021), 1347–1359

[22] Friedrich, A.; Necker, G.; Vesper, A.; Grune, J.; Kuznetsov, M.; Jordan, T., Experimental investigation on the burning behavior of homogeneous H<sub>2</sub>-CO-air mixtures in an obstructed, semiconfined channel, International Conference on Hydrogen Safety (ICHS 2021), Online, 21.–24. September 2021

[23] Gabriel, S.; Albrecht, G., Detailed investigations on flow boiling of water up to the critical heat flux, Annual Report 2019 of the Institute for Nuclear and Energy Technologies, 29–33, Karlsruhe Institut für Technologie (KIT)

[24] Gaus-Liu, X.; Cron, T.; Fluhrer, B.; Wenz, T., Experimental study and analytical analysis on the global heat transfer of stratified corium in LWR lower head, Nuclear engineering and design, 372, Art.-Nr.: 110999. [doi:10.1016/j.nucengdes.2020.110999](https://doi.org/10.1016/j.nucengdes.2020.110999)

[25] Gaus-Liu, X.; Stuckert, J., Current Severe Accident Researches in Germany, 28th International Conference on Nuclear Engineering (ICONE 2021), Online, 4.–6. August 2021

[26] Gaus-Liu, X.; Cron, T.; Fluhrer, B.; Stängle, R.; Vervoortz, M.; Wenz, T., JIMEC experiments to investigate jet impingement on a core catcher bottom and LIVE2D 2-Layer experiment, Annual Report 2019 of the Institute for Nuclear and Energy Technologies, 23–27, Karlsruhe Institut für Technologie (KIT)

[27] Grune, J.; Sempert, K.; Kuznetsov, M.; Jordan, T., Hydrogen Jet Structure in Presence of Forced Co-, Counter- and Cross-Flow Ventilation, Proceedings of the 9th International Conference on Hydrogen Safety (ICHS2021), 710–721

[28] Grune, J.; Sempert, K.; Kuznetsov, M.; Jordan, T., Hydrogen Jet Structure in Presence of Forced Co-, Counter- and Cross-Flow Ventilation, International Conference on Hydrogen Safety (ICHS 2021), Online, 21.–24. September 2021

- [29] Grune, J.; Sempert, K.; Kuznetsov, M.; Jordan, T., Experimental investigation of unconfined spherical and cylindrical flame propagation in hydrogen-air mixtures, International journal of hydrogen energy, 46 (23), 12487–12496. doi:10.1016/j.ijhydene.2020.09.062
- [30] Hanselka, H., Resilience by Design: Erneuerbare Energiesysteme nachhaltig gestalten, Redundanzen, Resilienzen und Nachhaltigkeit: Energie für die 20er Jahre, 80–87, Forum für Zukunftsenergien e.V
- [31] Hu, G.; Liu, Q., Characteristics of hemp radiation field on typical transport aircraft with frequency sweep method, Applied Sciences (Switzerland), 11 (19), 9284. doi:10.3390/app11199284
- [32] Hu, G.; Ma, Y.; Zhang, H.; Liu, Q., Investigation on Sub-models of Population Balance Model for Subcooled Boiling in Vertical Gas-liquid Flow by Comprehensive Evaluation, International journal of heat and mass transfer, 167, Art.-Nr.: 120816. doi:10.1016/j.ijheatmasstransfer.2020.120816
- [33] Hu, G.; Ma, Y.; Liu, Q., Evaluation on coupling of wall boiling and population balance models for vertical gas-liquid Subcooled boiling flow of first loop of nuclear power plant, Energies, 14 (21), 7357. doi:10.3390/en14217357
- [34] Hu, G.; Ma, Y.; Zhang, H.; Liu, Q., A mini-review on population balance model for gas-liquid subcooled boiling flow in nuclear industry, Annals of Nuclear Energy, 157, Art.-Nr.: 108174. doi:10.1016/j.anucene.2021.108174
- [34] Hu, G.; Wang, F.; Ba, Q.; Xiao, J.; Jordan, T., Numerical investigation of light gas release, stratification and dissolution in TH22 test facility using 3-D CFD code GASFLOW-MPI, International journal of hydrogen energy. doi:10.1016/j.ijhydene.2021.04.185
- [35] Hu, G.; Zhou, T.; Liu, Q., Data-Driven Machine Learning for Fault Detection and Diagnosis in Nuclear Power Plants: A Review, Frontiers in Energy Research, 9, Art.-Nr.: 663296. doi:10.3389/fenrg.2021.663296
- [36] Iannotta, J.; Eichinger, F.; Kuhn, D.; Seibt, A.; Würdemann, H.; Buse, C.; Teitz, S.; Otten, C.; Broda, B.; Schlegel, P., Prevention of carbonate precipitations in deep hydrothermal plants - Experiences from the long term application and operation of an eco-friendly degradable inhibitor, Der Geothermiekongress (DGK 2021), Essen, Deutschland, 30. November–2. Dezember 2021
- [37] Jordan, T.; Bernard, L.; Cirrone, D.; Coldrick, S.; Friedrich, A.; Hawksworth, S.; Jallais, S.; Kuznetsov, M.; Markert, F.; Molkov, V.; Proust, C.; Venetsanos, A.; Vesper, A.; Wen, J., Results of the Pre-Normative Research Project PRESLHY for the Safe Use of Liquid Hydrogen, Proceedings of the 9th International Conference on Hydrogen Safety (ICH2021), 189–207
- [38] Jordan, T.; Bernard, L.; Cirrone, D.; Coldrick, S.; Friedrich, A.; Proust, S.; Venetsanos, A.; Vesper, A.; Wen, J., Results of the Pre-Normative Research Project PRESLHY for the Safe Use of Liquid Hydrogen, International Conference on Hydrogen Safety (ICH2021), Online, 21.–24. September 2021
- [39] Jordan, T.; Friedrich, A., Stand der Wasserstoffsicherheit in Deutschland und Europa, DVGW-Schulung "H2 Sicherheit" (2021), Online, 28. September 2021
- [40] Jordan, T., Wasserstoff für die Energiewende, 6. Energieforschungsgespräche Disentis (2021), Online, 20.–22. Januar 2021
- [41] Jordan, T., Germany - LH2 Safety, Safe Net Zero 2021 - Hydrogen (2021), Online, 2.–4. März 2021
- [42] Jordan, T., Querschnittsübergreifende sicherheitstechnische Fragestellungen, Impulsvortrag Forschungsnetzwerk Wasserstoff (2021), Online, 24. März 2021
- [43] Jordan, T., Wasserstoff – aber sicher?! Wasserstoff: Echte Chance oder bloßer Trend? IHK Hochrhein Bodensee (2021), Konstanz, Deutschland, 2. Juli 2021
- [44] Jordan, T., Herausforderungen der flüssigen Wasserstoffspeicherung, Der Wasserstoffmotor (2021), Karlsruhe, Deutschland, 13.–14. September 2021

- [45] Jordan, T., PRESLHY Pre-normative Research for the Safe use of Liquid Hydrogen, FCH JU Programme Review Days (2021), Online, 2.–3. Dezember 2021
- [46] Jordan, T., LH2 Safety Research – State of the Art, International Gas Safety Seminar hosted by KGS (2021), Online, 16. Dezember 2021
- [47] Jordan, T.; Kuznetsov, M.; Friedrich, A.; Vesper, A.; Kotchourko, N., PRESLHY WP 4.4. (Ignition above the Pool) Experiment: 20200504 092719; Material of the ground: Grave04; High of the ignition point: 25cm; Camera: HIS PHOTRON; time 0-697ms, 2021
- [48] Jordan, T.; Kuznetsov, M.; Friedrich, A.; Vesper, A.; Kotchourko, N., PRESLHY WP 4.4. (Ignition above the Pool) Experiment: 20200504 092719; Material of the ground: Grave04; High of the ignition point: 25cm; Camera: HIS PHOTRON; time 0-82ms, 2021
- [49] Jordan, T.; Kuznetsov, M.; Friedrich, A.; Vesper, A.; Kotchourko, N., PRESLHY WP 4.4. (Ignition above the Pool) Experiment: 20200504 092719; Material of the ground: Grave04; High of the ignition point: 25cm; Camera: STEMMER, 2021
- [50] Jordan, T.; Kuznetsov, M.; Friedrich, A.; Vesper, A.; Kotchourko, N., PRESLHY WP 4.4. (Ignition above the Pool) Experiment: 20200504 092719; Material of the ground: Grave04; High of the ignition point: 25cm; Camera: PANASONIC I, 2021
- [51] Jordan, T.; Kuznetsov, M.; Friedrich, A.; Vesper, A.; Kotchourko, N., PRESLHY WP 4.4. (Ignition above the Pool) Experiment: 20200504 092719; Material of the ground: Grave04; High of the ignition point: 25cm; Camera: CANON II, 2021
- [52] Jordan, T.; Kuznetsov, M.; Friedrich, A.; Vesper, A.; Kotchourko, N., PRESLHY WP 4.4. (Ignition above the Pool) Experiment: 20200427 142349; Material of the ground: Water02; High of the ignition point: 25cm; Camera: CANON II, 2021
- [53] Jordan, T.; Kuznetsov, M.; Friedrich, A.; Vesper, A.; Kotchourko, N., PRESLHY WP 4.4. (Ignition above the Pool) Experiment: 20200427 142349; Material of the ground: Water02; High of the ignition point: 25cm; Camera: CANON I, 2021
- [54] Jordan, T.; Kuznetsov, M.; Friedrich, A.; Vesper, A.; Kotchourko, N., PRESLHY WP 4.4. (Ignition above the Pool) Experiment: 20200427 142349; Material of the ground: Water02; High of the ignition point: 25cm; Camera: HIS PHOTRON, 2021
- [55] Jordan, T.; Kuznetsov, M.; Friedrich, A.; Vesper, A.; Kotchourko, N., PRESLHY WP 4.4. (Ignition above the Pool) Experiment: 20200427 142349; Material of the ground: Water02; High of the ignition point: 25cm; Camera: PANASONIC I, 2021
- [56] Jordan, T.; Kuznetsov, M.; Friedrich, A.; Vesper, A.; Kotchourko, N., PRESLHY WP 4.4. (Ignition above the Pool) Experiment: 20200427 134405; Material of the ground: Concrete07; High of the ignition point: 08cm; Camera: PANASONIC I, 2021
- [57] Jordan, T.; Kuznetsov, M.; Friedrich, A.; Vesper, A.; Kotchourko, N., PRESLHY WP 4.4. (Ignition above the Pool) Experiment: 20200427 134405; Material of the ground: Concrete07; High of the ignition point: 08cm; Camera: CANON II, 2021
- [58] Jordan, T.; Kuznetsov, M.; Friedrich, A.; Vesper, A.; Kotchourko, N., PRESLHY WP 4.4. (Ignition above the Pool) Experiment: 20200427 134405; Material of the ground: Concrete07; High of the ignition point: 08cm; Camera: CANON I, 2021
- [59] Jordan, T.; Kuznetsov, M.; Friedrich, A.; Vesper, A.; Kotchourko, N., PRESLHY WP 4.4. (Ignition above the Pool) Experiment: 20200427 132430; Material of the ground: Concrete06; High of the ignition point: 15cm; Camera: CANON I, 2021
- [60] Jordan, T.; Kuznetsov, M.; Friedrich, A.; Vesper, A.; Kotchourko, N., PRESLHY WP 4.4. (Ignition above the Pool) Experiment: 20200427 132430; Material of the ground: Concrete06; High of the ignition point: 15cm; Camera: CANON II, 2021
- [61] Jordan, T.; Kuznetsov, M.; Friedrich, A.; Vesper, A.; Kotchourko, N., PRESLHY WP 4.4.

- (Ignition above the Pool) Experiment: 20200427 132430; Material of the ground: Concrete06; High of the ignition point: 15cm; Camera: HIS PHOTRON, 2021
- [62] Jordan, T.; Kuznetsov, M.; Friedrich, A.; Vesper, A.; Kotchourko, N., PRESLHY WP 4.4. (Ignition above the Pool) Experiment: 20200427 132430; Material of the ground: Concrete06; High of the ignition point: 15cm; Camera: STEMMER, 2021
- [63] Jordan, T.; Kuznetsov, M.; Friedrich, A.; Vesper, A.; Kotchourko, N., PRESLHY WP 4.4. (Ignition above the Pool) Experiment: 20200427 132430; Material of the ground: Concrete06; High of the ignition point: 15cm; Camera: PANASONIC I, 2021
- [64] Jordan, T.; Kuznetsov, M.; Friedrich, A.; Vesper, A.; Kotchourko, N., PRESLHY WP 4.4. (Ignition above the Pool) Experiment: 20200427 130148; Material of the ground: Concrete05; High of the ignition point: 25cm; Camera: PANASONIC I, 2021
- [65] Jordan, T.; Kuznetsov, M.; Friedrich, A.; Vesper, A.; Kotchourko, N., PRESLHY WP 4.4. (Ignition above the Pool) Experiment: 20200427 130148; Material of the ground: Concrete05; High of the ignition point: 25cm; Camera: STEMMER, 2021
- [66] Jordan, T.; Kuznetsov, M.; Friedrich, A.; Vesper, A.; Kotchourko, N., PRESLHY WP 4.4. (Ignition above the Pool) Experiment: 20200427 130148; Material of the ground: Concrete05; High of the ignition point: 25cm; Camera: HIS PHOTRON, 2021
- [67] Jordan, T.; Kuznetsov, M.; Friedrich, A.; Vesper, A.; Kotchourko, N., PRESLHY WP 4.4. (Ignition above the Pool) Experiment: 20200427 130148; Material of the ground: Concrete05; High of the ignition point: 25cm; Camera: CANON II, 2021
- [68] Jordan, T.; Kuznetsov, M.; Friedrich, A.; Vesper, A.; Kotchourko, N., PRESLHY WP 4.4. (Ignition above the Pool) Experiment: 20200427 130148; Material of the ground: Concrete05; High of the ignition point: 25cm; Camera: CANON I, 2021
- [69] Jordan, T.; Kuznetsov, M.; Friedrich, A.; Vesper, A.; Kotchourko, N., PRESLHY WP 4.4. (Ignition above the Pool) Experiment: 20200427 123016; Material of the ground: Concrete04; High of the ignition point: 45cm; Camera: CANON I, 2021
- [70] Jordan, T.; Kuznetsov, M.; Friedrich, A.; Vesper, A.; Kotchourko, N., PRESLHY WP 4.4. (Ignition above the Pool) Experiment: 20200427 123016; Material of the ground: Concrete04; High of the ignition point: 45cm; Camera: CANON II, 2021
- [71] Jordan, T.; Kuznetsov, M.; Friedrich, A.; Vesper, A.; Kotchourko, N., PRESLHY WP 4.4. (Ignition above the Pool) Experiment: 20200427 123016; Material of the ground: Concrete04; High of the ignition point: 45cm; Camera: HIS PHOTRON, 2021
- [72] Jordan, T.; Kuznetsov, M.; Friedrich, A.; Vesper, A.; Kotchourko, N., PRESLHY WP 4.4. (Ignition above the Pool) Experiment: 20200427 123016; Material of the ground: Concrete04; High of the ignition point: 45cm; Camera: STEMMER, 2021
- [73] Jordan, T.; Kuznetsov, M.; Friedrich, A.; Vesper, A.; Kotchourko, N., PRESLHY WP 4.4. (Ignition above the Pool) Experiment: 20200427 123016; Material of the ground: Concrete04; High of the ignition point: 45cm; Camera: PANASONIC I, 2021
- [74] Jordan, T.; Kuznetsov, M.; Friedrich, A.; Vesper, A.; Kotchourko, N., PRESLHY WP 4.4. (Ignition above the Pool) Experiment: 20200427 113920; Material of the ground: Sand11; High of the ignition point: 45cm; Camera: PANASONIC I, 2021
- [75] Jordan, T.; Kuznetsov, M.; Friedrich, A.; Vesper, A.; Kotchourko, N., PRESLHY WP 4.4. (Ignition above the Pool) Experiment: 20200427 113920; Material of the ground: Sand11; High of the ignition point: 45cm; Camera: STEMMER, 2021
- [76] Jordan, T.; Kuznetsov, M.; Friedrich, A.; Vesper, A.; Kotchourko, N., PRESLHY WP 4.4. (Ignition above the Pool) Experiment: 20200427 113920; Material of the ground: Sand11; High of the ignition point: 45cm; Camera: HIS PHOTRON, 2021

- [77] Jordan, T.; Kuznetsov, M.; Friedrich, A.; Vesper, A.; Kotchourko, N., PRESLHY WP 4.4. (Ignition above the Pool) Experiment: 20200427 113920; Material of the ground: Sand11; High of the ignition point: 45cm; Camera: CANON I, 2021
- [78] Jordan, T.; Kuznetsov, M.; Friedrich, A.; Vesper, A.; Kotchourko, N., PRESLHY WP 4.4. (Ignition above the Pool) Experiment: 20200427 113920; Material of the ground: Sand11; High of the ignition point: 45cm; Camera: CANON II, 2021
- [79] Jordan, T.; Kuznetsov, M.; Friedrich, A.; Vesper, A.; Kotchourko, N., PRESLHY WP 4.4. (Ignition above the Pool) Experiment: 20200427 111712; Material of the ground: Sand10; High of the ignition point: 08cm; Camera: CANON II, 2021
- [80] Jordan, T.; Kuznetsov, M.; Friedrich, A.; Vesper, A.; Kotchourko, N., PRESLHY WP 4.4. (Ignition above the Pool) Experiment: 20200427 111712; Material of the ground: Sand10; High of the ignition point: 08cm; Camera: CANON I, 2021
- [81] Jordan, T.; Kuznetsov, M.; Friedrich, A.; Vesper, A.; Kotchourko, N., PRESLHY WP 4.4. (Ignition above the Pool) Experiment: 20200427 111712; Material of the ground: Sand10; High of the ignition point: 08cm; Camera: HIS PHOTRON, 2021
- [82] Jordan, T.; Kuznetsov, M.; Friedrich, A.; Vesper, A.; Kotchourko, N., PRESLHY WP 4.4. (Ignition above the Pool) Experiment: 20200427 111712; Material of the ground: Sand10; High of the ignition point: 08cm; Camera: STEMMER, 2021
- [83] Jordan, T.; Kuznetsov, M.; Friedrich, A.; Vesper, A.; Kotchourko, N., PRESLHY WP 4.4. (Ignition above the Pool) Experiment: 20200427 111712; Material of the ground: Sand10; High of the ignition point: 08cm; Camera: PANASONIC I, 2021
- [84] Jordan, T.; Kuznetsov, M.; Friedrich, A.; Vesper, A.; Kotchourko, N., PRESLHY WP 4.4. (Ignition above the Pool) Experiment: 20200427 102617; Material of the ground: Sand09; High of the ignition point: 35cm; Camera: PANASONIC I, 2021
- [85] Jordan, T.; Kuznetsov, M.; Friedrich, A.; Vesper, A.; Kotchourko, N., PRESLHY WP 4.4. (Ignition above the Pool) Experiment: 20200427 102617; Material of the ground: Sand09; High of the ignition point: 35cm; Camera: HIS PHOTRON, 2021
- [86] Jordan, T.; Kuznetsov, M.; Friedrich, A.; Vesper, A.; Kotchourko, N., PRESLHY WP 4.4. (Ignition above the Pool) Experiment: 20200427 102617; Material of the ground: Sand09; High of the ignition point: 35cm; Camera: CANON I, 2021
- [87] Jordan, T.; Kuznetsov, M.; Friedrich, A.; Vesper, A.; Kotchourko, N., PRESLHY WP 4.4. (Ignition above the Pool) Experiment: 20200427 102617; Material of the ground: Sand09; High of the ignition point: 35cm; Camera: CANON II, 2021
- [88] Jordan, T.; Kuznetsov, M.; Friedrich, A.; Vesper, A.; Kotchourko, N., PRESLHY WP 4.4. (Ignition above the Pool) Experiment: 20200427 095604; Material of the ground: Sand08; High of the ignition point: 40cm; Camera: CANON II, 2021
- [89] Jordan, T.; Kuznetsov, M.; Friedrich, A.; Vesper, A.; Kotchourko, N., PRESLHY WP 4.4. (Ignition above the Pool) Experiment: 20200427 095604; Material of the ground: Sand08; High of the ignition point: 40cm; Camera: CANON I, 2021
- [90] Jordan, T.; Kuznetsov, M.; Friedrich, A.; Vesper, A.; Kotchourko, N., PRESLHY WP 4.4. (Ignition above the Pool) Experiment: 20200427 095604; Material of the ground: Sand08; High of the ignition point: 40cm; Camera: PANASONIC I, 2021
- [91] Jordan, T.; Kuznetsov, M.; Friedrich, A.; Vesper, A.; Kotchourko, N., PRESLHY WP 4.4. (Ignition above the Pool) Experiment: 20200427 095604; Material of the ground: Sand08; High of the ignition point: 40cm; Camera: HIS PHOTRON, 2021
- [92] Jordan, T.; Kuznetsov, M.; Friedrich, A.; Vesper, A.; Kotchourko, N., PRESLHY WP 4.4. (Ignition above the Pool) Experiment: 20200424 113916; Material of the ground: Sand06; High of the ignition point: 15cm; Camera: CANON II, 2021

- [93] Jordan, T.; Kuznetsov, M.; Friedrich, A.; Vesper, A.; Kotchourko, N., PRESLHY WP 4.4. (Ignition above the Pool) Experiment: 20200424 113916; Material of the ground: Sand06; High of the ignition point: 15cm; Camera: CANON I, 2021
- [94] Jordan, T.; Kuznetsov, M.; Friedrich, A.; Vesper, A.; Kotchourko, N., PRESLHY WP 4.4. (Ignition above the Pool) Experiment: 20200424 113916; Material of the ground: Sand06; High of the ignition point: 15cm; Camera: HIS PHOTRON, 2021
- [95] Jordan, T.; Kuznetsov, M.; Friedrich, A.; Vesper, A.; Kotchourko, N., PRESLHY WP 4.4. (Ignition above the Pool) Experiment: 20200424 113916; Material of the ground: Sand06; High of the ignition point: 15cm; Camera: PANASONIC I; time 1400-4100 ms, 2021
- [96] Jordan, T.; Kuznetsov, M.; Friedrich, A.; Vesper, A.; Kotchourko, N., PRESLHY WP 4.4. (Ignition above the Pool) Experiment: 20200424 113916; Material of the ground: Sand06; High of the ignition point: 15cm; Camera: PANASONIC I, 2021
- [97] Jordan, T.; Kuznetsov, M.; Friedrich, A.; Vesper, A.; Kotchourko, N., PRESLHY WP 4.4. (Ignition above the Pool) Experiment: 20200424 113916; Material of the ground: Sand06; High of the ignition point: 15cm; Camera: STEMMER, 2021
- [98] Jordan, T.; Kuznetsov, M.; Friedrich, A.; Vesper, A.; Kotchourko, N., PRESLHY WP 4.4. (Ignition above the Pool) Experiment: 20200424 103252; Material of the ground: Sand05; High of the ignition point: 25cm; Camera: STEMMER, 2021
- [99] Jordan, T.; Kuznetsov, M.; Friedrich, A.; Vesper, A.; Kotchourko, N., PRESLHY WP 4.4. (Ignition above the Pool) Experiment: 20200424 103252; Material of the ground: Sand05; High of the ignition point: 25cm; Camera: PANASONIC I, 2021
- [100] Jordan, T.; Kuznetsov, M.; Friedrich, A.; Vesper, A.; Kotchourko, N., PRESLHY WP 4.4. (Ignition above the Pool) Experiment: 20200424 103252; Material of the ground: Sand05; High of the ignition point: 25cm; Camera: CANON II, 2021
- [101] Jordan, T.; Kuznetsov, M.; Friedrich, A.; Vesper, A.; Kotchourko, N., PRESLHY WP 4.4. (Ignition above the Pool) Experiment: 20200424 103252; Material of the ground: Sand05; High of the ignition point: 25cm; Camera: CANON I, 2021
- [102] Jordan, T.; Kuznetsov, M.; Friedrich, A.; Vesper, A.; Kotchourko, N., PRESLHY WP 4.4. (Ignition above the Pool) Experiment: 20200424 103252; Material of the ground: Sand05; High of the ignition point: 25cm; Camera: HIS PHOTRON, 2021
- [103] Jordan, T.; Kuznetsov, M.; Friedrich, A.; Vesper, A.; Kotchourko, N., PRESLHY WP 4.4. (Ignition above the Pool) Experiment: 20200424 090012; Material of the ground: Sand04; High of the ignition point: 25cm; Camera: HIS PHOTRON, 2021
- [104] Jordan, T.; Kuznetsov, M.; Friedrich, A.; Vesper, A.; Kotchourko, N., PRESLHY WP 4.4. (Ignition above the Pool) Experiment: 20200424 090012; Material of the ground: Sand04; High of the ignition point: 25cm; Camera: STEMMER, 2021
- [105] Jordan, T.; Kuznetsov, M.; Friedrich, A.; Vesper, A.; Kotchourko, N., PRESLHY WP 4.4. (Ignition above the Pool) Experiment: 20200424 090012; Material of the ground: Sand04; High of the ignition point: 25cm; Camera: CANON II, 2021
- [106] Jordan, T.; Kuznetsov, M.; Friedrich, A.; Vesper, A.; Kotchourko, N., PRESLHY WP 4.4. (Ignition above the Pool) Experiment: 20200424 090012; Material of the ground: Sand04; High of the ignition point: 25cm; Camera: CANON I, 2021
- [107] Jordan, T.; Kuznetsov, M.; Friedrich, A.; Vesper, A.; Kotchourko, N., PRESLHY WP 4.4. (Ignition above the Pool) Experiment: 20200424 090012; Material of the ground: Sand04; High of the ignition point: 25cm; Camera: PANASONIC I, 2021
- [108] Jordan, T.; Kuznetsov, M.; Friedrich, A.; Vesper, A.; Kotchourko, N., PRESLHY Experiment series WP 5.3 (Flame propagation over a spill of LH2); warm55\_br0, 2021

- [109] Jordan, T.; Kuznetsov, M.; Friedrich, A.; Vesper, A.; Kotchourko, N., PRESLHY Experiment series WP 5.3 (Flame propagation over a spill of LH2); warm44\_br30, 2021
- [110] Jordan, T.; Kuznetsov, M.; Friedrich, A.; Vesper, A.; Kotchourko, N., PRESLHY Experiment series WP 5.3 (Flame propagation over a spill of LH2); warm44\_br0\_02, 2021
- [111] Jordan, T.; Kuznetsov, M.; Friedrich, A.; Vesper, A.; Kotchourko, N., PRESLHY Experiment series WP 5.3 (Flame propagation over a spill of LH2); warm\_44\_b40\_01, 2021
- [112] Jordan, T.; Kuznetsov, M.; Friedrich, A.; Vesper, A.; Kotchourko, N., PRESLHY Experiment series WP 5.3 (Flame propagation over a spill of LH2); warm30\_br60, 2021
- [113] Jordan, T.; Kuznetsov, M.; Friedrich, A.; Vesper, A.; Kotchourko, N., PRESLHY Experiment series WP 5.3 (Flame propagation over a spill of LH2); warm30\_br30, 2021
- [114] Jordan, T.; Kuznetsov, M.; Friedrich, A.; Vesper, A.; Kotchourko, N., PRESLHY Experiment series WP 5.3 (Flame propagation over a spill of LH2); warm30\_br0, 2021
- [115] Jordan, T.; Kuznetsov, M.; Friedrich, A.; Vesper, A.; Kotchourko, N., PRESLHY Experiment series WP 5.3 (Flame propagation over a spill of LH2); warm25\_br60, 2021
- [116] Jordan, T.; Kuznetsov, M.; Friedrich, A.; Vesper, A.; Kotchourko, N., PRESLHY Experiment series WP 5.3 (Flame propagation over a spill of LH2); warm25\_br30, 2021
- [117] Jordan, T.; Kuznetsov, M.; Friedrich, A.; Vesper, A.; Kotchourko, N., PRESLHY Experiment series WP 5.3 (Flame propagation over a spill of LH2); warm15\_br60, 2021
- [118] Jordan, T.; Kuznetsov, M.; Friedrich, A.; Vesper, A.; Kotchourko, N., PRESLHY Experiment series WP 5.3 (Flame propagation over a spill of LH2); warm\_15\_br30, 2021
- [119] Jordan, T.; Kuznetsov, M.; Friedrich, A.; Vesper, A.; Kotchourko, N., PRESLHY Experiment series WP 5.3 (Flame propagation over a spill of LH2); warm15\_br0, 2021
- [120] Jordan, T.; Kuznetsov, M.; Friedrich, A.; Vesper, A.; Kotchourko, N., PRESLHY Experiment series WP 5.3 (Flame propagation over a spill of LH2); warm10\_br60, 2021
- [121] Jordan, T.; Kuznetsov, M.; Friedrich, A.; Vesper, A.; Kotchourko, N., PRESLHY Experiment series WP 5.3 (Flame propagation over a spill of LH2); warm10\_br30, 2021
- [122] Jordan, T.; Kuznetsov, M.; Friedrich, A.; Vesper, A.; Kotchourko, N., PRESLHY Experiment series WP 5.3 (Flame propagation over a spill of LH2); warm10\_br0, 2021
- [123] Jordan, T.; Kuznetsov, M.; Friedrich, A.; Vesper, A.; Kotchourko, N., PRESLHY Experiment series WP 5.3 (Flame propagation over a spill of LH2); cold55\_br0, 2021
- [124] Jordan, T.; Kuznetsov, M.; Friedrich, A.; Vesper, A.; Kotchourko, N., PRESLHY Experiment series WP 5.3 (Flame propagation over a spill of LH2); cold43\_br0, 2021
- [125] Jordan, T.; Kuznetsov, M.; Friedrich, A.; Vesper, A.; Kotchourko, N., PRESLHY Experiment series WP 5.3 (Flame propagation over a spill of LH2); cold30\_br60, 2021
- [126] Jordan, T.; Kuznetsov, M.; Friedrich, A.; Vesper, A.; Kotchourko, N., PRESLHY Experiment series WP 5.3 (Flame propagation over a spill of LH2); cold30\_br0, 2021
- [127] Jordan, T.; Kuznetsov, M.; Friedrich, A.; Vesper, A.; Kotchourko, N., PRESLHY Experiment series WP 5.3 (Flame propagation over a spill of LH2); cold25\_br60, 2021
- [128] Jordan, T.; Kuznetsov, M.; Friedrich, A.; Vesper, A.; Kotchourko, N., PRESLHY Experiment series WP 5.3 (Flame propagation over a spill of LH2); cold15\_br60, 2021
- [129] Jordan, T.; Kuznetsov, M.; Friedrich, A.; Vesper, A.; Kotchourko, N., PRESLHY Experiment series WP 5.3 (Flame propagation over a spill of LH2); cold15\_br30, 2021
- [130] Jordan, T.; Kuznetsov, M.; Friedrich, A.; Vesper, A.; Kotchourko, N., PRESLHY Experiment series WP 5.3 (Flame propagation over a spill of LH2); cold15\_br0, 2021

- [131] Jordan, T.; Kuznetsov, M.; Friedrich, A.; Veser, A.; Kotchourko, N., PRESLHY Experiment series WP 5.3 (Flame propagation over a spill of LH2) ; cold\_br60, 2021
- [132] Jordan, T.; Kuznetsov, M.; Friedrich, A.; Veser, A.; Kotchourko, N., PRESLHY Experiment series WP 5.3 (Flame propagation over a spill of LH2); cold10\_br30, 2021
- [133] Jordan, T.; Kuznetsov, M.; Friedrich, A.; Veser, A.; Kotchourko, N., PRESLHY Experiment series WP 5.3 (Flame propagation over a spill of LH2), 2021
- [134] Jordan, T.; Reinecke, E., Sicherheit im Umgang mit Wasserstoff, Jahrestagung 2021 des Forschungsverbunds Erneuerbare Energien (FVEE): Mit Wasserstoff zur Klimaneutralität - von der Forschung in die Anwendung (2021), Berlin, Deutschland, 10.–11. November 2021
- [135] Kamienowska, M.; Niedermeier, K.; Stoppel, L.; Bender, M.; Wetzl, T., Experimental set-up for the production of formaldehyde using sodium vapour, 13th European Congress of Chemical Engineering (ECCE 13) & 6th European Congress of Applied Biotechnology (ECAB 6 2021), Online, 20.–23. September 2021
- [136] Kotchourko, A.; Lelyakin, A.; Yanez, J.; Halmer, G., COM3D: Turbulent Combustion Code User's Guides, 2021, August 16. doi:10.5445/IR/1000136328
- [137] Kropp, C.; Ley, A.; Ottenburger, S. S.; Ufer, U. (Hrsg.), Climate-neutral and intelligent cities in Europe : Mission statements, paths, risks, Zeitschrift für Technikfolgenabschätzung in Theorie und Praxis, 30 (1), 10–55. doi:10.14512/tatup.30.1.10
- [138] Kropp, C.; Ley, A.; Ottenburger, S. S.; Ufer, U., Making intelligent cities in Europe climate-neutral : About the necessity to integrate technical and socio-cultural innovations, Zeitschrift für Technikfolgenabschätzung in Theorie und Praxis, 30 (1), 11–16. doi:10.14512/tatup.30.1.11
- [139] Kryková, M.; Schulenberg, T.; Arnoult Růžičková, M.; Sáez-Maderuelo, A.; Otic, I.; Czifrus, S.; Cizelj, L.; Pavel, G. L., European Research Program on Supercritical Water-Cooled Reactor, Journal of nuclear engineering and radiation science, 7 (2), 021301. doi:10.1115/1.4048901
- [140] Kuznetsov, M., Flame acceleration and detonation transition of hydrogen-air mixtures at cryogenic temperatures, International Workshop on Explosion and Reactive Flow, Beijing Institute of Technology (2021), Peking, China, 24.–25. Juni 2021
- [141] Kuznetsov, M., Flame acceleration and DDT at cryogenic temperatures, Web-conference organized by the State Key Laboratory of Explosion Science and Technology, Beijing Institute of Technology (2021), Peking, China, 10. Juni 2021
- [142] Kuznetsov, M.; Denkevits, A.; Veser, A.; Friedrich, A.; Necker, G.; Jordan, T., Shock tube experiments on flame propagation regimes and critical conditions for flame acceleration and detonation transition for hydrogen-air mixtures at cryogenic temperatures, Proceedings of the 9th International Conference on Hydrogen Safety (ICH2021), 818–831
- [143] Kuznetsov, M.; Denkevits, A.; Veser, A.; Friedrich, A.; Necker, G.; Jordan, T., Shock tube experiments on flame propagation regimes and critical conditions for flame acceleration and detonation transition for hydrogen-air mixtures at cryogenic temperatures, International Conference on Hydrogen Safety (ICH2021), Online, 21.–24. September 2021
- [144] Kuznetsov, M.; Yanez, J.; Veiga-López, F., Near Limit Flame Propagation in a Thin Layer Geometry at Low Peclet Numbers, Proceedings of the Eighteenth International Conference on Flow Dynamics, 688–692
- [145] Kuznetsov, M.; Yanez, J.; Veiga-López, F., Near Limit Flame Propagation in a Thin Layer Geometry at Low Peclet Numbers, 18th International Conference on Flow Dynamics (ICFD 2021), Sendai, Japan, 27.–29. Oktober 2021
- [146] Laube, T.; Dietrich, B.; Marocco, L.; Wetzl, T., Experimentelle Bestimmung des Wärmeübergangs in turbulenten Flüssigmetailströmungen bei komplexen thermischen

Randbedingungen, Jahrestreffen der Process-Net-Fachgruppen Fluidverfahrenstechnik und Wärme- und Stoffübertragung (2021), Online, 24.–26. Februar 2021

[147] Laube, T.; Emmendorfer, F.; Dietrich, B.; Marocco, L.; Wetzels, T., Thermophysical properties of the near eutectic liquid Ga-In-Sn alloy, 2021, November 19. doi:10.5445/IR/1000140052

[148] Li, Y.; Xiao, J.; Zhang, H.; Breitung, W.; Travis, J.; Kuznetsov, M.; Jordan, T., Numerical analysis of hydrogen release, dispersion and combustion in a tunnel with fuel cell vehicles using all-speed CFD code GASFLOW-MPI, International journal of hydrogen energy, 46 (23), 12474–12486. doi:10.1016/j.ijhydene.2020.09.063

[149] Litfin, K.; Klupp, J.; Class, A., Blockage formation experiments in a water rod bundle, Annual Report 2019 of the Institute for Nuclear and Energy Technologies, 63–69, Karlsruhe Institut für Technologie (KIT)

[150] Lyons, K., Fuel Cells and Hydrogen Joint Undertaking (FCH JU), 2021, August 16. doi:10.5445/IR/1000136285

[151] Lyons, K.; Coldrick, S.; Atkinson, G., Fuel Cells and Hydrogen Joint Undertaking (FCH JU); Summary of experiment series E3.5 2021, August 16. doi:10.5445/IR/1000136281

[152] Lyons, K.; Hooker, P., Electrostatic Ignition (Summary of experiment series E4.3 results), 2021, August 16. doi:10.5445/IR/1000136330

[153] Lyons, K.; Hooker, P., Summary of experiment series E4.3 (Electrostatic Ignition) results, 2021, August 16. doi:10.5445/IR/1000136282

[154] Makarov, D.; Cirrone, D.; Shentsov, V.; Kashkarov, S.; Molkov, V.; Xu, Z.; Kuznetsov, M.; Venetsanos, A.; Giannissi, S.; Toliás, I.; Vaagsaether, K.; Pursell, M.; Rattigan, W.; Markert, F.; Giuliani, L.; Bernard, A.; Sanz Millán, M.; Brauner, C.; Kummer, U., Overview of first outcomes of PNR project HyTunnel-CS International Conference on Hydrogen Safety (ICHS 2021), Online, 21.–24. September 2021

[155] Makarov, D.; Cirrone, D.; Shentsov, V.; Kashkarov, S.; Molkov, V.; Xu, Z.; Kuznetsov, M.; Venetsanos, A.; Giannissi, S.; Toliás, I.; Vaagsaether, K.; Gaathaug, A.; Pursell, M.; Rattigan, W.; Markert, F.; Giuliani, L.; Bernad, A.; Sanz Millán, A.; Brauner, C.; Kummer, U., Overview of first outcomes of PNR project HyTunnel-CS, Proceedings of the 9th International Conference on Hydrogen Safety (ICHS2021), 1248–1262

[156] Makarov, D.; Shentsov, V.; Kuznetsov, M.; Molkov, V., Hydrogen Tank Rupture in Fire in the Open Atmosphere: Hazard Distance Defined by Fireball, Hydrogen, 2 (1), 134–146. doi:10.3390/hydrogen2010008

[157] Marthaler, P. G.; Class, A. G., Integral effects of the Debye layer on a sedimenting particle with zeta-potential variations, Proceedings in applied mathematics and mechanics, 21 (1), Art.-Nr.: e202100209. doi:10.1002/pamm.202100209

[158] Marthaler, P. G.; Class, A. G., Integral jump conditions for singular problems – applied to Debye-layer phenomena, Proceedings in applied mathematics and mechanics, 20 (1), Art.-Nr.: e202000044. doi:10.1002/pamm.202000044

[160] Mistrangelo, C.; Bühler, L.; Alberghi, C.; Bassini, S.; Candido, L.; Courtessole, C.; Tassone, A.; Urgorri, F. R.; Zikanov, O., Mhd r&d activities for liquid metal blankets, Energies, 14 (20), 6640. doi:10.3390/en14206640

[161] Mistrangelo, C.; Bühler, L.; Koehly, C.; Ricapito, I., Magnetohydrodynamic velocity and pressure drop in manifolds of a WCLL TBM, Nuclear fusion, 61 (9), Art.-Nr. 096037. doi:10.1088/1741-4326/ac18dc

[162] Mistrangelo, C.; Bühler, L.; Smolentsev, S.; Klüber, V.; Maione, I.; Aubert, J., MHD flow in liquid metal blankets: Major design issues. MHD guidelines and numerical analysis, Fusion engineering and design, 173, Art.Nr. 112795 doi:10.1016/j.fusengdes.2021.112795

[163] Möhrle, S., Knowledge Management for Enhanced Decision-Making. Developments and Future Challenges for Remediation, IAEA Network of Environmental Management and Remediation (ENVIRONET), Web Seminar:

- Remediation Approaches and Knowledge Management in Context of the Aftermath of a Nuclear Accident (2022), Online, 6. April 2021
- [164] Möhrle, S.; Ottenburger, S. S.; Müller, T. O.; Trybushnyi, D.; Deines, E.; Raskob, W., Strengthening Resilience in Critical Infrastructure Systems: A Deep Learning Approach for Smart Early Warning of Critical States, 31st European Safety and Reliability Conference (ESREL 2021), Angres, Frankreich, 19.–23. September 2021
- [165] Möhrle, S.; Ottenburger, S. S.; Müller, T. O.; Trybushnyi, D.; Deines, E.; Raskob, W., Strengthening Resilience in Critical Infrastructure Systems: A Deep Learning Approach for Smart Early Warning of Critical States, Proceedings of the 31st European Safety and Reliability Conference (ESREL 2021). Hrsg.: B. Castanier, 1894–1901, Research Publishing. doi:10.3850/978-981-18-2016-8\_239-cd
- [166] Müller, T.; Möhrle, S.; Bai, S.; Raskob, W., Multi Criteria Decision Analysis: Uncertainties and Combining Decision Making Methods, Annual Report 2019 of the Institute for Nuclear and Energy Technologies, 39–47, Karlsruher Institut für Technologie (KIT)
- [167] Müller-Trefzer, F.; Niedermeier, K.; Daubner, M.; Wetzel, T., Experimental investigations of a dual-media thermal energy storage system with liquid metals, 15th International Conference on Renewable Energy Storage (IRES 2021), Online, 16.–18. März 2021
- [168] Müller-Trefzer, F.; Niedermeier, K.; Fellmoser, F.; Flesch, J.; Pacio, J.; Wetzel, T., Experimental results from a high heat flux solar furnace with a molten metal-cooled receiver SOMMER, Solar energy, 221, 176–184. doi:10.1016/j.solener.2021.03.066
- [167] Ottenburger, S.; Raskob, W., Smart grid resilience - The role of future power systems in critical infrastructure protection [in press], Modelling the Resilience of Infrastructure Networks Remenyte-Priscott, Rasa; Kopustinskias, Vytiš (Eds.), 148–165, Det Norske Veritas AS (DNS)
- [168] Ottenburger, S. S., Criticality-Based Designs of Power Distribution Systems: Metrics for Identifying Urban Resilient Smart Grids Information Technology Applications for Crisis Response and Management. Ed.: J. Beard, 150–175, Engineering Science Reference. doi:10.4018/978-1-7998-7210-8.ch008
- [169] Pacio, J.; Daubner, M.; Fellmoser, F.; Litfin, K.; Wetzel, T., Corrigendum to “Experimental study of heavy-liquid metal (LBE) flow and heat transfer along a hexagonal 19-rod bundle with wire spacers” [Nucl. Eng. Des. 301 (2016) 111–127], Nuclear engineering and design, 371, Art. Nr.: 110928. doi:10.1016/j.nucengdes.2020.110928
- [170] Schröder, E.; Kraml, M.; Thomauske, K.; Kuhn, D.; Jodocy, M.; Thorwart, K.; Wolfram, M., In-situ Measurement of Physico-Chemical Parameters of Geothermal Waters and Brines - Results of R&D Project PETHER, 2021, Juni 14. World Geothermal Congress (WGC 2021), Reykjavík, Island, 21.–26. Mai 2021
- [171] Tolias, I. C.; Venetsanos, A. G.; Kuznetsov, M.; Koutsoukos, S., Evaluation of an improved CFD model against nine vented deflagration experiments, International journal of hydrogen energy, 46 (23), 12407–12419. doi:10.1016/j.ijhydene.2020.09.231
- [172] Tromm, T. W., Heutige Situation und Energiestrategien, Energieforschungsgespräche Disentis (2021), Disentis, Schweiz, 20.–22. Januar 2021
- [173] Tromm, W., Structure and Laboratories of the Institute of Nuclear and Energy Technologies, Annual Report 2019 of the Institute for Nuclear and Energy Technologies, 1–6, Karlsruher Institut für Technologie (KIT)
- [174] Tromm, W. (Hrsg.), Annual Report 2019 of the Institute for Nuclear and Energy Technologies (KIT Scientific Reports ; 7759), KIT Scientific Publishing. doi:10.5445/KSP/1000123340
- [175] Tromm, W.; Gaus-Liu, X., KIT-JMEC Experiments to Investigate Jet Impingement on the Ablation of Core Catcher Bottom 30th International Conference Nuclear Energy for New Europe (NENE 2021), Veldes, Slowenien, 6.–9. September 2021

- [176] Vesper, A.; Friedrich, A.; Kuznetsov, M.; Jordan, T.; Kotchourko, N., Hydrogen Blow-down Release Experiments at Different Temperatures in the DISCHA-Facility, Proceedings of the 9th International Conference on Hydrogen Safety (ICHS2021), 442–454
- [177] Vesper, A.; Friedrich, A.; Kuznetsov, M.; Jordan, T.; Kotchourko, N., Hydrogen Blow-down Release Experiments at Different Temperatures in the DISCHA-Facility, International Conference on Hydrogen Safety (ICHS 2021), Online, 21.–24. September 2021
- [178] Vesper, A.; Friedrich, A.; Necker, G.; Denkevits, A.; Kuznetsov, M.; Jordan, T., Flame propagation regimes at cryogenic temperature, 2021, August 16. doi:10.5445/IR/1000136188
- [179] Wiemer, H.-J.; Schneider, V. B., Thermodynamical and Economical Valuation of Low-Temperature ORC with Alternative Working Fluids, Proceedings of the World Geothermal Congress 2020+1, Reykjavik, Iceland, April - October 2021
- [180] Wiemer, H.-J.; Schneider, V. B., Thermodynamical and Economical Valuation of Low-Temperature ORC with Alternative Working Fluids [in press], World Geothermal Congress (WGC 2021), Reykjavík, Island, 21.–26. Mai 2021
- [181] Xiao, J.; Jordan, T., Simulation Capabilities Requirements of CFD-Based Tool for Hydrogen Safety Analysis in Large-Scale Infrastructures, The International Symposium on Hydrogen Fire, Explosion and Safety Standard (ISHFESS2021 2021), Hefei, China, 21.–23. Mai 2021
- [182] Xu, Z.; Jiang, F.; Jordan, T., Investigation on cooling effect of water sprays on tunnel fires of hydrogen, Proceedings of the 9th International Conference on Hydrogen Safety (ICHS2021), 975–983
- [184] Xu, Z.; Jiang, F.; Jordan, T., Investigation on cooling effect of water sprays on tunnel fires of hydrogen, International Conference on Hydrogen Safety (ICHS 2021), Online, 21.–24. September 2021
- [185] Yanez, J.; Veiga-López, F., Theoretical analysis of the condensation of combustion products in thin gaseous layers, Physics of Fluids, 33 (8), 083601. doi:10.1063/5.0056831
- [186] Yáñez Escanciano, J.; Kuznetsov, M.; Veiga-López, F., Characterization of unconventional hydrogen flame propagation in narrow gaps, Physical review / E, 103 (3), 033101. doi:10.1103/PhysRevE.103.033101
- [187] Zhang, H.; Sauerschell, S.; Ba, Q.; Hu, G.; Jordan, T.; Bajohr, S.; Xiao, J., Numerical simulation of accidental released hazardous gas dispersion at a methanation plant using GASFLOW-MPI, International journal of hydrogen energy, 46 (2), 2804–2823. doi:10.1016/j.ijhydene.2020.10.100
- [188] Zhang, Y.; Hu, G.; Zhang, H.; Liu, Q.; Zhou, J., Thermodynamic analysis and optimization for steam methane reforming hydrogen production system using high temperature gas-cooled reactor pebble-bed module, Journal of Nuclear Science and Technology, 58 (12), 1359–1372. doi:10.1080/00223131.2021.1951863

KIT Scientific Working Papers  
ISSN 2194-1629

[www.kit.edu](http://www.kit.edu)